



**Politecnico  
di Torino**

Politecnico di Torino

MSc Automotive Engineering

A.Y. 2020/2021

October 2021

**Effect of Key Design Variables on  
Adhesively Bonded Joints with  
Additive Manufacturing  
Substrates**

Advisors:

prof. Luca Goglio

prof. Sayed A. Nassar

Candidate:

Daniel Nappi

ID Number:

276981

© Copyright by Daniel Nappi, 2021  
All rights are reserved

*To whoever has struggled before success*

## ACKNOWLEDGMENT

Firstly, I would like to deeply thank my Thesis advisors, Sayed Nassar and Luca Goglio, for the continuous support: even by remote I have always felt their *presence* and their bi-weekly precious comments and add-ons have made this work possible.

Then I would like to thank to whoever has participated in this research, starting from my head-tutors from Stellantis S.P.A.: eng. Stefano Slaghenaufi, from the very first day, showed me great passion and professionalism in his work. Then, a very special mention is needed to eng. Maura Fontana, who has helped a young and ambitious student to cope with complicated finite element models with constant dedication and interest, I could have never asked for better tutoring (such a shame it was not in person!).

Moreover I would like to thank eng. Raffaele Ciardiello and the staff of PoliTo's laboratory with which I have shared several months.

Last but not least, I would thank sincerely Marco Gerini Romagnoli, with his constant presence whenever it was needed: since the very first day of this experience he really taught me a lot and made me grow up remarkably.

Finally, I just want to dedicate the research to whoever always fights for his dreams, struggling, making plans to transform them into objectives: *Velle est posse!*

Daniel Nappi

## ABSTRACT

### EFFECT OF KEY DESIGN VARIABLES ON ADHESIVELY BONDED JOINTS WITH ADDITIVE MANUFACTURING SUBSTRATES

by

Daniel Nappi

Adviser: Sayed A. Nassar, Ph.D.

This research study investigates on the effect of key design variables on adhesively bonded single lap joints and the FE modelling of an aluminum additive manufacturing (AM) automotive joint using commercially available finite element software like HYPERMESH and ABAQUS. The main objective is the realization of a reliable finite element model able to simulate the mechanical behavior of a complex bonded joint configuration, assembled to the structure with injected adhesive in static conditions. The effect of key design variables for Single Lap Joints (SLJs) is analyzed with analytical models like the ones provided by Volkersen and Goland Reissner. Then, the effect of adhesive thickness and overlap length on the overall mechanical properties of the 3D printed aluminum SLJ is discussed by assessing the optimal design choices for the sample automotive bonded joint.

Numerical results from cohesive FEA modeling are compared both with classical analytical models and validation test data are given. In order to assess the proper parameters to describe the mechanical behavior of the adhesive, also AM Double

Cantilever Beams (DCBs) have been considered to evaluate the fracture toughness properties for the development of the joint simulation. The test samples are all bonded using the same commercially available single-part epoxy. Accordingly, after having characterized the adhesive, the additive manufacturing automotive joint FEA model can be assessed.

## TABLE OF CONTENTS

ACKNOWLEDGMENTS	iv
ABSTRACT	v
LIST OF TABLES	x
LIST OF FIGURES	xi
NOMENCLATURE	xvii
CHAPTER ONE	
INTRODUCTION AND LITERATURE SURVEY	1
1.1 Introduction	1
1.2 Literature Survey	6
1.3 Objectives	9
CHAPTER TWO	
CLASSICAL ANALYTICAL MODELS	11
2.1 Analytical Formulation from Literature	11
2.1.1 Generalized Adhesive Yielding Criterion	14
2.1.2 Volkersen Model [21]	15
2.1.3 Goland-Reissner Model [22]	17
2.1.4 Hart-Smith Approach [24]	21
2.1.5 Design Methodology	22
2.2 Classical Analytical Models Effect on Key Design Variables	24
2.2.1 Effect of Adhesive Material	24
2.2.2 Effect of Adherend Thickness	30

## TABLE OF CONTENTS – Continued

2.2.3 Effect of Joint Width	33
2.2.4 Effect of Adhesive Thickness	37
2.2.5 Effect of Overlap Length	40
<b>CHAPTER THREE</b>	
<b>EXPERIMENTAL SETUP AND TEST PROCEDURE</b>	<b>44</b>
3.1 Experimental Procedure	44
3.2 Single Lap Joint Test	46
3.2.1 Joint Geometry	46
3.2.2 Bonding Process	49
3.2.3 Shear-Tensile Testing	50
3.3 Double Cantilever Beam Test	52
3.3.1 Joint Geometry	52
3.3.2 Peel Testing	55
<b>CHAPTER FOUR</b>	
<b>FINITE ELEMENT MODELS</b>	<b>59</b>
4.1 Finite Element Modeling	59
4.2 Cohesive Zone Modeling	60
4.3 Single Lap Joint	63
4.4 Automotive Bonded Joint	66
<b>CHAPTER FIVE</b>	
<b>RESULTS AND DISCUSSION</b>	<b>71</b>
5.1 Experimental Testing Results	71

## TABLE OF CONTENTS – Continued

5.1.1 Single Lap Joint	71
5.1.2 Double Cantilever Beam	86
5.2 Finite Element Results	91
5.2.1 Single Lap Joint	91
5.2.2 Sample Automotive Application	98
CHAPTER SIX CONCLUSIONS	102
6.1 Conclusions	102
6.2 Continuation Studies	102
REFERENCES	103

## LIST OF TABLES

Table 1.1	Additive Manufacturing Pros and Cons	5
Table 2.1	Analytical Models Range of Applicability	12
Table 2.2	Equations for Bending Moment Factors	23
Table 2.3	Single Lap Joint Fixed Parameters for Analytical Analysis	26
Table 2.4	Polyurethane Material Properties	26
Table 2.5	Epoxy Material Properties	28
Table 2.6	Summary of the Results for the Adhesive Stress Using Classical Analytical Models	43
Table 3.1	Experimental Testing Configurations	45
Table 3.2	Single Lap Joint Geometry Data	48
Table 3.3	Double Cantilever Beam Geometry Data	53
Table 3.4	Crack Length Monitoring in Double Cantilever Beam Testing	56
Table 5.1	Effect of Adhesive Thickness on Joint Failure Loads	75
Table 5.2	Effect of Adhesive Thickness on Joint Stiffness	76
Table 5.3	Effect of Overlap Length on Joint Failure Loads	80
Table 5.4	Summary of the Single Lap Joint Shear Tests with Additive Manufacturing Substrates	85
Table 5.5	Mode I Fracture Toughness	90
Table 5.6	Effect of Adhesive Thickness on Joint Behavior: Comparison FEA vs. Experimental Tests	96
Table 5.7	Effect of Overlap Length on Joint Behavior: Comparison FEA vs. Experimental Tests	97

## LIST OF FIGURES

Figure 1.1	Schematics of Adhesion Topics	2
Figure 2.1	Single Lap Joint Deformation	13
Figure 2.2	Simplified Shear Stress Model	14
Figure 2.3	Differential Shear Model	15
Figure 2.4	Local Equilibrium of Single Lap Joint Elements	16
Figure 2.5	Goland-Reissner Model [22]	18
Figure 2.6	Adams Design Methodology	23
Figure 2.7	Polyurethane Joint Peel Stress predicted by Goland Reissner Analytical Model [22]	27
Figure 2.8	Polyurethane Joint Shear Stress predicted by Volkersen [21] and Goland-Reissner [22] Models	27
Figure 2.9	Epoxy Joint Peel Stress predicted by Goland Reissner Analytical Model [22]	29
Figure 2.10	Epoxy Joint Shear Stress predicted by Volkersen [21] and Goland-Reissner [22] Analytical Models	29
Figure 2.11	Effect of Adherend Thickness on Maximum Shear Stress	31
Figure 2.12	Effect of Adherend Thickness on Maximum Peel Stress	31
Figure 2.13	3D Effect of Adherend Thickness on Shear Stress	32
Figure 2.14	3D Effect of Adherend Thickness on Peel Stress	32
Figure 2.15	Effect of Adherend Thickness on Equivalent von Mises Stress	33
Figure 2.16	Effect of Joint Width on Maximum Shear Stress	34
Figure 2.17	Effect of Joint Width on Maximum Peel Stress	35

## LIST OF FIGURES – Continued

Figure 2.18	3D Effect of Joint Width on Shear Stress	35
Figure 2.19	3D Effect of Joint Width on Peel Stress	36
Figure 2.20	Effect of Joint Width on Equivalent von Mises Stress	36
Figure 2.21	Effect of Adhesive Thickness on Maximum Shear Stress	37
Figure 2.22	Effect of Adhesive Thickness on Maximum Peel Stress	38
Figure 2.23	3D Effect of Adhesive Thickness on Shear Stress	38
Figure 2.24	3D Effect of Adhesive Thickness on Peel Stress	39
Figure 2.25	Effect of Adhesive Thickness on Equivalent von Mises Stress	39
Figure 2.26	Effect of Overlap Length on Maximum Shear Stress	40
Figure 2.27	Effect of Overlap Length on Maximum Peel Stress	41
Figure 2.28	3D Effect of Overlap Length on Shear Stress	41
Figure 2.29	3D Effect of Overlap Length on Peel Stress	42
Figure 2.30	Effect of Overlap Length on Equivalent von Mises Stress	42
Figure 3.1	Preliminary Design Choice for Substrate Thickness of Single Lap Joints	47
Figure 3.2	Bending Moment Factor vs. Substrate Thickness	47
Figure 3.3	Schematics of Test Single Lap Joint	48
Figure 3.4	Additive Manufacturing Surface	49
Figure 3.5	Bonded Single Lap Joint	50

## LIST OF FIGURES – Continued

Figure 3.6	MTS 8801 Material Test System	51
Figure 3.7	Double Cantilever Beam Geometry	52
Figure 3.8	Double Cantilever Beam Adhesion Process	53
Figure 3.9	Bonded Double Cantilever Beam	54
Figure 3.10	Equivalent Crack Length and Fracture Process Zone	58
Figure 4.1	Cohesive Zone Model Traction Separation Law	62
Figure 4.2	Contact Definition between Adhesive and Adherends	64
Figure 4.3	Load Case of Single Lap Joint: Lateral View	65
Figure 4.4	Load Case of Single Lap Joint: 3D View	65
Figure 4.5	Numerical Model Workflow	66
Figure 4.6	Sample Automotive Bonded Joint Mesh	67
Figure 4.7	Quality of the Mesh for the Automotive Joint	68
Figure 4.8	Contact Definition in the Adhesive Layer	69
Figure 4.9	Contact Definition among Adhesive and Adherends of the Automotive Bonded Joint	69
Figure 4.10	Contact Definition among the Metals of the Adherends	70
Figure 5.1	Illustration of some Failure Modes of Bonded Single Lap Joints	71
Figure 5.2	Load-Displacement Data for Adhesive Thickness = 0.5 mm	73
Figure 5.3	Load-Displacement Data for Adhesive Thickness = 1 mm	73

## LIST OF FIGURES – Continued

Figure 5.4	Load-Displacement Data for Adhesive Thickness = 2 mm	74
Figure 5.5	Average Load-Displacement Data for Different Adhesive Thicknesses	74
Figure 5.6	Effect of Adhesive Thickness on Single Lap Joints Bonded with Additive Manufacturing Substrates	76
Figure 5.7	Fracture Surface: Adhesive Thickness = 0.5 mm	78
Figure 5.8	Fracture Surface: Adhesive Thickness = 1 mm	78
Figure 5.9	Fracture Surface: Adhesive Thickness = 2 mm	78
Figure 5.10	Load-Displacement Data for Overlap Length = 19.05 mm and Adhesive Thickness = 0.5 mm	79
Figure 5.11	Average Load-Displacement Data for Different Overlap Lengths	80
Figure 5.12	Effect of Overlap Length on Single Lap Joints Bonded with Additive Manufacturing Substrates	81
Figure 5.13	Fracture Surface of the Single Lap Joint with L = 19.05 mm	82
Figure 5.14	Joint Average Shear Stress with Additive Manufacturing Substrates	83
Figure 5.15	Joint Average Shear Stress with Additive Manufacturing and Extruded Substrates	84
Figure 5.16	Comparison of Joint Strength: Additive Manufacturing vs. Extruded Substrates	84
Figure 5.17	Double Cantilever Beam Load-Displacement Curves	86
Figure 5.18	Double Cantilever Beam Compliance	87
Figure 5.19	Double Cantilever Beam Equivalent Crack Length	87

## LIST OF FIGURES – Continued

Figure 5.20	Crack Length Measurement	88
Figure 5.21	Comparison of Single Beam Theory, Double Beam Theory and Compliance Based Beam Method	88
Figure 5.22	Mode I Fracture Toughness from Double Cantilever Beam	89
Figure 5.23	Mode I Fracture Toughness Test Data	90
Figure 5.24	Finite Element Analysis: Single Lap Joint Shear Testing with Adhesive Thickness 0.5 mm and Overlap Length 12.7 mm	91
Figure 5.25	Finite Element Analysis: Single Lap Joint Shear Testing with Adhesive Thickness 1 mm and Overlap Length 12.7 mm	92
Figure 5.26	Finite Element Analysis: Single Lap Joint Shear Testing with Adhesive Thickness 2 mm and Overlap Length 12.7 mm	92
Figure 5.27	Finite Element Analysis: Single Lap Joint Shear Testing with Adhesive Thickness 0.5 mm and Overlap Length 19.05 mm	93
Figure 5.28	Quadratic Nominal Stress Criterion of the Adhesive in the Finite Element Analysis	94
Figure 5.29	Stiffness Degradation of the Adhesive in the Finite Element Analysis	94
Figure 5.30	Effect of Adhesive Thickness on Load - Displacement Curves: Comparison Finite Element Analysis vs. Experimental Tests	95
Figure 5.31	Effect of Overlap Length on Load-Displacement Curves: Comparison Finite Element Analysis vs. Experimental Tests	97
Figure 5.32	Equivalent Stress in the Sample Automotive Bonded Joint: Overall View	99

LIST OF FIGURES – Continued

Figure 5.33	Equivalent Stress in the Sample Automotive Bonded Joint: Lateral View	99
Figure 5.34	Quadratic Nominal Stress in the Sample Automotive Bonded Joint Adhesive	100
Figure 5.35	Stiffness Degradation in the Sample Automotive Bonded Joint Adhesive	100
Figure 5.36	Sample Automotive Bonded Joint Load Transfer Capacity	101

## NOMENCLATURE

### Latin Symbols

a	Crack Length
b	Joint Width
c	Half of the Overlap Length
C	Compliance
D	Adherend Bending Stiffness
E	Young's Modulus
G	Shear Modulus
$G_{Ic}$	Fracture Toughness
h	Adherend Thickness
k	Bending Moment Factor
k'	Transverse Force Factor
L	Overlap Length
M	Bending Moment
P	Best Estimate Variance
$\bar{P}$	Applied Tensile Load per Unit Width
x	Longitudinal Co-ordinate
X	Normalized Longitudinal Co-ordinate
t	Thickness
u	Horizontal Displacement

## NOMENCLATURE – Continued

$w$	Vertical Displacement
$y$	Transverse Co-ordinate

### Symbols

$\gamma$	Shear Strain
$\nu$	Poisson's Ratio
$\tau$	Shear Stress
$\sigma$	Peel Stress

### Subscripts

$a$	Adhesive
$e$	Elastic
$eq$	Equivalent
$f$	Flexural
$p$	Plastic
$0$	Initial
$1$	Top Adherend
$2$	Bottom Adherend

# CHAPTER ONE

## INTRODUCTION AND LITERATURE SURVEY

### 1.1 Introduction

Adhesive bonding has been used for thousands of years for very different applications joining materials with natural products, but only in the last century they found a relevant role in the industries along with polymers' diffusion.

Adhesion process design is characterized by very different phases, from the spreading of the adhesive on the surface, to its hardening and the evaluation of stresses along the overlap line under external service loads: hence, to obtain reliable results in adhesive bonding it is needed to have control over many sciences, from surface chemistry and polymers' physics to materials engineering and mechanical engineering (Fig. 1.1).

The number of variables involved in proper bonding between substrates is very wide: there is a large amount of theories that try to model what happens locally in the adhesion process. According to electrostatic and mechanical interlocking theories, the surface roughness is one of the parameters which affects the most bonding of the adherends.

Surface treatment and adhesive's *wettability*, therefore, are key aspects to consider when joining adhesive substrates depending on:

- Chemical compatibility among adherends and adhesive.
- Surface roughness.
- Cleaning of the surfaces.
- Adhesive type

The usage of adhesive bonded joints has been definitely increasing during the years: from

machine building and aerospace industry to the civil and automotive sectors. These latter are increasingly becoming an alternative to the conventional mechanical fasteners because they provide many advantages: strength-to-weight ratio, cost effectiveness, the ability to join dissimilar materials (which in conventional joints would cause corrosion), more uniform stress distribution and ease of fabrications are just few of the advantages of the bonded joints over the bolted ones.

Although these positive aspects, adhesive bonding is also associated to some main disadvantages like the limited resistance to extreme temperature and humidity, the cure process time and also the peel and cleavage loading which could induce to poor joint strength.

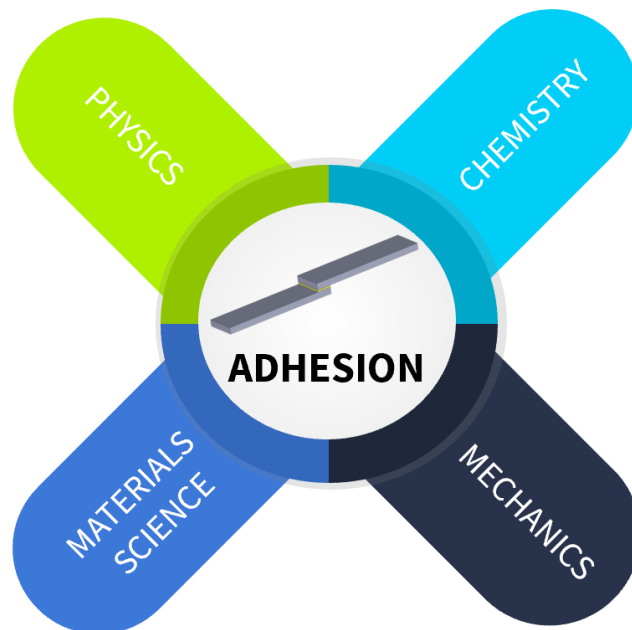


Figure 1.1 Schematics of Adhesion Topics

Many different structural adhesives exist: from the acrylics and polyurethanes up to the epoxies. Polyurethanes adhesives are much *softer*, allowing therefore more deformations to the joint, whereas epoxies are more *brittle* with a stiffer behavior and higher bearing capacity.

The choice of the adhesive is directly connected to the type of application for which they are needed. It is therefore becoming more and more important providing the process and design engineers tools which are able to predict and control the stresses and the mechanical characteristics of the adhesive bonded joints in order to simplify its already complicated design.

In this research, many aspects of the adhesive bonding have been considered: starting from the analytical and FEA models up to experimental test on real bonded joints, the influence of the main design variables for single lap joints (SLJ) and the correct parametrization (DCB) of the used Non Commercially Available (NCA) adhesive are assessed. Therefore, experimental tests have been carried out considering additive manufacturing substrates and regular extruded aluminum specimens: the different surface roughness and fabrication will lead to different bonding results and failure mode. The main outputs of the tests are fundamental to create a proper and reliable FEA model of the adhesive and to apply this to a real patented joint by Stellantis.

Additive manufacturing and 3D printing are likely to become the most revolutionary technologies introduced in this century. The term "3D printing" can refer to a variety of processes in which material is deposited, joined or solidified under computer control to create a three-dimensional object starting from a CAD model: material such as plastics, liquids or powder grains (being fused together) are added, typically layer by

layer. The trend in the industries is tending more and more to the creation and design of lightweight structures and complex geometries in reasonable times.

Conventional manufacturing main problems are related to high cost for prototyping and small runs, long design time, materials waste (subtractive methods), limited materials combinations and complex assembly in case of complex geometries. Most of these concerns can be easily addressed by exploiting some of the additive manufacturing techniques like Fused Filament Fabrication (FFF), Powder Bed Fusion (PBF) and Electrical Discharge Machining (EDM).

These techniques guarantee to cope also with very non-usual geometries: the more complex (or, the less solid the object is), the faster and cheaper it can be made through additive manufacturing. Moreover, if a part needs to be changed, the change can simply be made on the original CAD file, and the new product can be printed right away, without changing radically the process. Other advantages of this innovative design technique are related to the little lead time, since moving parts such as hinges and bicycle chains can be printed in metal directly into the product, significantly reducing part numbers and engineers, as soon as the part has printed, may then begin testing its properties instead of waiting weeks or months for a prototype or part to come in.

However, additive manufacturing is not always the right choice a priori, every advantage comes along with some disadvantages and according to the application the most proper decision must be assessed. Indeed build rates are remarkably slow: many printers lay down material at a speed of one to five cubic inches per hour; depending on the part needed, other manufacturing processes may be significantly faster.

The production costs are still high since sometimes parts can be made faster using

techniques other than additive manufacturing, the extra time may lead to higher costs.

Additionally, high-quality additive manufacturing machines can cost anywhere from \$300,000 to \$1.5 million, and materials can cost \$100 to \$150 per pound.

Moreover, the production process is discontinuous (preventing economics of scale) and the component requires post-processing: the surface finish and dimensional accuracy may be lower quality than other manufacturing methods. In most cases, also, the build volume must be constrained by the machine volume; nevertheless, larger machines are available but they will come at a cost. Table 1.1 summarizes the main pros and cons relative to the usage of additive manufacturing with respect to traditional design techniques.

Table 1.1 Additive Manufacturing Pros and Cons

<b>Advantages</b>	<b>Disadvantages</b>
Complex Geometries	High Costs
Less waste	Poor Mechanical Properties
No assembly required	Discontinuous Production Process
Little Lead Time	Slow Build Rate
Little-Skill Manufacturing	Requires Post-Processing

## 1.2 Literature Survey

The scientific community investigated multiple general aspects of the adhesive bonding for different applications and joint materials.

Da Silva et al. [1] and [2] developed an extensive and full review of the present literature for bonding stress evaluation along single lap joints and their accuracy on strength prediction. In the first reference, the described analytical models are the ones provided by Volkersen and Goland-Reissner, considering a study case to analyze the stress trend along the overlap. In the second reference of the literature survey more complex formulations have been analyzed (from Hart-Smith to Frostig) and the influence of adhesive thickness and overlap length on joint strength is discussed along with experimental testing: nevertheless, they considered regular manufactured substrates.

Subsequently, Adams [3] studied the stresses in standard metal-to-metal adhesive bonded lap joints using two-dimensional finite-element modeling to compare with classical analytical models. In his work he also considered Volkersen and Goland-Reissner models, but he did not exploit those models to assess the effect of the key design variables on joint mechanical behavior made with additive manufacturing substrates.

Banea et al. [4] have analysed multiple material applications in order to optimize the performance of adhesion for different families of materials, using fibre-reinforced plastic (FRP) composites and metals. They considered numerical approaches covering both linear and non-linear models. The main outcome is that the increase of the overlap length results in a nonlinear increase in load bearing capacity, while increasing the adherend thickness (especially for CFRP/HS combinations) caused no significant variation of the joint strength, allowing favourable weight reductions. Other studies are

currently exploring the effects of the modification of the base line adhesive by addition of particles in the adhesive matrix, therefore modifying the adhesive behaviour. Indeed, an accurate strength prediction of the adhesively bonded joints is essential to decrease the amount of expensive testing at the design stage. Nevertheless, these results might not be effective when the surface roughness of the 3D printed substrates is considered.

Garcia [5], explored the use of polymer additive manufacturing technology for imparting texture to bond regions in adhesively bonded joints. Towards that, computational models were first developed to simulate stress distribution along the overlap region of single lap shear joints, and four models that performed the best were chosen for physical testing. Peak loads, shear stresses, and failure types were compared between these models.

Overall, using a combined computational and experimental approach, it is established that the 3D printed reinforcements have the potential to drastically improve the apparent shear strength of adhesively bonded single lap joints. This outcome has been reached for plastic reinforcements; the purpose of this research is to perform similar numerical-experimental approach for a model of an aluminum 3D printed adhesive bonded joint to expand the literature on the combination of these two techniques.

Arenas et al. [6], instead, investigated on one of the most used methods in rapid prototyping: FDM. A novel method of construction by assembling parts with structural adhesive joints is proposed designing the adhesive joints specifically to fit the plastic substrate and the FDM manufacturing technology. To achieve this, the most suitable structural adhesive selection is firstly required. Therefore, their study analyzes five different families of adhesives (cyanoacrylate, polyurethane, epoxy, acrylic and silicone),

and, by means of the application of technical multi-criteria decision analysis based on the analytic hierarchy process (AHP), they obtained the structural adhesive that better conjugates mechanical benefits and adaptation to the FDM manufacturing process among the considered ones. This was just a preliminary study on the adhesive selection which better fit the 3D printed adherends, but nor a virtual model nor the influence of the design parameters on the overall strength are discussed.

More recent studies on additive manufacturing bonded joints were conducted by Frascio et al: in the first [7], they investigated on the building parameters of the AM process Fused Filed Fabrication which affected the joint strength, wettability and morphology. In this study, two materials are considered, acrylonitrile butadiene styrene and polylactideacid. Wettability, surface morphology and mechanical strength have been determined at different combinations of nozzle temperature, print speed and layer thickness. Although they started to consider the possibility of AM joints, their focus was on process parameters, whereas in this research the design parameters affecting the mechanical strength of bonded AM joints are discussed.

Additionally in a follow up study, Frascio et al. [8] emphasize the critical need of surface preparation to improve the performance of adhesively bonded 3D printed Acrylonitrile Butadiene Styrene (ABS) adherends obtained using Fused Filament Fabrication (FFF). In particular, mechanical abrasion and two different plasma pre-treatment were compared through the qualitative analysis of surface wettability, using static and dynamic contact angle measurements, and the quantitative evaluation of surface roughness measured using optical profilometry. In addition, mechanical tests were carried out using the single lap joint configuration and the interaction between the

treated ABS substrates and three different adhesive materials, epoxy, polyurethane and modified silane, were carefully ascertained. The results showed that the actual mechanism of fracture shifted from adhesive failure, typical of solvent cleaned and abraded surfaces, to full cohesive failure within either the substrates or the adhesive layer, with a difference of joint strength of over 300%. Additive manufacturing is, indeed, increasingly used by industries due to its revolutionary features: the possibility of printing very complex geometries, the little lead time, material waste and skill-manufacturing techniques are just some of the advantages of this technique but nevertheless they are still related to high production costs and (sometimes) to poor mechanical properties.

### 1.3 Objectives

Within this context there is a now growing research interest in combining additive manufacturing with adhesive bonding, striving to achieve an innovative and streamlined manufacturing processes, improve the mechanical performance of bonded joints and enable the introduction of capabilities and features to adhesive joints that cannot be achieved via conventional manufacturing methods. For example, additive manufacturing opens several novel possibilities in the design of substrate configurations and the creation of precisely controlled adhesive layers, allowing a practical implementation of graded material properties. Research is also being carried out on how to bond additively manufactured components, approaching subjects such as surface preparation and geometrical design optimization, to achieve ideal stress distributions. Although the topic has already been covered in some papers, most of the time it is difficult for the end-user to understand and deal with the design parameters related to adhesive bonding.

The complexity of the problems of strength prediction of adhesive joints, especially under long-term operations in variable environmental conditions, must be addressed in very different perspectives in order to control as much as possible the phenomena.

The purpose of this study is to provide, at first glance, simple and general guidance for the design to the final users: analyzing how the peak stresses along the overlap vary (with analytical tools and experimental testing) with the key parameters can be a very useful tool to have an idea on the improvement and control of the bonded design.

The development of reliable techniques and predictive methodologies for adhesives could lead to a better and more efficient way to exploit their characteristics: analyzing joints' stresses and strains properly can avoid the overdesign of bonded joints which is usually made when the parameters' influence on the stress distributions are not clear to the final users. Stress analysis, in general, can be approached in two different ways: a full analytical approach exploiting the classical mathematical theories or a numerical approach exploiting the modern softwares for finite element modeling. This work has been divided into four main sections: in the first one, the formulation of the analytical models (Volkersen, Goland-Reissner) implemented in MATLAB and the key design parameters' effect is presented from the analytical point of view. In the second section, the experimental setup and testing procedure is discussed. In the third section, the detailed description of the finite element modeling for SLJ and the real component is treated, whereas in the final section, the results carried out from real experimental testing and their virtual models are proposed in order to assess the influence of parameters such as adhesive thickness and overlap length on SLJ: effectiveness of the analytical predictions with respect to additive manufacturing bonded joints is analyzed.

## CHAPTER TWO

### CLASSICAL ANALYTICAL MODELS

#### 2.1 Analytical Formulation from Literature

Adhesive bonding stress evaluation along the overlap of a single lap joint configuration can be assessed in two ways: *analytically*, exploiting classical mathematical models (e.g. Volkersen, Goland-Reissner) and *numerically*, exploiting FEA through commercial softwares (e.g. Hypermesh, Abaqus).

Both methodologies have their own advantages and disadvantages but the right trade off in accuracy of the results and computational cost must be found. In this research, both approaches have been chosen, exploiting the classical formulations by Volkersen, Goland-Reissner, Hart-Smith and Adams such to evaluate the influence of the key design variables on the overlap trend and failure load. Therefore, experimental and numerical studies have been conducted in the next chapters.

In general, the stress analysis in the thin adhesive layer is rather complex because of their three-dimensional development: indeed there is no predominant stress above the others (peel, shear) but they are all strictly related and comparable to each other. The approach followed in the study is such to consider the simplest and the most applicable theories: using very complicated 3D elastic-plastic analytical models is not advisable, in complex problems it is better to exploit FEM softwares. The possibility of having direct results by varying the parameters influencing the mechanical behavior of the joint allows the possibility of the parametric study, evaluating the influence of both geometric

(adherend and adhesive thickness and overlap length) and both mechanic (external load and material) properties. Each studied analytical model comes along with some assumptions: in order to have a better understanding of the applicability range of the models, in Table 2.1 the respective assumptions have been reported.

Table 2.1 Analytical Models Range of Applicability

		<b>Simplified Stress Model</b>	<b>Volkersen</b>	<b>Goland and Reissner</b>	<b>Hart-Smith</b>
	<i>Adhesive</i>	Linear	Linear	Linear	Linear and Non Linear
	<i>Adherend</i>	Linear	Linear	Linear	Linear
<b>Adherend</b>	<i>Isotropic</i>	X	X	X	X
	<i>Similar</i>	X	X	X	X
	<i>Dissimilar Thickness</i>	X	X		
<b>Adhesive Stress</b>	$\sigma_x$				
	$\sigma_y$			X	X
	$\tau_{xy}$	X	X	X	X
<b>Solution</b>	<i>Closed - form</i>	X	X	X	X

The main analyzed geometry is represented in Fig. 2.1, the well-known single lap joint configuration obtained by simple superposition of the substrates. It is important to highlight that, because of the eccentricity of the loading, a bending moment will be induced into the structure contributing to its deformation.

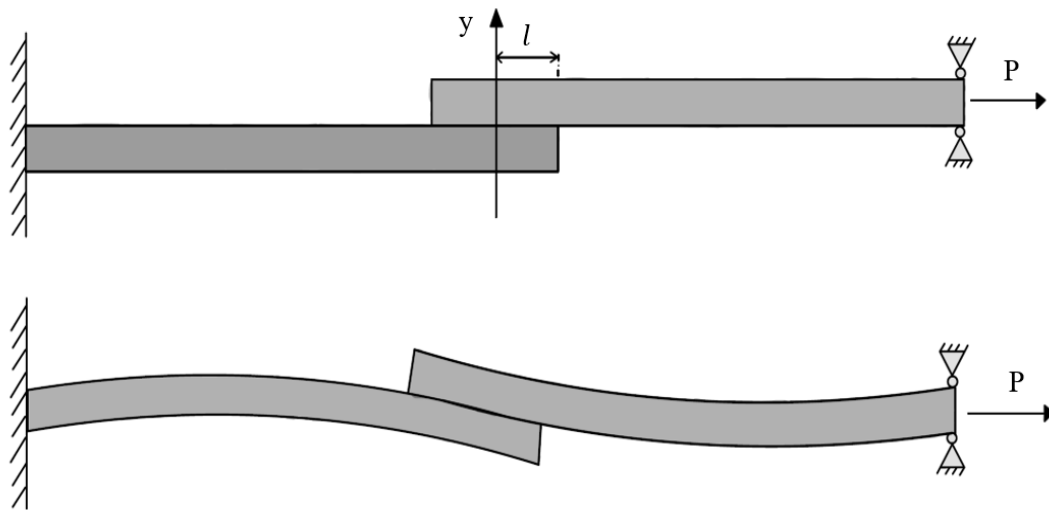


Figure 2.1 Single Lap Joint Deformation

The state of stress of a bonded joint, indeed, is very similar to a *welded joint* since it is distributed on extensive areas but with some differences such as the reduced possibility of plastic redistribution of the stresses since some structural adhesives may be rather fragile (i.e. acrylics or epoxies). Additionally peak stresses at the end of the overlaps are present in the bonded joints and the field of stresses due to the geometries and discontinuities of the material is rather different than the one that can be appreciated in welded joints.

### 2.1.1 Generalized Adhesive Yielding Criterion

The simplest approach is to assume that the substrates are effectively rigid. This means that as the load passes from substrate to substrate a *uniform* shear stress distribution is generated, as shown in Fig. 2.2.

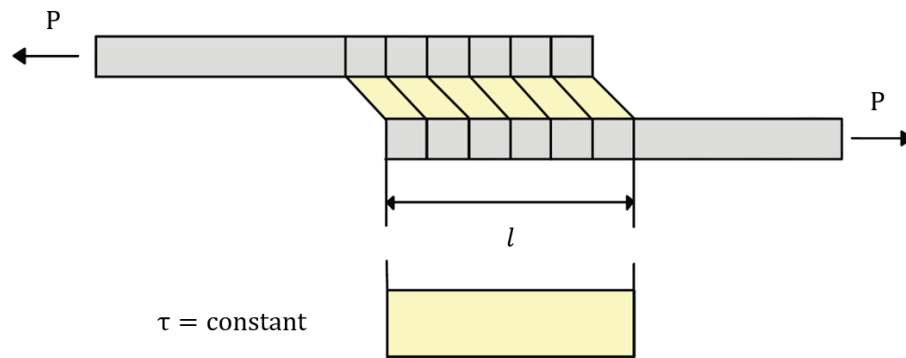


Figure 2.2 Simplified Shear Stress Model

In this simplified stress model, the *cells* corresponding to the adherends do not change and the relative displacements of the adherends causes a deformation by shear strain in the adhesive cells. Therefore, the adhesive shear stress  $\tau_{xy}$  is constant along the overlap length  $l$ , thus, given as external load  $P$  and joint width  $b$

$$\tau = \frac{P}{bl} \quad (1)$$

This model is as simple as inaccurate: it is not able to catch the shear stress increase at the end of the overlaps, but it is still a good reference as it represents the average shear stress acting on the adhesive layer (especially for very ductile adhesives).

### 2.1.2 Volkersen Model [21]

The approach described in paragraph 2.1.1 is over-simplified, since the adhesive potential could not be fully exploited; its performances might be underestimated by the wrong approximation provided by the generalized adhesive yielding criterion: in other words, variation of the values of allowable mean stress of one order could lead to overestimated safety coefficients ( $10 \div 20$ ). This would contribute to uncertainty and mistrust in the use of the adhesives, hence, more refined assumptions should be considered, like the differential shear model which assumes that, applying a load, also the adherends deform longitudinally.

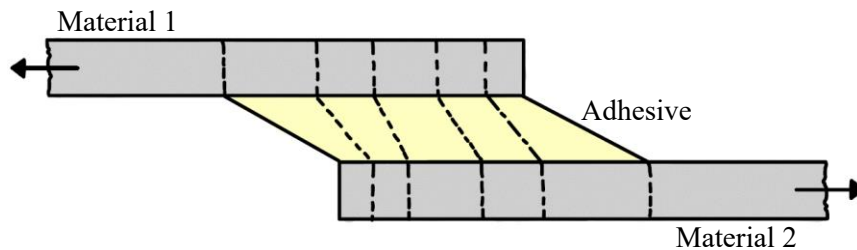


Figure 2.3 Differential Shear Model

The elongation of the cells in each adherend increases as the material gets closer to the external applied load: in this way the relative displacement of the adherends lead to a greater slippage in the adhesive at the extremes with a non-uniform tangent stress  $\tau$ .

This simple reasoning covers the fundamental aspects of the concept of *differential shear* that is caught with more details by Volkersen analytical theory.

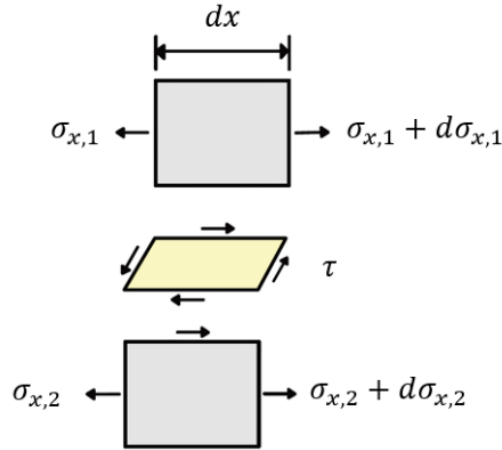


Figure 2.4 Local Equilibrium of Single Lap Joint Elements

It was assumed that the adhesive deforms only in shear and the adherends only in tension remaining in the elastic region. As qualitatively explained in Fig. 2.3, the strain must progressively reduce from the loaded zone to the free edge. The reduction of the strain in the adherends along the overlap and the continuity of the adhesive interface cause a non-uniform shear strain (and stress) distribution in the adhesive layer. The tangential stress is maximum at the ends of the overlap and is much lower in the middle. Analytically, balancing the upper and lower adherend

$$\sigma_1 b t_1 + \tau b dx = (\sigma_1 + d\sigma_1) b t_1 \quad (2.a)$$

$$\sigma_2 b t_2 = \tau b dx + (\sigma_2 + d\sigma_2) b t_2 \quad (2.b)$$

Considering also joint equilibrium and shear deformation in the adhesive

$$P = \sigma_1 b t_1 + \sigma_2 b t_2 \quad (3.a)$$

$$\gamma = \frac{\tau}{G_a} = \frac{1}{t_a} (u_1 - u_2) \quad (3.b)$$

Combining these results, the differential equation solved by Volkersen is

$$\frac{d^2\sigma_2(x)}{dx^2} - \frac{G_a}{t_a} \left( \frac{1}{E_1 t_1} + \frac{1}{E_2 t_2} \right) \sigma_2(x) + \frac{P}{t_a b E_2 t_2 t_1} G_a = 0 \quad (4)$$

From equation (4), the closed formula for tangential stress  $\tau$

$$\tau = \frac{P}{bl} \frac{w}{2} \frac{\cosh(wX)}{\sinh\left(\frac{w}{2}\right)} + \left( \frac{t_1 - t_2}{t_1 + t_2} \right) \frac{w}{2} \frac{\sinh(wX)}{\cosh\left(\frac{w}{2}\right)} \quad (5)$$

with  $X=x/l$  where  $-0.5 \leq X \leq 0.5$ , with

$$w = \sqrt{\frac{G_a l^2}{E t_1 t_a} \left( 1 + \frac{t_1}{t_2} \right)} \quad (6)$$

where  $t_1$  is the top adherend thickness,  $t_2$  the bottom adherend thickness,  $E$  the adherend modulus,  $G_a$  the adhesive shear modulus,  $t_a$  the adhesive thickness. The origin of the reference system has been positioned in the middle of the overlap. Volkersen theory, although it considers the possibility of having different adherent thicknesses, does not account for the bending effect caused by the eccentric load path of single lap joint. Thus, it better represents Double Lap Joint (DLJ) since the bending effect is less prominent.

### 2.1.3 Goland-Reissner Model [22]

To take into account the eccentric load path of a SLJ a bending moment ( $M$ ) and a transverse force ( $V$ ) are induced in the joint ends along with the applied tensile load per unit width ( $\bar{P}$ ). In Fig. 2.5, it is qualitatively shown the rotation of the joint due to the bending moment, varying the direction of the load line: the applied tensile force will tend to realign the joint. As this latter rotates, the bending moment will decrease, giving rise to a nonlinear geometric problem where the large deflections of the adherends must be accounted for: this is the main idea developed by Goland and Reissner.

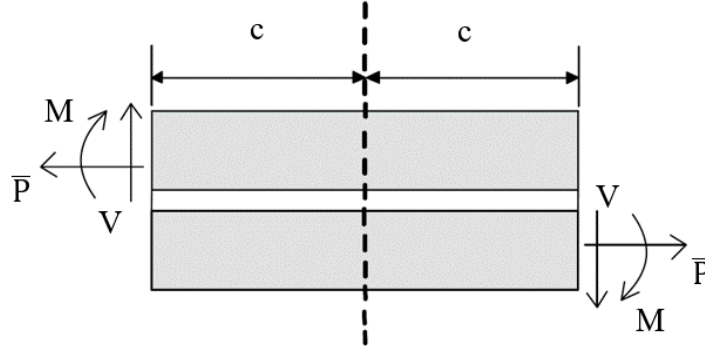


Figure 2.5 Goland-Reissner Model [22]

A bending moment factor  $k$  (7.a) and a transverse force factor  $k'$  (7.b) are introduced.

$$M = \frac{k\bar{P}t}{2} \quad (7.a)$$

$$V = \frac{k'\bar{P}t}{2} \quad (7.b)$$

where  $t$  is the adherend thickness (indeed in this model  $t_1 = t_2$ ) and  $c$  is the half of the overlap length. For very small rotations of the joint  $k$  and  $k'$  will tend to 1, as soon as it rotates more they tend to decrease, hence the bending moment and transverse load will also decrease. Goland-Reissner expression for the bending moment factor is defined.

$$k_{GR} = \frac{\cosh(u_2c)}{\cosh(u_2c) + 2\sqrt{2}\sinh(u_2c)} \quad (8)$$

defining, given  $\nu$  as the Poisson's ratio:

$$u_2 = \frac{1}{t} \sqrt{\frac{3P(1-\nu^2)}{2tE}} \quad (9)$$

Instead of solving a nonlinear geometric problem, a linear problem has been solved by considering the loads applied in the ends: in this way they avoided a more complex

problem with the consideration of the geometric nonlinearity effect.

Two limit cases were considered in order to evaluate adhesive stresses: in the first, the adhesive layer is assumed relatively not flexible and the overlap is considered as a single deformed body with adherend properties, whereas, in the second, the adhesive is assumed relatively flexible and the joint flexibility is mainly due to the adhesive presence. The first case is more suited for wood joints whereas the second is proper for metals. In the second case, the adherends' deformation was due only to the longitudinal normal stress  $\sigma_x$ : adherends bending leads to a transverse normal stress through the thickness direction in the adhesive layer (the also known as peel stress).

For this reason, the adhesive layer was modelled as an infinite number of shear and tension/compression springs through the thickness direction, giving rise to shear and transverse stresses in the adhesive layer, neglecting the longitudinal direct stress. Since the adhesive layer thickness was considered to be negligible compared to the adherend thickness, the stress in the adhesive was assumed to be constant through the thickness: this case is very common in metallic joints. These assumptions reduce the range of applicability of this model in the following requirements

$$\frac{tG_a}{t_a G} < 0.1 \quad (10.a)$$

$$\frac{tE_a}{t_a E} < 0.1 \quad (10.b)$$

where  $G$  is the adherend shear modulus,  $G_a$  the adhesive shear modulus and  $E_a$  the adhesive Young's Modulus. These requirements can be summarized in the assumption that the adherends shear and transverse deformations are negligible with respect to the ones in the adhesive layer. The closed formulation for tangential stress proposed by

Goland and Reissner is reported in equation 11, given k by equation 8

$$\tau(x) = -\frac{\bar{P}}{8c} \left( \frac{\beta c(1+3k) \cosh\left(\frac{\beta x}{t}\right)}{t \sinh\left(\frac{\beta c}{t}\right)} + 3(1-k) \right) \quad (11)$$

where

$$\beta = \sqrt{\frac{8G_a t}{Et_a}} \quad (12)$$

In addition to what proposed by Volkersen, they considered also the presence of peel stress induced by the bending moment M

$$\begin{aligned} \sigma(x) = \frac{\bar{P}t}{\Delta c^2} & \left[ \left( R_2 \lambda^2 \frac{k}{2} + \lambda k' \cosh(\lambda) \cos(\lambda) \right) \cosh\left(\frac{\lambda x}{c}\right) \cos\left(\frac{\lambda x}{c}\right) \right. \\ & \left. + \left( R_1 \lambda^2 \frac{k}{2} + \lambda k' \sinh(\lambda) \sin(\lambda) \right) \sinh\left(\frac{\lambda x}{c}\right) \sin\left(\frac{\lambda x}{c}\right) \right] \end{aligned} \quad (13)$$

where the required variables are given by

$$\psi = \sqrt[4]{\frac{6E_a t}{Et_a}} \quad (14.a)$$

$$\lambda = \frac{\psi c}{t} \quad (14.b)$$

$$k' = \frac{kc}{t} \sqrt{\frac{3(1-\nu^2)P}{tE}} \quad (14.c)$$

$$R_1 = \cosh(\lambda) \sin(\lambda) + \sinh(\lambda) \cos(\lambda) \quad (14.d)$$

$$R_2 = \sin(\lambda) \cos(\lambda) - \cosh(\lambda) \sinh(\lambda) \quad (14.e)$$

$$\Delta = \frac{1}{2}(\sin(2\lambda) + \sinh(2\lambda)) \quad (14.f)$$

#### 2.1.4 Hart-Smith Approach [24]

Hart-Smith approach is one of the first models to implement adhesive plasticity for single and double lap joints, creating an elastic-plastic  $\tau$  stress model with the *maximum shear* strain as the failure criterion. In order to characterize the adhesive behavior, the elastic-plastic model is such that the ultimate shear stresses and strains in the model are equal to the ultimate shear stresses and strains of the adhesive, defined by the same strain energy. Their model allows plasticity (failure strain) of the adhesive within the ends of the overlap, whereas in the middle the adhesive is remain elastic.

This refined numerical-analytical model is required only if there is yielding of the adhesive/adherends and substantial peeling load is present (especially in SLJ), but still the more complete is the analysis, the more complicated gets the model and in this case FEA is advised for more precise and effective calculations. Analytical models, indeed, are never fully representative of real life mechanical behavior of the joint, thus, they must be considered just as a preliminary guidance for the design of the adhesively bonded joints. For this reason, in this research, the full analytical model of Hart-Smith has only been partly considered: the bending moment factor equation has been inserted in the Adams [23] design methodology to predict failure load in single lap joints more effectively.

$$k_{HS} = \left(1 + \frac{t_a}{t}\right) \frac{1}{1 + \xi c + \frac{(\xi c)^2}{6}} \quad (15)$$

### 2.1.5 Design Methodology

A simple design methodology was proposed by Adams [23] based on adherend and adhesive yielding limit. When choosing dimensions for specimens or for quick design of the joint, a universal criterion is not defined yet, but the powerful methodology illustrated is effective for first rough design choices. Considering uniform the yield in the *adhesive* corresponding to total plastic deformation, a failure load  $P_a$  can be identified

$$P_a = \tau_y bl \quad (16)$$

The stress acting in the *adherend* is the sum of the direct tensile stress (when applied load P) and the bending stress (due to joint rotation), hence the failure load relative the adherend yield  $P_s$  will be

$$P_s = \frac{\sigma_y bt}{1 + 3k} \quad (17)$$

This equation has been therefore (over) simplified by Adams, stating that for low loads and short overlaps k tends to 1, and oppositely it tends to zero

$$P_s = \frac{\sigma_y bt}{4} \quad \frac{l}{t} < 20 \quad (18.a)$$

$$P_s = \sigma_y bt \quad \frac{l}{t} \geq 20 \quad (18.b)$$

From Fig 2.6 the design methodology is illustrated (in blue, the adhesive global yielding and in red the adherend yielding), but this model is not very robust in case of brittle adhesives and non-yielding adherends, for this reason a more refined model should be considered: bending moment factors provided by other analytical theories allow to have a continuous dependency on variables like the overlap length and adherend thickness.

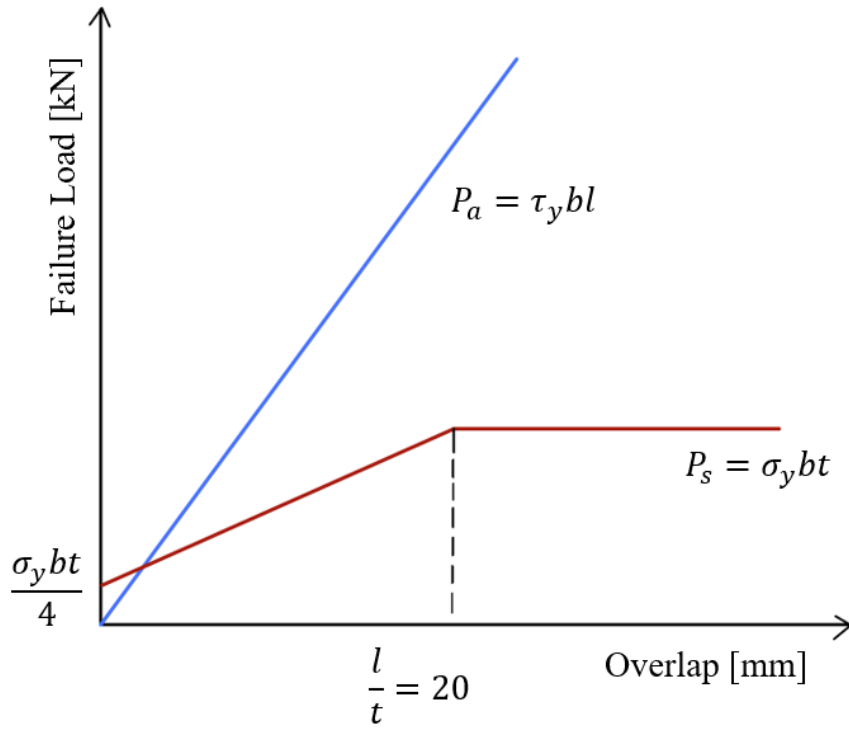


Figure 2.6 Adams Design Methodology

Table 2.2 Equations for Bending Moment Factors

Analytical Model	Bending Moment Factors
<i>Goland and Reissner [22]</i>	$k_{GR} = \frac{\cosh(u_2 c)}{\cosh(u_2 c) + 2\sqrt{2}\sinh(u_2 c)}$
<i>Hart-Smith [24]</i>	$k_{HS} = \left(1 + \frac{t_a}{t}\right) \frac{1}{1 + \xi c + \frac{(\xi c)^2}{6}}$
<i>Zhao et al. [12]</i>	$k_{ZH} = \frac{1}{1 + \xi c}$

Indeed considering equation 17, and taking into account the different models proposed (Goland-Reissner and Hart-Smith), it can be utilized by considering the bending moment factor for each theory (Table 2.2).

Mixing the classical models with the basic idea of Adams et al. design methodology it is possible to obtain a more *reliable* design tool software for the final failure load, allowing the first design choices concerning SLJs when numerical or experimental testing are not possible yet.

## 2.2 Classical Analytical Models Effect on Key Design Variables

The generalized adhesive yielding criterion, Volkersen and Goland-Reissner equations have been implemented in MATLAB environment in order to obtain the 3D stress trend along the overlap by varying one parameter (positioning the origin of the reference system in the center of the overlap) and fixing all the other variables. In the second part of the script, a design methodology is proposed exploiting the Adams [23] failure criterion and implementing the bending moment factor formulations by Goland-Reissner, Hart-Smith and the simplified and improved one by Zhao et al. [12]

### 2.2.1 Effect of Adhesive Material

The main role of the adhesive in the bonded joint is to transfer the load from one adherend to the other: engineers have to design the joint such that this load transfer occurs mainly through shear stress avoiding peel or cleavage loadings which could reduce joint strength. For this reason, the shear resistance and deformability are the most important mechanical properties to define a structural adhesive behavior.

The main classification among structural adhesives is between *brittle* structural adhesives, which are characterized by high resistance and stiffness to shear, but limited

deformability (one or two part epoxies) and *ductile* structural adhesives, which are characterized by lower resistance and stiffness to shear, but enhanced deformability (polyurethanes). The choice of the type of adhesive will have relevant influence on adhesive bonded stress along the overlap and to the kind of failure mode: the ductility of the adhesive, indeed plays an important role on the reduction of shear and normal stress peaks. The different performances of these two kinds of adhesive on the single lap joint adhesive stress can be compared considering the parameters shown in Table 2.3.

#### 2.2.1.1 Polyurethane-Based Adhesive Joint

Polyurethane (PU), as already mentioned, is a very ductile adhesive which will deform considerably before failing. The generalized adhesive yielding criterion (constant model) usually has excellent results for this kind of adhesives especially when joining very stiff adherends. The polyurethane properties utilized for this evaluation are summarized in Table 2.4.

In Figure 2.7, the peel stress in a polyurethane-aluminum joint is shown and it is present for the only model which considered also the bending load due to the eccentricity of the single lap joint geometry (i.e. Goland-Reissner). In Figure 2.8, instead, the shear stress trend is presented: in this case, three models are proposed (i.e. Simplified Stress Model, Volkersen and Goland-Reissner). All the analytical models are clearly symmetrical and go from the constant modelling to the *parabolic* trend of the Volkersen and Goland-Reissner formulation. This latter analytical theory shows higher peaks in the end of the overlaps with respect to the other two models, making this model the most conservative among the three.

Analyzing the trends it can be appreciated that in shear stress, the variation among the

constant and Goland-Reissner modelling is not negligible in the end of the overlaps with an increase of more than 10%. In the middle of the overlaps, instead, the simplified stress model provides a remarkable overestimation of the stresses with respect to the other model with an increase of more than 7%. Nevertheless, Volkersen stresses for this *ductile* configuration, are very close to the simplified model.

Table 2.3 Single Lap Joint Fixed Parameters for Analytical Analysis

<b>Parameters for Analytical Analysis</b>	
Overlap Length L [mm]	25.4
Joint Width b [mm]	25.4
Adhesive Thickness $t_{adh}$ [mm]	2.0
Adherend Young Modulus E [MPa]	70,000
Adhesive Shear Modulus $G_{adh}$ [MPa]	570
External Load P [N]	5,000

Table 2.4 Polyurethane Material Properties

<b>Polyurethane</b>	
Adhesive Shear Strength $\tau_{max}$ [MPa]	5
Adhesive Young Modulus E [MPa]	600
Adhesive Shear Modulus G [MPa]	230

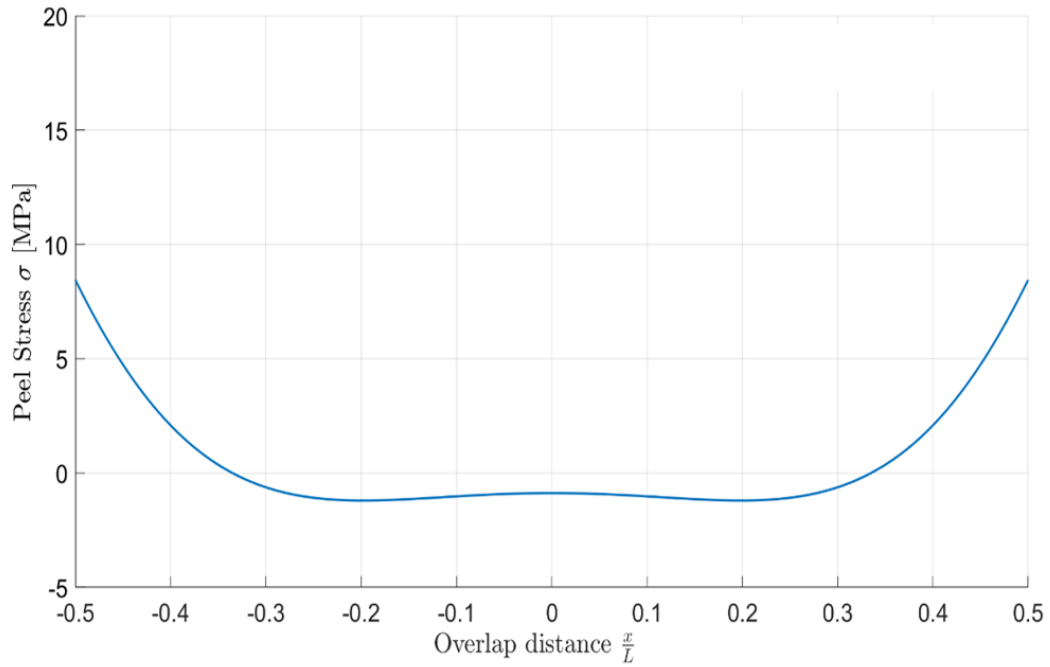


Figure 2.7 Polyurethane Joint Peel Stress predicted by Goland-Reissner Model [22]

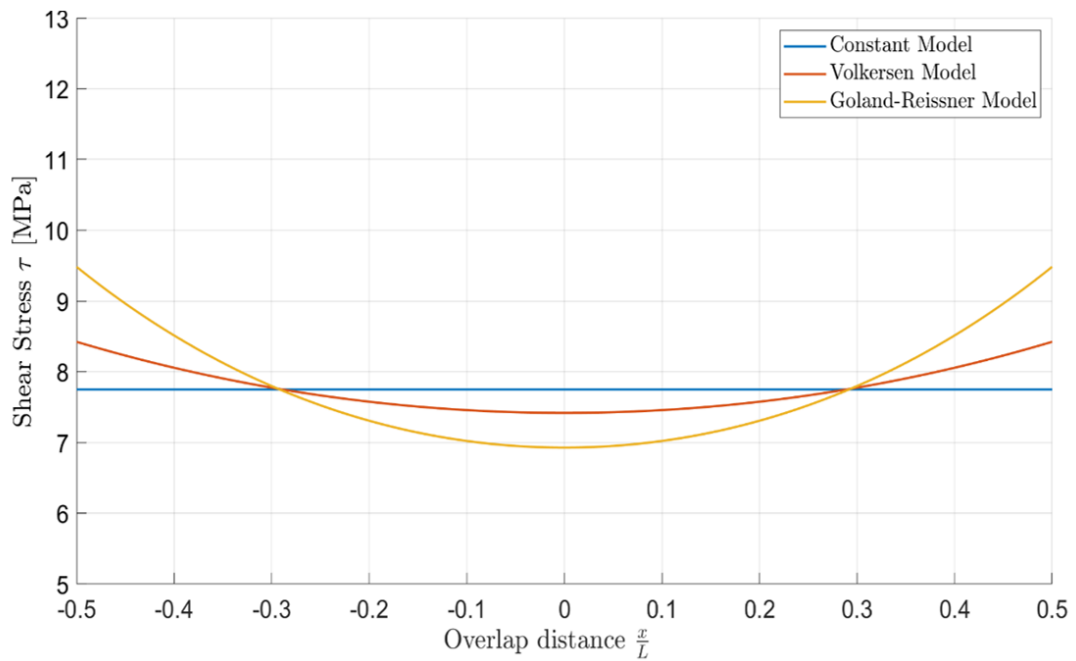


Figure 2.8 Polyurethane Joint Shear Stress predicted by Volkersen [21] and Goland-Reissner [22] Models

All the presented analytical models, though, have some limitations because they do not account for variations of the adhesive stresses through the thickness direction (interface stresses) and they ignore the stress free condition overestimating the stress at the ends of the overlap providing conservative failure load predictions.

This is why, in this research, different approaches to evaluate the adhesively bonded joints' mechanical behavior (SLJs and real joint) have been used: analytical models may just provide a starting general guidance, but they must always be compared with numerical and/or experimental tests.

#### 2.2.1.2 Epoxy-Based Joint

Epoxy-based adhesives, instead, are very brittle: thus, they will not deform considerably before failing and will have much higher stiffness. The epoxy properties utilized for this evaluation are summarized in Table 2.5.

Table 2.5 Epoxy Material Properties

<b>Epoxy</b>	
Adhesive Shear Strength $\tau_{max}$ [MPa]	18
Adhesive Young Modulus E [MPa]	1700
Adhesive Shear Modulus G [MPa]	660

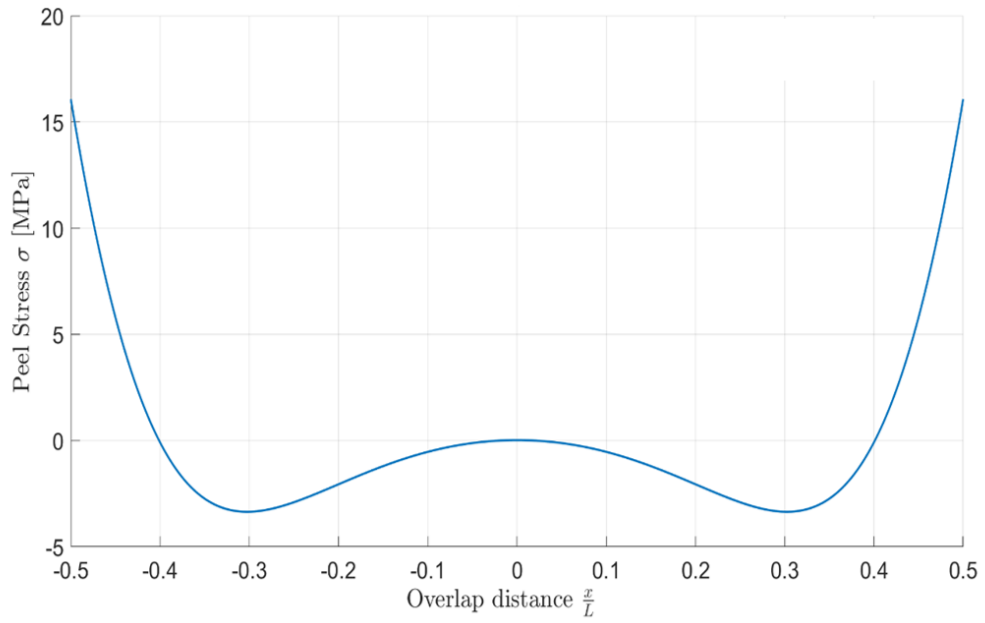


Figure 2.9 Epoxy Joint Peel Stress predicted by Goland-Reissner Analytical Model [22]

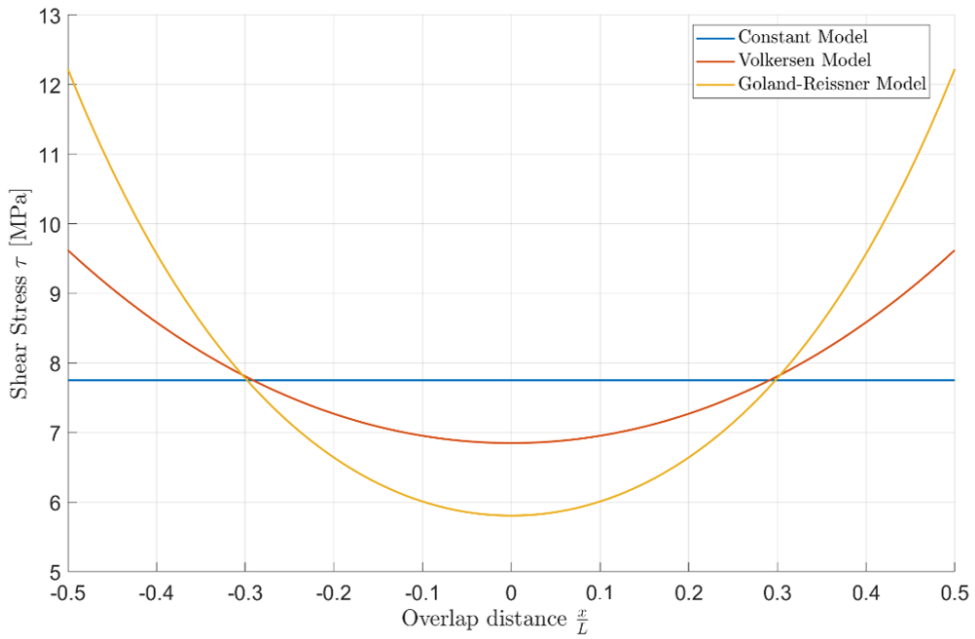


Figure 2.10 Epoxy Joint Shear Stress predicted by Volkersen [21] and Goland-Reissner [22] Analytical Models

In Figures 2.9 and 2.10, respectively, the peel stress and the shear stress induced on the epoxy-aluminum single lap joint are reported. With respect to the PU, the peak stresses at the end of the overlaps, both in shear and peel, are much higher due to the different nature of the adhesive. Indeed, epoxy is much stiffer and can transfer higher loads to the adherends before failing; also the induced peel stress is almost double with respect to the PU joint: the peel stress distribution in the PU configuration is much flatter, whereas in the epoxy reaches exactly zero in the middle and higher values in the edges.

### 2.2.2 Effect of Adherend Thickness

When designing experiments, the proper adherend thickness must be chosen to reduce as much as possible the effect of yielding in the adherend which would lead to wrong characterization of the adhesive. Fixing the other parameters, and varying the adherend thickness between 1 and 10 mm, the effect of each key design variable can be assessed: first the 2D variations of the stresses are evaluated, then the models are implemented to obtain 3D plots to observe directly the wave form of stresses along the overlap length of the aluminum single lap joint considered in the analysis.

From Figure 2.11, it is evident that the shear stress in the adhesive, as expected, is not affected at all by the variations of the adherend thickness since it does not influence the adhesive quantity along the overlap area: also the waveform of the shear stress remains unchanged. For what concerns the peel, instead in Figure 2.12, it is interesting to highlight how for low values of adherend thickness, the peel stress has a non-linear behavior due to the increased eccentricity of the load (larger bending for the specimens) before stabilizing when larger thicknesses are involved.

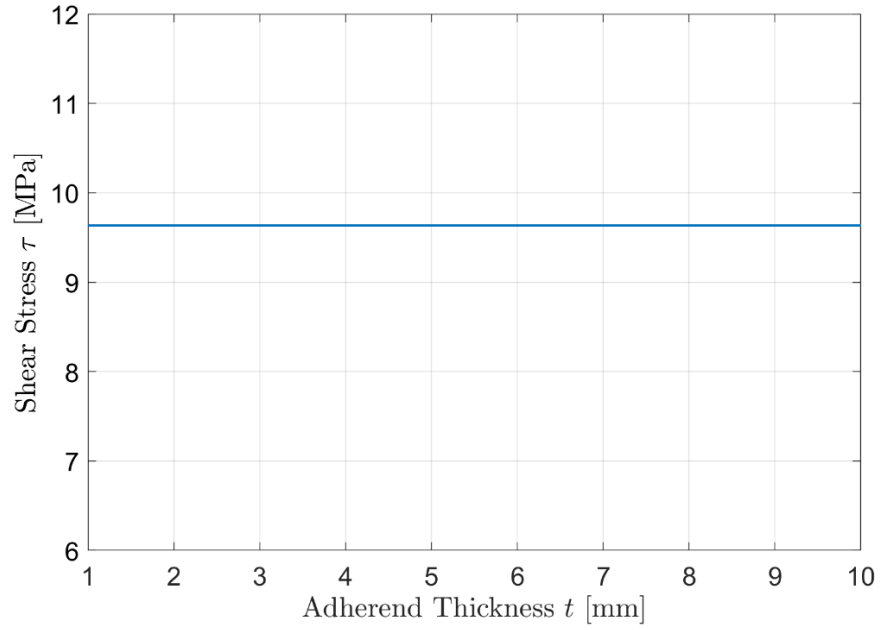


Figure 2.11 Effect of Adherend Thickness on Maximum Shear Stress

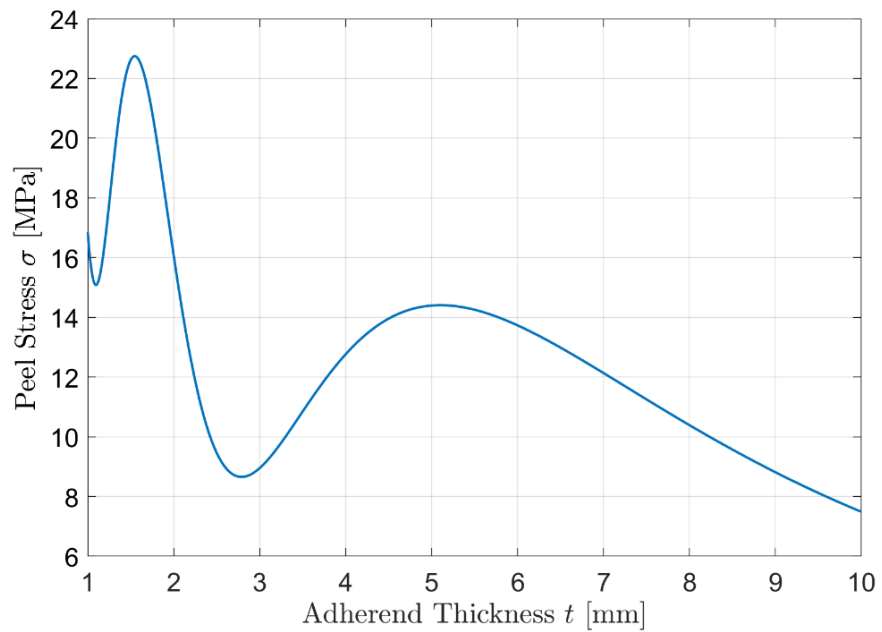


Figure 2.12 Effect of Adherend Thickness on Maximum Peel Stress

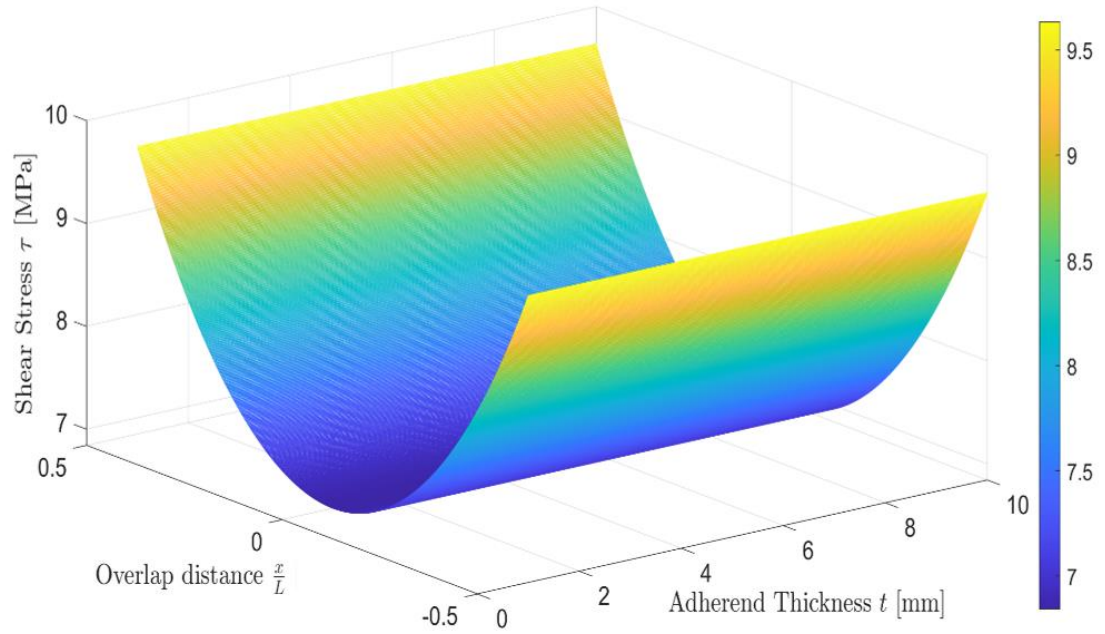


Figure 2.13 3D Effect of Adherend Thickness on Shear Stress

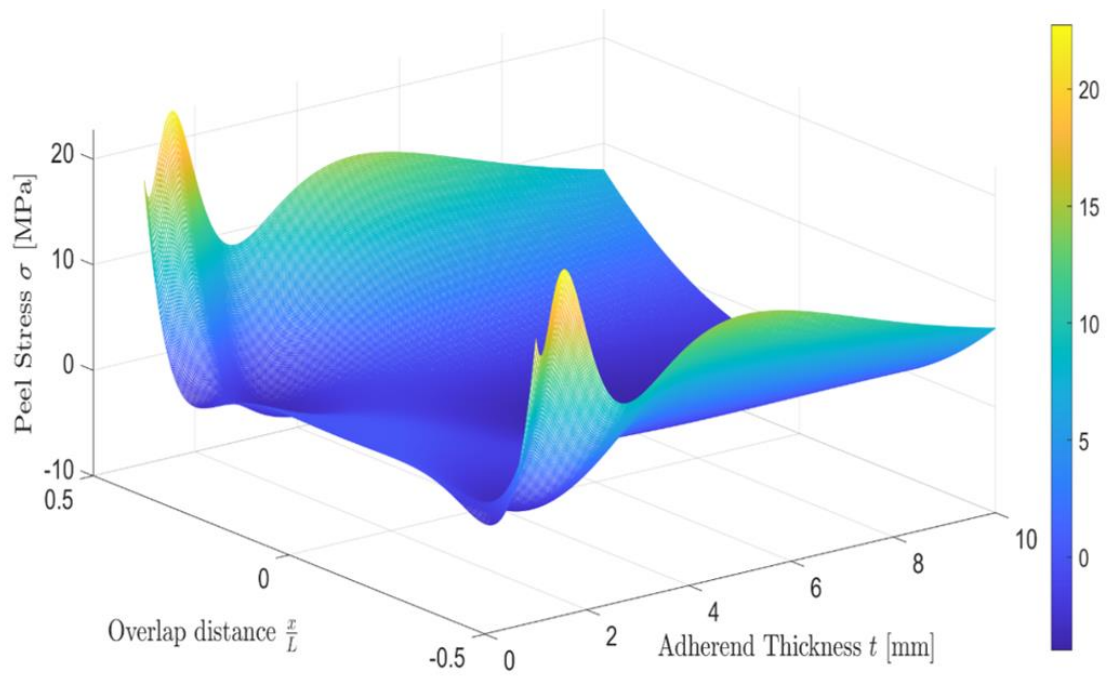


Figure 2.14 3D Effect of Adherend Thickness on Peel Stress

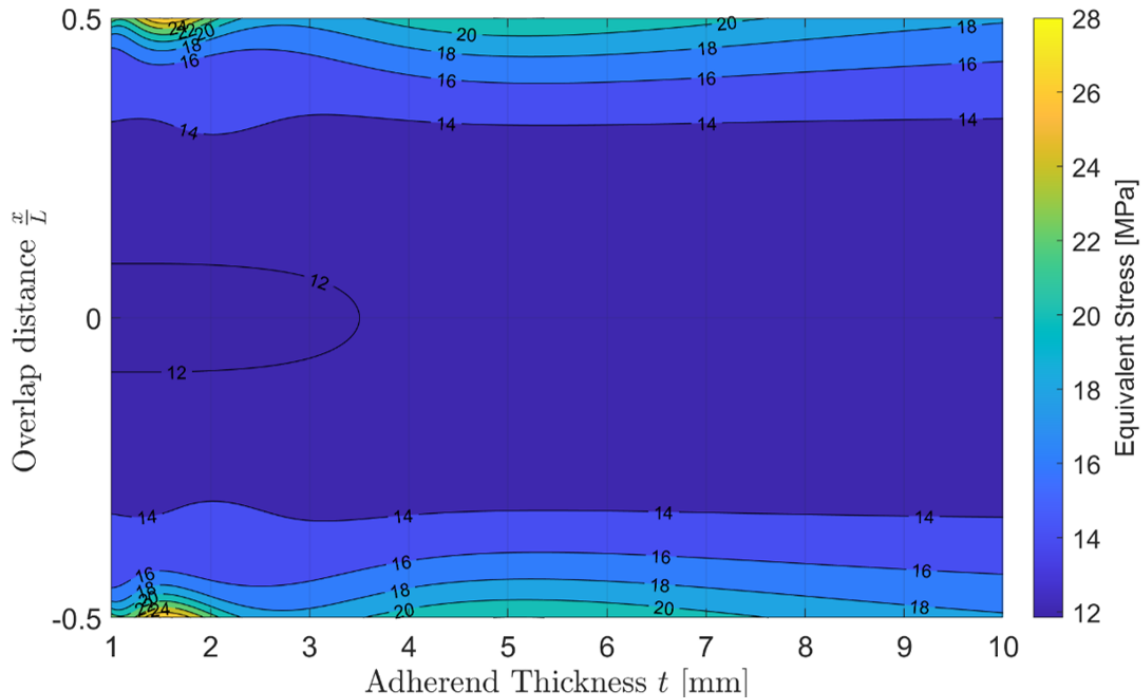


Figure 2.15 Effect of Adherend Thickness on Equivalent von Mises Stress

Combined effects of peel and shear stress can be observed in Figure 2.15 with the equivalent von Mises stress. Since the adherend thickness is not affecting the shear stress at all, the change in equivalent stress is due only to the variations in the peel stress, which is remarkable when low adherend thicknesses for the SLJs are considered.

### 2.2.3 Effect of Joint Width

The joint width is a relevant variable of the single lap joint configuration previously described. Its influence is often not considered remarkable for the mechanical behavior of SLJs, but in reality, it affects considerably the performances of the adhesive: if the other design variables are fixed and the joint width is varying from half inch to two inches, it is possible to appreciate how the stress trends along the overlap differ from one

configuration to the other. Indeed, in Figure 2.18 it is noticeable how the shear stress varies as the joint width increases: for low values of  $b$ , the difference between the edges and the middle is very significant, for higher values of the width, instead the stress trend flattens and the generalized adhesive yielding criterion becomes a better approximation of the reality. In Figure 2.19, the peel stress behavior is very similar to the shear stress pattern: with the increase of the joint width the stress trend tends to flatten and to lower since a wider portion of the adhesive is present, “redistributing”, therefore, transversally the stress in all the bonding area.

Also in this case, it is possible to observe the combination of the variation of shear and peel stress in the adhesive: both the shear and peel stress are decreasing as the joint width increases. For this reason, the effect on the equivalent von Mises stress is much more noticeable since the highest stresses are for lower joint width at the overlap ends.

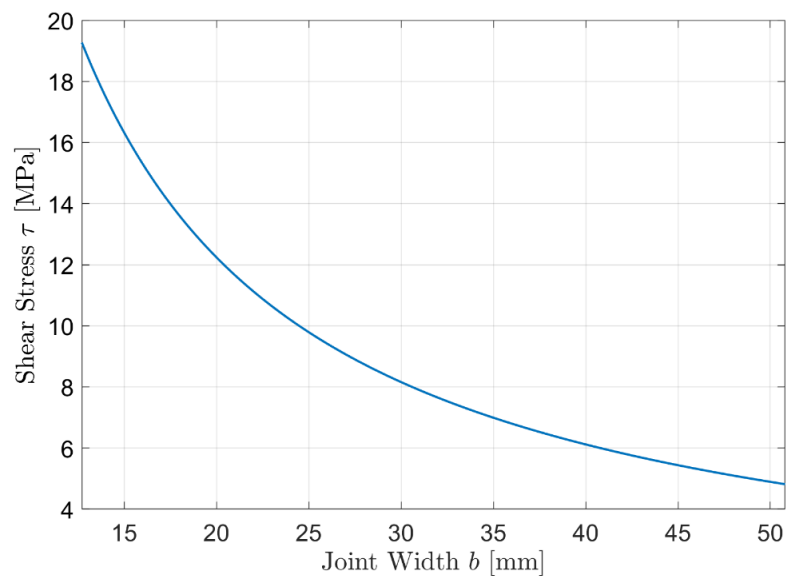


Figure 2.16 Effect of Joint Width on Maximum Shear Stress

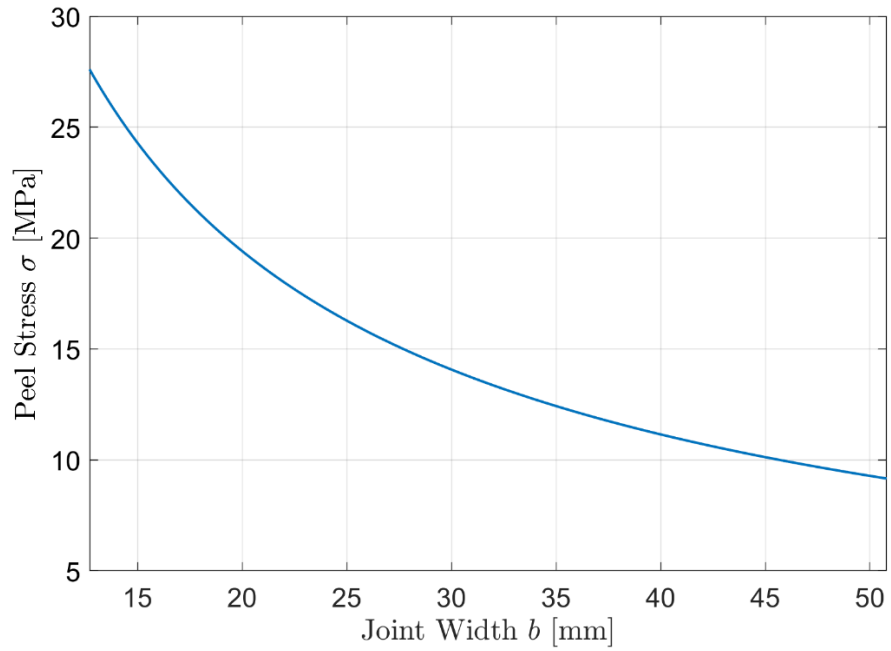


Figure 2.17 Effect of Joint Width on Maximum Peel Stress

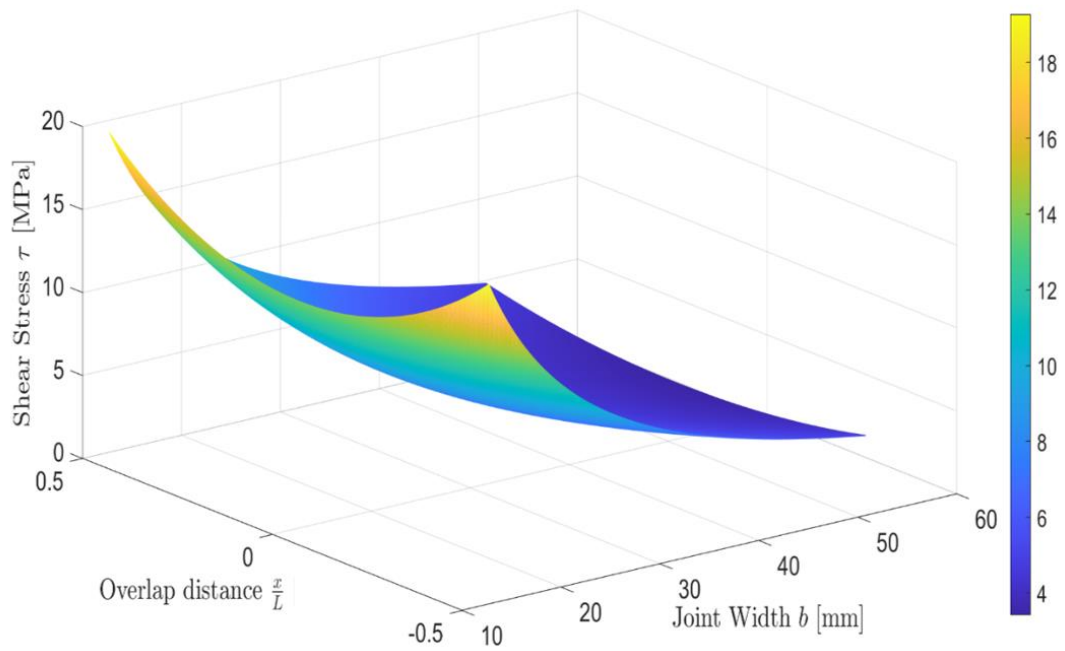


Figure 2.18 3D Effect of Joint Width on Shear Stress

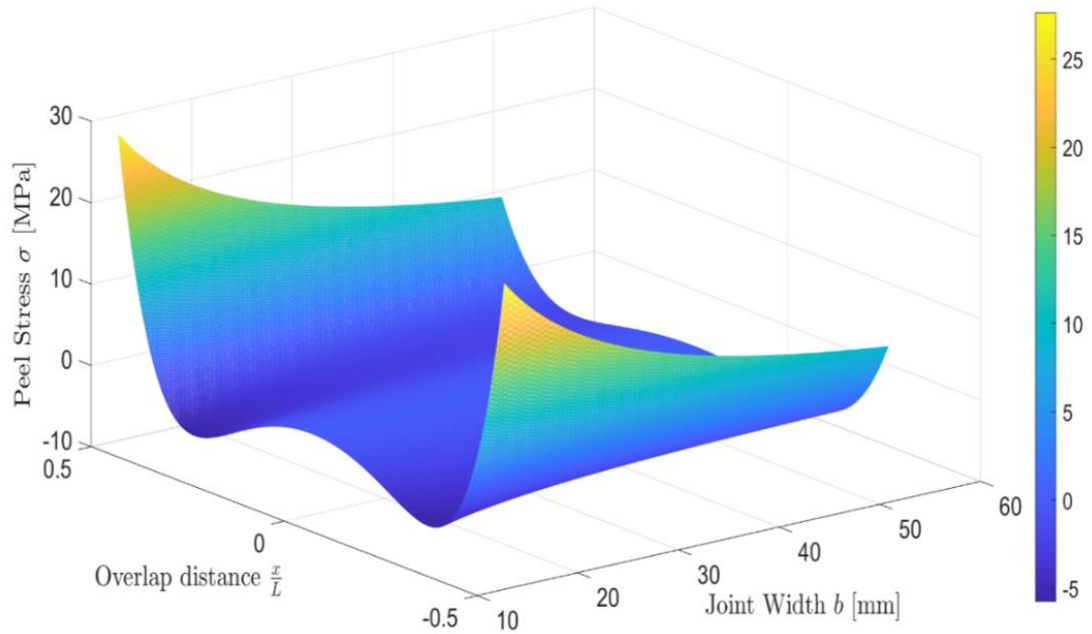


Figure 2.19 3D Effect of Joint Width on Peel Stress

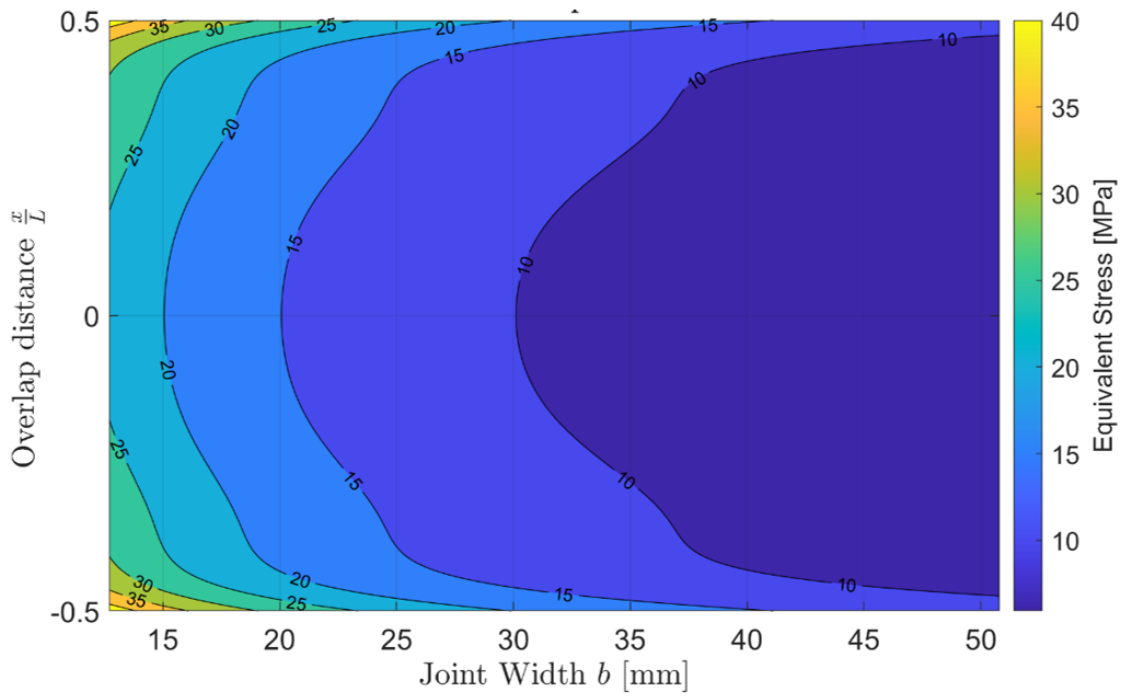


Figure 2.20 Effect of Joint Width on Equivalent von Mises Stress

#### 2.2.4 Effect of Adhesive Thickness

The adhesive thickness is an essential variable for SLJs: its influence on the stress trends, nevertheless, is often misleading since the analytical models are not able to account for through-thickness variation of stresses. This is why numerical models are considered in this study to compare the results. Fixing the other variables and making the adhesive thickness vary between 0.1 and 3 mm, the analytical trend observable in Fig. 2.21 and 2.22 is clear: increasing the adhesive thickness, the stress in the bonded joint is reduced. This might not be always verified, hence, experimental tests or reliable virtual FEA models are required. An interesting observation is that for a thickness value among 0.1 and 0.5 mm the peel stress has a local minimum: this is compatible with the practical *optimal* value of adhesive thickness for structural adhesives which is set to 0.2 mm.

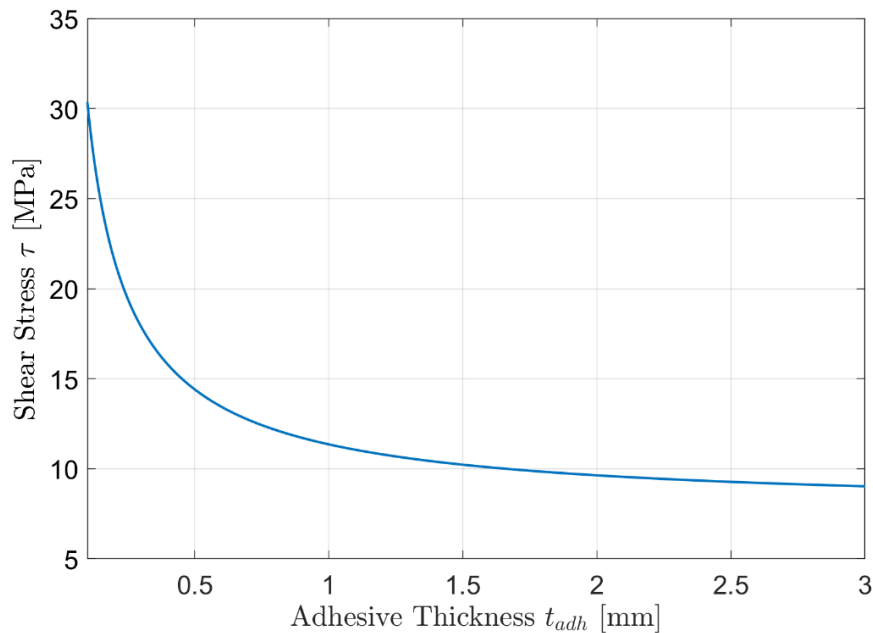


Figure 2.21 Effect of Adhesive Thickness on Maximum Shear Stress

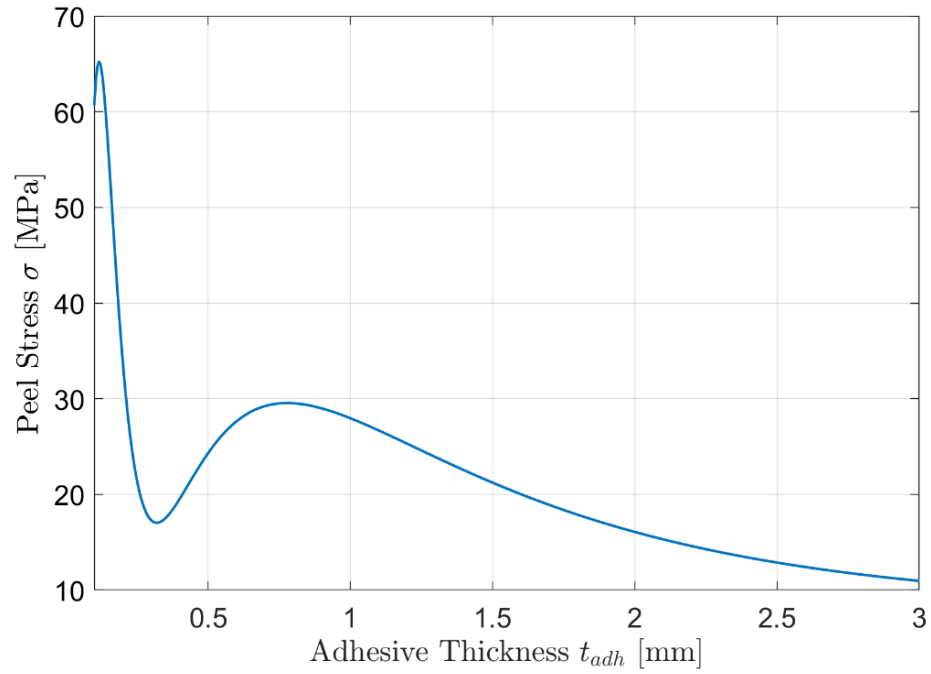


Figure 2.22 Effect of Adhesive Thickness on Maximum Peel Stress

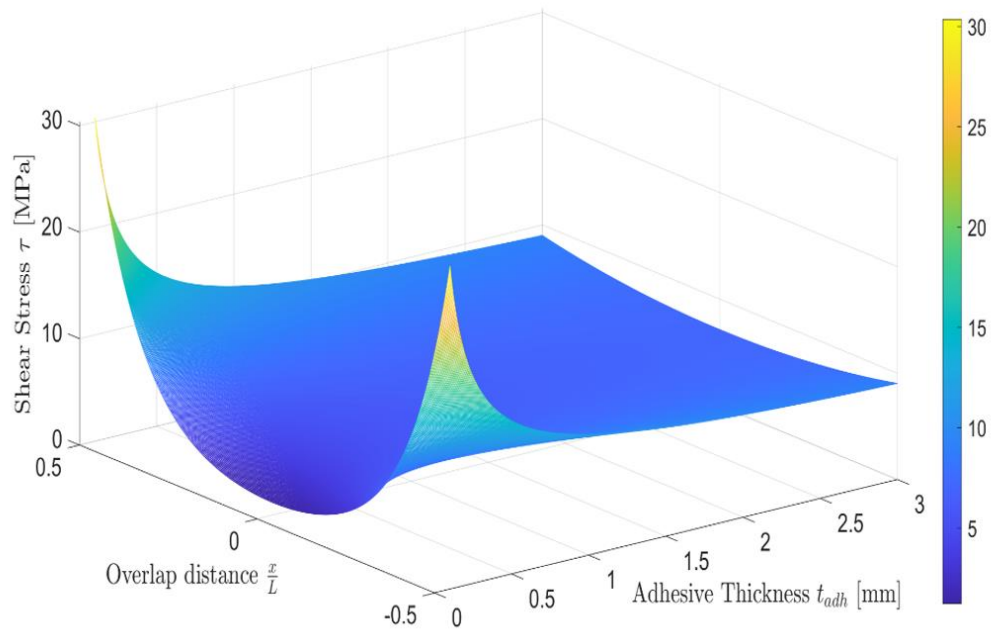


Figure 2.23 3D Effect of Adhesive Thickness on Shear Stress

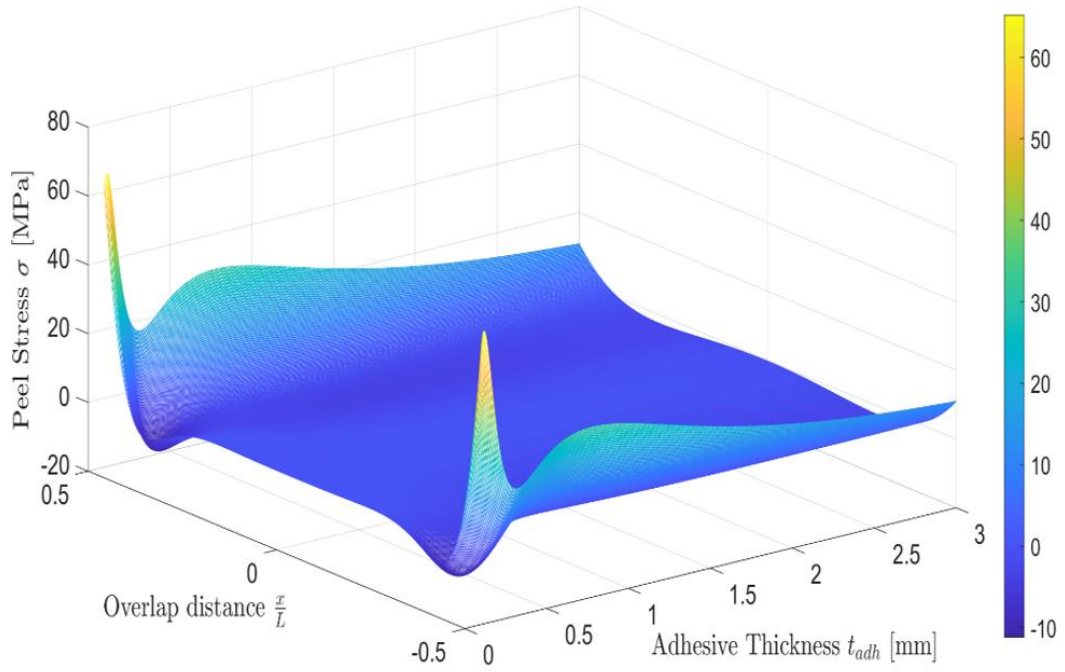


Figure 2.24 3D Effect of Adhesive Thickness on Peel Stress

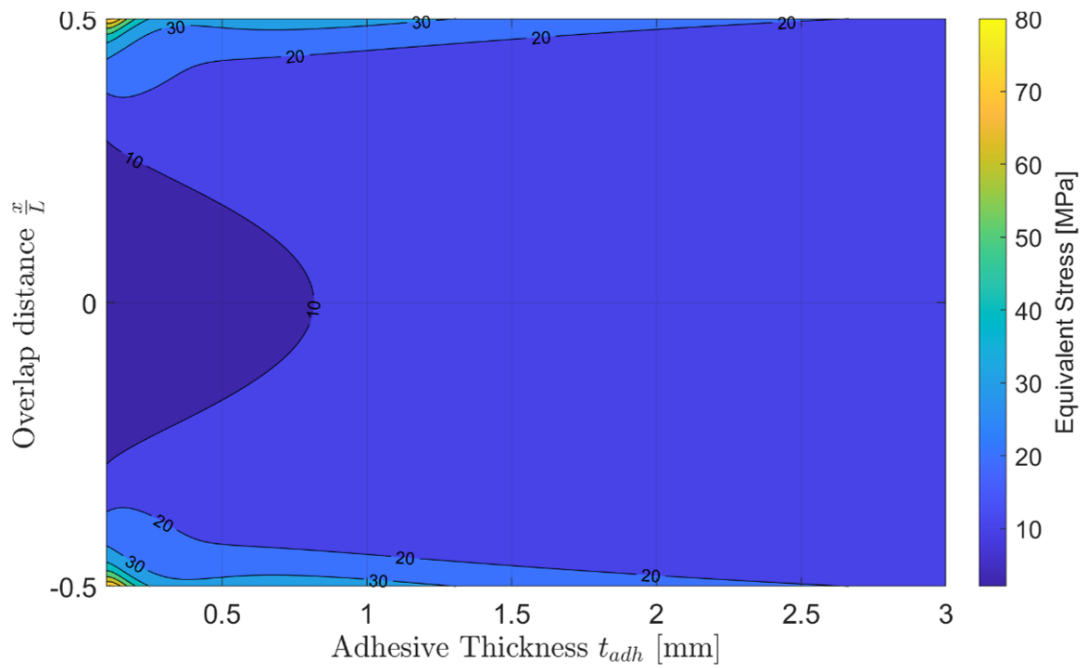


Figure 2.25 Effect of Adhesive Thickness on Equivalent von Mises Stress

### 2.2.5 Effect of Overlap Length

The last key design variable considered in this study is the overlap length. This parameter must be carefully increased when performing experimental tests on SLJs, because also a slight increase could lead to a remarkable improvement on the performance of the adhesive, leading therefore to the bending of the substrates. Fixing the other parameters and varying the overlap length from half inch to two inches, the mechanical behavior of the SLJ with different overlaps can be observed. Combined effects can be noticed also in the case of overlap length and adhesive thickness, confirming what the 2D variations show respectively.

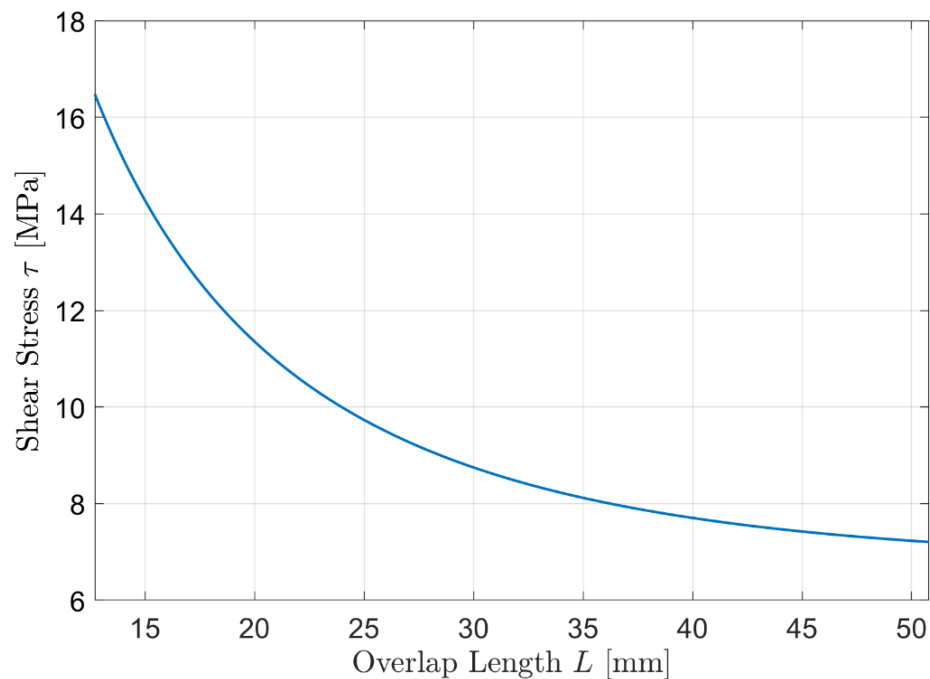


Figure 2.26 Effect of Overlap Length on Maximum Shear Stress

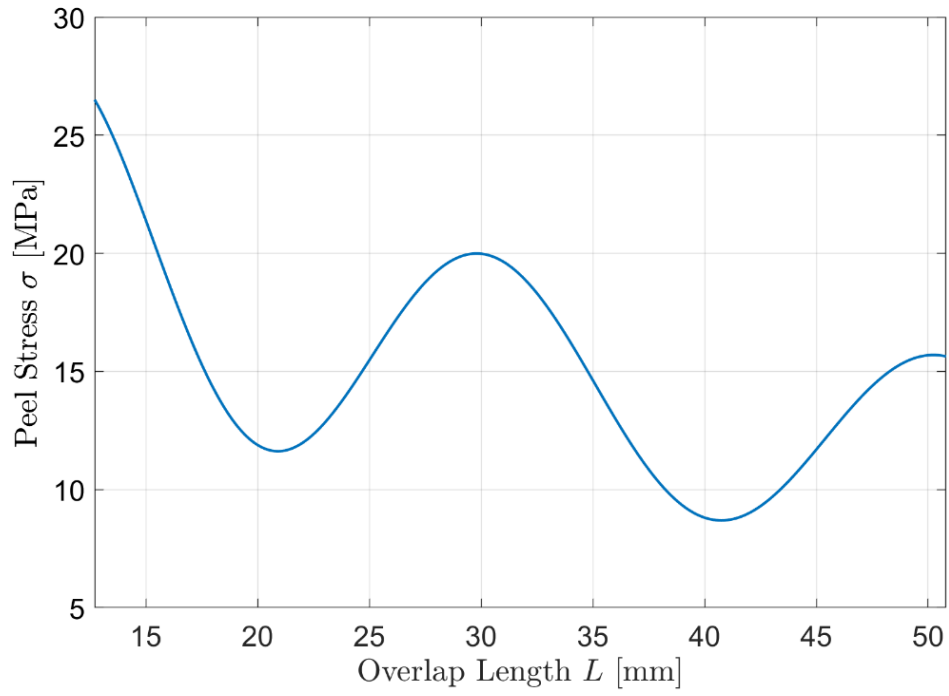


Figure 2.27 Effect of Overlap Length on Maximum Peel Stress

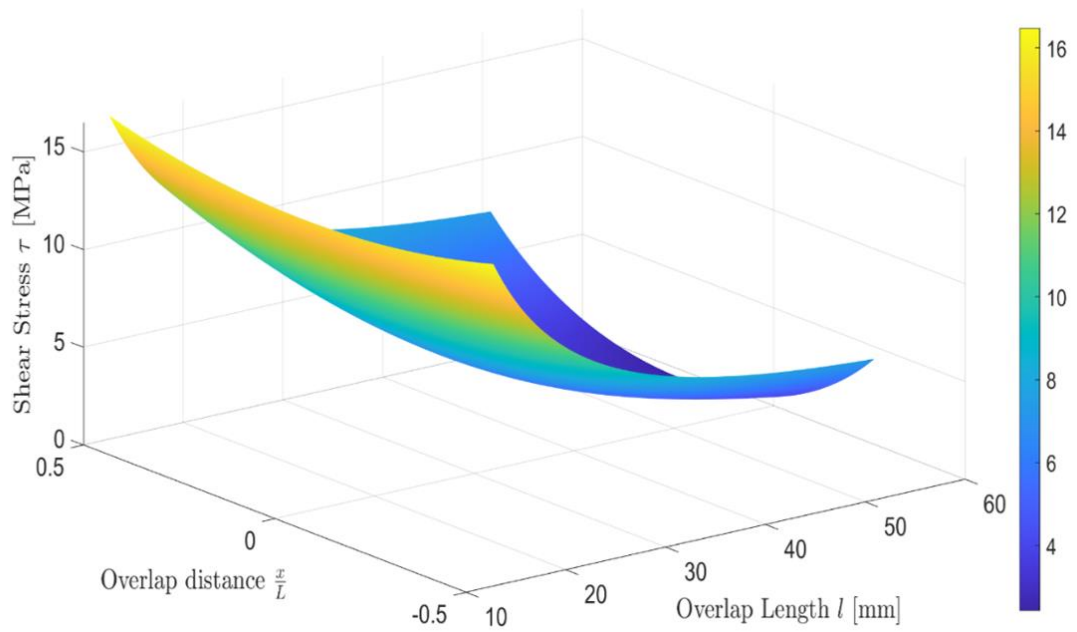


Figure 2.28 3D Effect of Overlap Length on Shear Stress

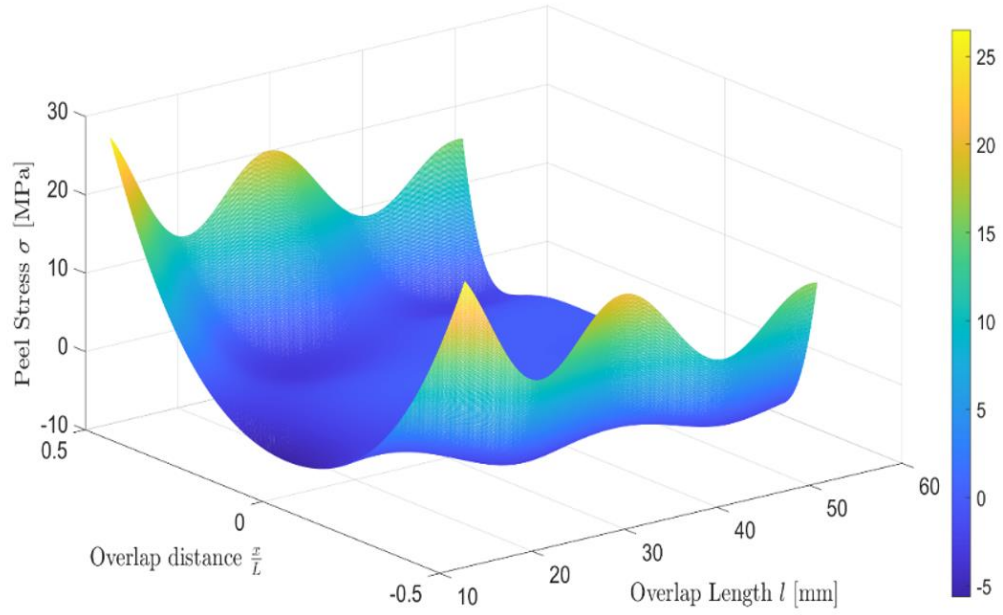


Figure 2.29 3D Effect of Overlap Length on Peel Stress

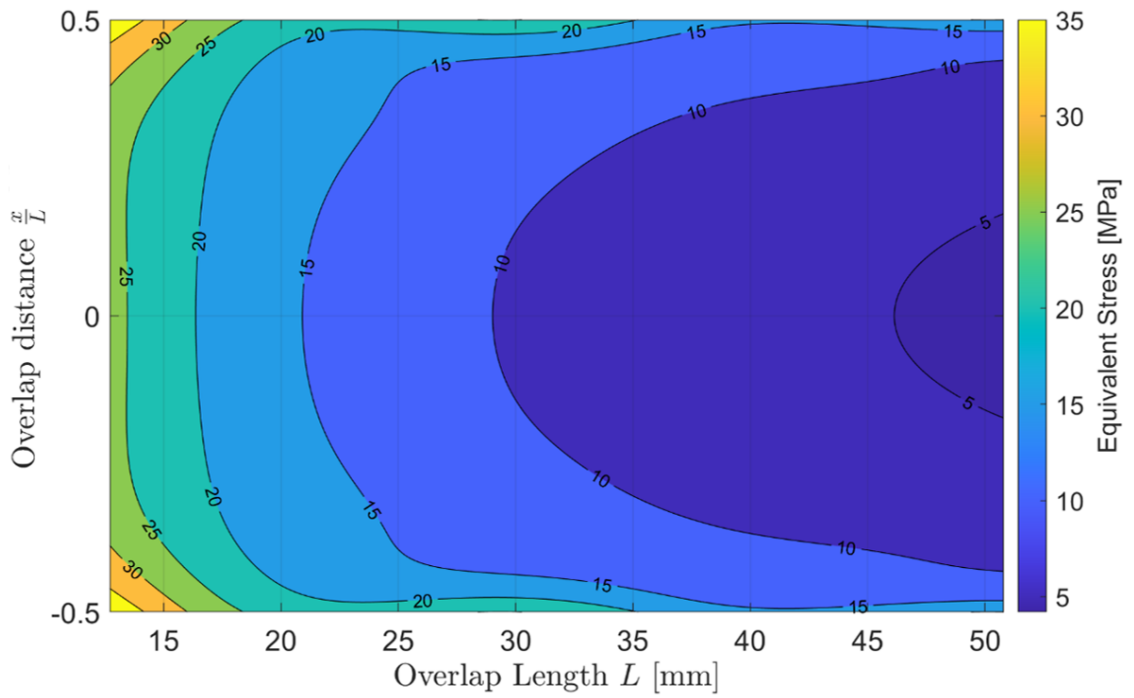


Figure 2.30 Effect of Overlap Length on Equivalent von Mises Stress

From Figure 2.28, the influence of the overlap length on the shear stress is clear: as the overlap increases the shear stress in the overlap decreases, thus leading to higher failure loads in the single lap joint. From Figure 2.29, instead, the peel stress has not a uniform trend as the overlap length increases, but since the decrease in the shear is higher, overall the mechanical performance of the bonded configuration will be better. Combined effects can be appreciated in Figure 2.30. The overall results coming from this analytical analysis have been summarized in Table 2.6.

Table 2.6 Summary of the Results for the Adhesive Stress Using Classical Analytical Models

<b>Effect of the Key Design Variables with Analytical Models</b>	
Adherend Thickness ↑	Adhesive Shear Stress =
Joint Width ↑	Adhesive Shear Stress ↓
Adhesive Thickness ↑	Adhesive Shear Stress ↓
Overlap Length ↑	Adhesive Shear Stress ↓

## CHAPTER THREE

### EXPERIMENTAL SETUP AND TEST PROCEDURE

In this chapter, the experimental setup and test procedure are outlined for adhesively bonded single lap joints and double cantilever beams, showing the adopted procedure for the bonding process.

#### 3.1 Experimental Procedure

In order to properly parametrize the non-commercially available epoxy-based adhesive used in this study, an experimental plan involving single lap joints and double cantilever beams has been designed.

The purpose of the experiments for the SLJs is to analyze the influence of key design variables, such as adhesive thickness and overlap length on very stiff aluminum substrates made in additive manufacturing (AlSi 10Mg). The main output of the testing for the SLJs, therefore, will be the average shear strength of the joints in each considered condition: this parameter is key for the successive parametrization of the adhesive in the finite element model. Moreover, the results obtained with additive manufacturing (AM) substrates have been compared with preliminary tests realized by Stellantis with a mixed configuration, with joints realized with a 3D printed surface and an extruded one (AM-EXTR). Even though these latter presented a different geometry, the results will be normalized by the bonding area to have comparable results.

Single lap Joints are not the only specimens considered in the plan, also DCBs have been manufactured in order to evaluate another fundamental parameter for the cohesive modeling of the adhesive: the fracture toughness.

Table 3.1 Experimental Testing Configurations

<b>Sample Size</b>	<b>Material</b>	<b>Adherend Thickness [mm]</b>	<b>Overlap Length [mm]</b>	<b>Adhesive Thickness [mm]</b>	<b>Adhesive Type</b>
<i>Joint Configurations</i>			<i>Adhesive Bonding</i>		
4 SLJs	AM-AM	6.0	12.7	2.0	NCA Single Part Epoxy
4 SLJs	AM-AM	6.0	12.7	1.0	NCA Single Part Epoxy
4 SLJs	AM-AM	6.0	12.7	0.5	NCA Single Part Epoxy
4 SLJs	AM-AM	6.0	19.05	0.5	NCA Single Part Epoxy
3 SLJs	AM-EXTR	2.0	20.0	2.0	NCA Single Part Epoxy
5 DCBs	AM-AM	13.0	250.0	1.0	NCA Single Part Epoxy

## 3.2 Single Lap Joint Test

### 3.2.1 Joint Geometry

The first step to design the correct geometry of the specimens, although the values of the adhesive thickness, joint width and overlap lengths are standardized, the adherend thickness must be carefully chosen in order to achieve the yielding load first in the adhesive with respect to the substrates to properly characterize the adhesive.

Reducing as much as possible the influence of the peel stress, indeed, allows the joint shear strength (evaluated through the single lap joint shear stress) to be more accurate.

For this purpose, as shown in the methodology, Adams [23] criterion has been used but implementing different bending moment factors formulations such to have more reliable models that are able to correctly assess, in the design phase, the desired value of adherend thickness. All the equations described in the analytical formulation have been implemented in MATLAB.

For the most-stressed configuration (with higher overlap), the design tool assessed that the minimum value of the adherend thickness for the tests such to avoid yielding in the substrates is 6mm: for lower adherend thickness, the test would be more affected by the material of the substrates. Indeed, Figure 3.1 illustrates how the design tool works: it intercepts the adherend and adhesive yield load varying the joint thickness. The minimum value of the joint thickness after the interception is the one that guarantees the yielding of the adhesive to occur first. In Figure 3.2 the bending moment factors utilized for the design tool are represented: it is clear that the trends converge to the same value as the joint thickness increases. For low thicknesses, though, a significant difference is noticeable: the most conservative formulation (i.e. Goland-Reissner) is suggested.

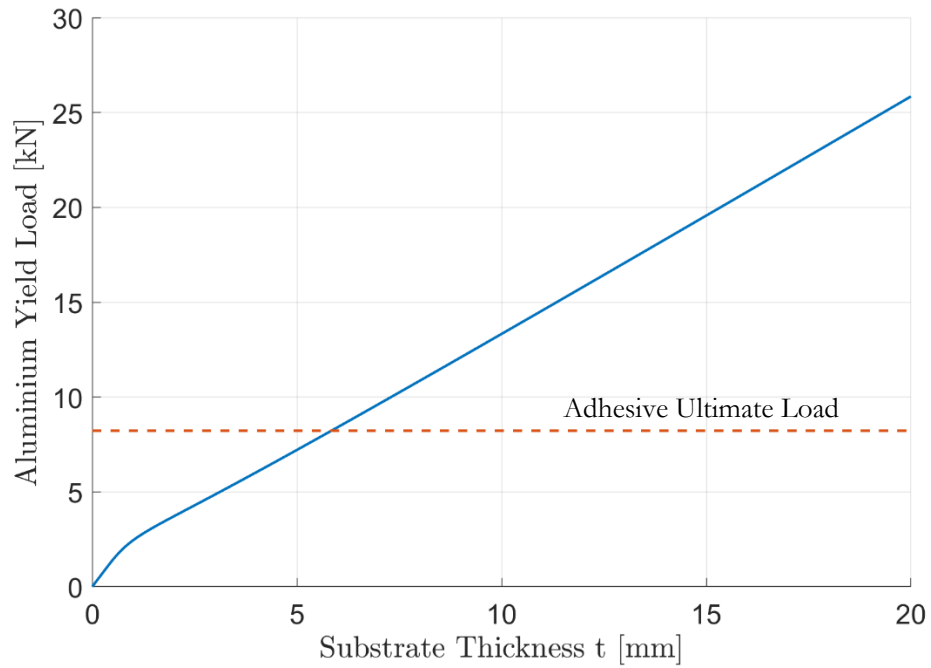


Figure 3.1 Preliminary Design Choice for Substrate Thickness of Single Lap Joints

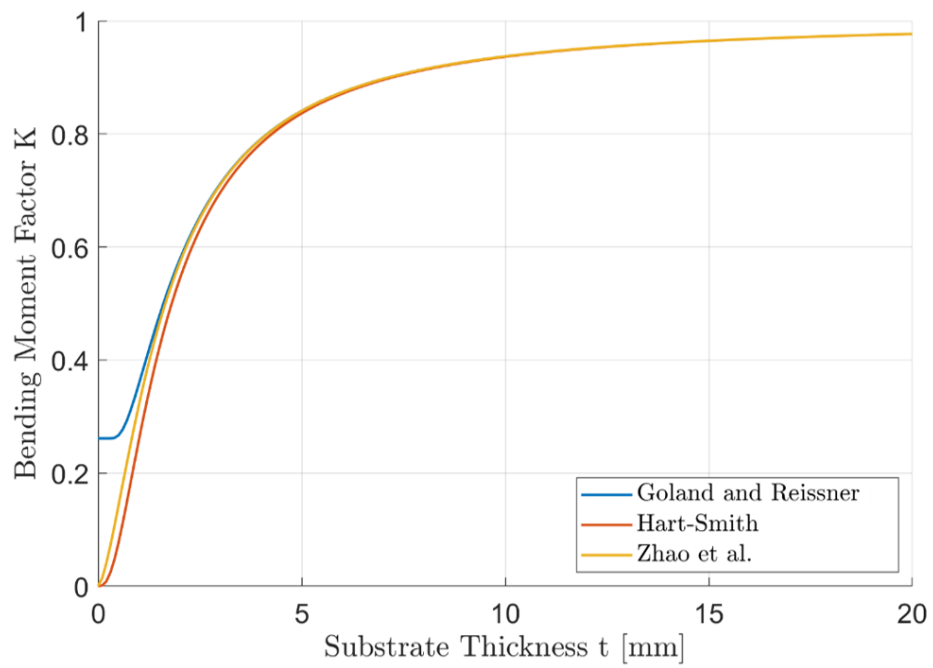


Figure 3.2 Bending Moment Factor vs. Substrate Thickness

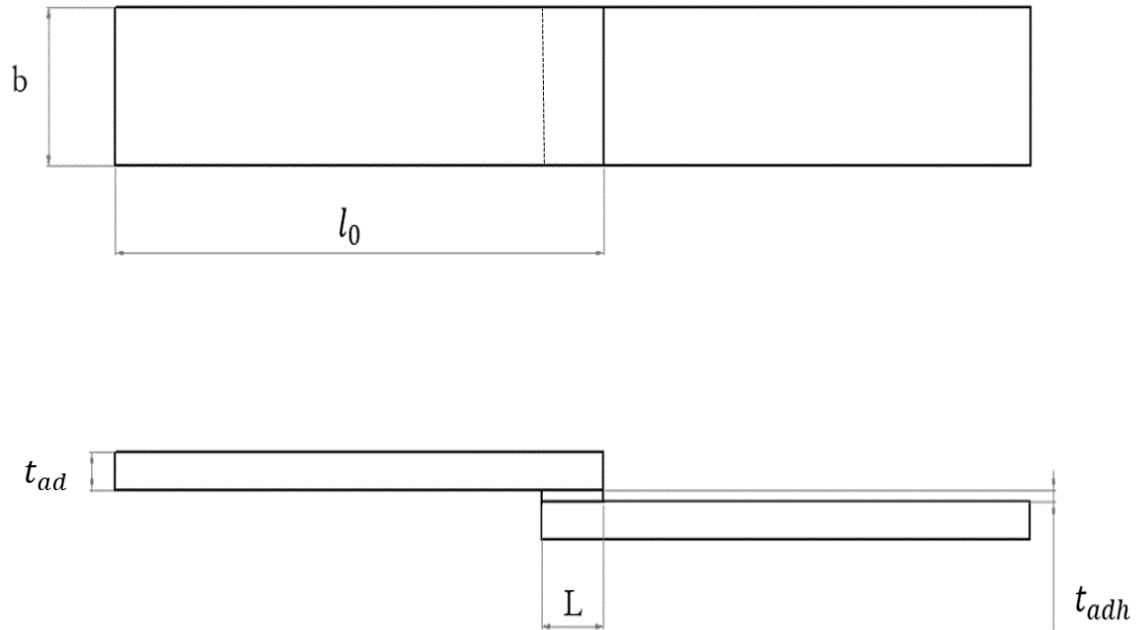


Figure 3.3 Schematics of Test Single Lap Joint

Table 3.2 Single Lap Joint Geometry Data

<b>Single Lap Joint Geometry</b>	
Overlap Length $L$ [mm]	12.7
Substrate Width $b$ [mm]	25.4
Adherend Thickness $t_{adh}$ [mm]	6
Adherend Young Modulus $E$ [MPa]	70,000
Substrate Length $l_0$ [mm]	101.6

### 3.2.2 Bonding Process

The bonding of the single lap joints is a fundamental part of the testing setup: the proper adhesion of the substrates' surfaces is a complicated process involving very different sciences (from chemistry up to materials 'science).

The adherends' preparation is a delicate step that could affect considerably the performance and the failure mode of the joint from adhesive to cohesive: usually, the surface roughness of the adherends is unified through sand paper, increasing the asperities of the material to encourage the mechanical interlocking of the adhesive.

In this study, the additive manufacturing substrates have been kept as they are, in order to evaluate the adhesion with the very particular surface roughness of 3D printed elements.



Figure 3.4 Additive Manufacturing Surface

Although the surface has not been modified, the substrates have been carefully cleaned with acetone to remove the oxide layers present in the aluminum. The bonding of the substrates has been realized exploiting calibrated glass layers such to guarantee the required thickness room for the adhesive (0.5, 1 and 2 mm). The curing of the considered adhesive has been performed at 180°C for 30 minutes with calibrated weights on the bonding area and the free edges of the SLJs, to guarantee alignment and proper pressure on the bonding surfaces.

### 3.2.3 Shear-Tensile Testing

Once the SLJ specimen has been prepared, another step is required before the testing. In order to reduce as much as possible the eccentricity of the load, calibrated tabs have been designed for each adhesive thickness such that to align the specimen in the testing machine.

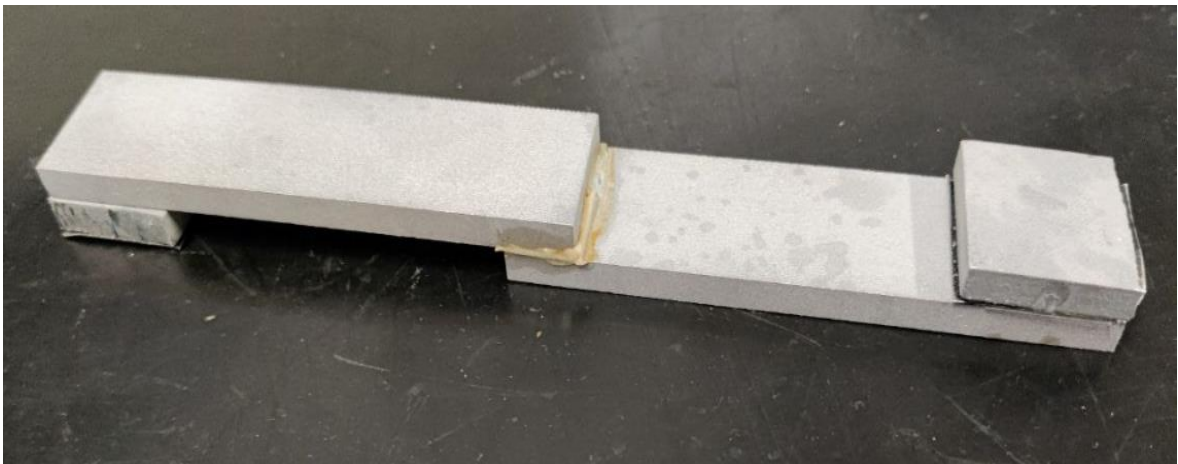


Figure 3.5 Bonded Single Lap Joint

Tests have been conducted using an MTS machine (Figure 3.6) with a strain rate of 1 mm/min to reproduce a quasi-static test. The used joint dimensions are specified in the Fig. 3.3. The substrates are 25.4 mm (1”) wide and 101.6 mm (4”) long, the overlap between the substrates is 12.7 mm (0.5”), with the modifications (on adhesive thickness and overlap length) described in the experimental testing procedure.

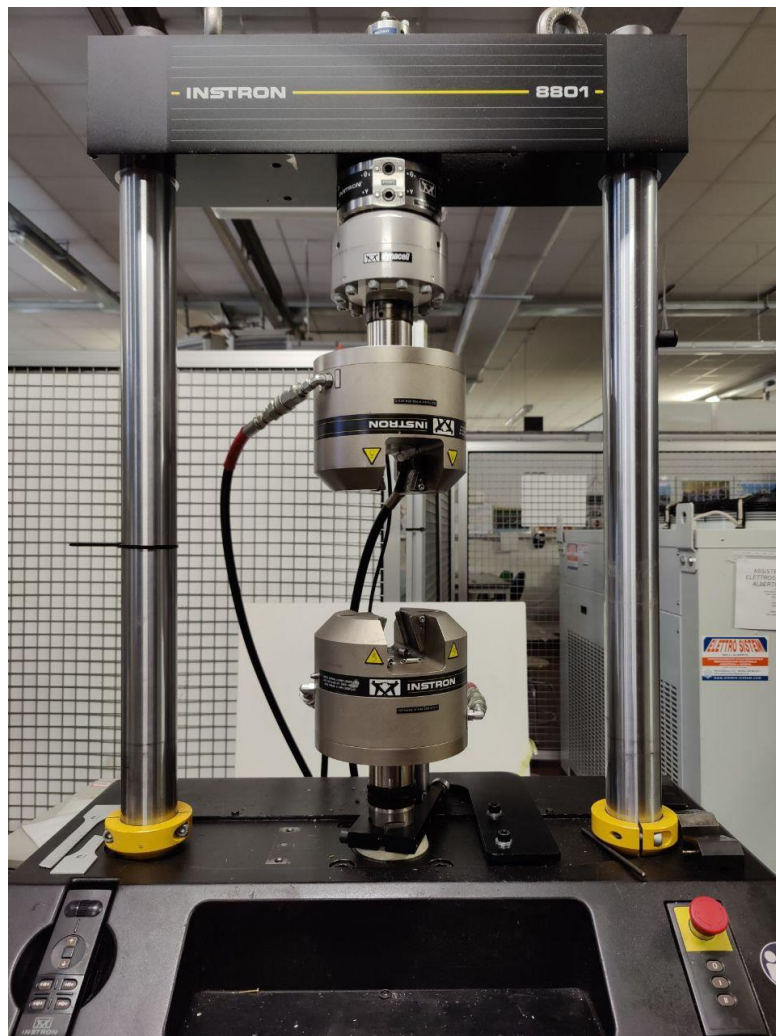


Figure 3.6 MTS 8801 Material Test System

### 3.3 Double Cantilever Beam Test

#### 3.3.1 Joint Geometry

Double Cantilever Beams specimens' dimensions have been chosen according to a slightly modified version of the standard ASTM D3433-99; exploiting the additive manufacturing techniques, in proximity of the holes, the thickness has been increased to avoid stress concentration in the substrates. The preparation of the DCBs requires more practical experience with respect to the SLJs: additional steps such as the creation of a small crack in the adhesive are needed. In order to control the adhesive thickness, calibrated shims (red elements in Fig. 3.8) in both ends of the joint have been used such that, applying pressure with grip elements, the desired adhesive layer bonds with the substrates and the overflow is removed after the curing process.

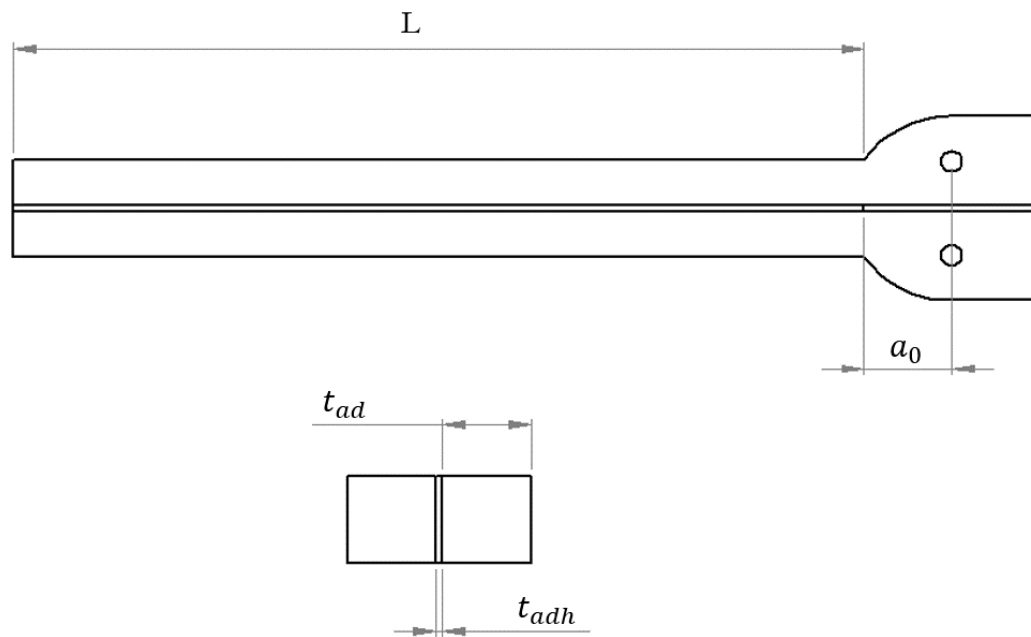


Figure 3.7 Double Cantilever Beam Geometry

Table 3.3 Double Cantilever Beam Geometry Data

<b>Double Cantilever Beam</b>	
Overlap Length $L$ [mm]	249
Joint Width $b$ [mm]	25.4
Adherend Thickness $t_{ad}$ [mm]	13
Adhesive Thickness $t_{adh}$ [mm]	1
Initial Crack Length $a_0$ [mm]	25

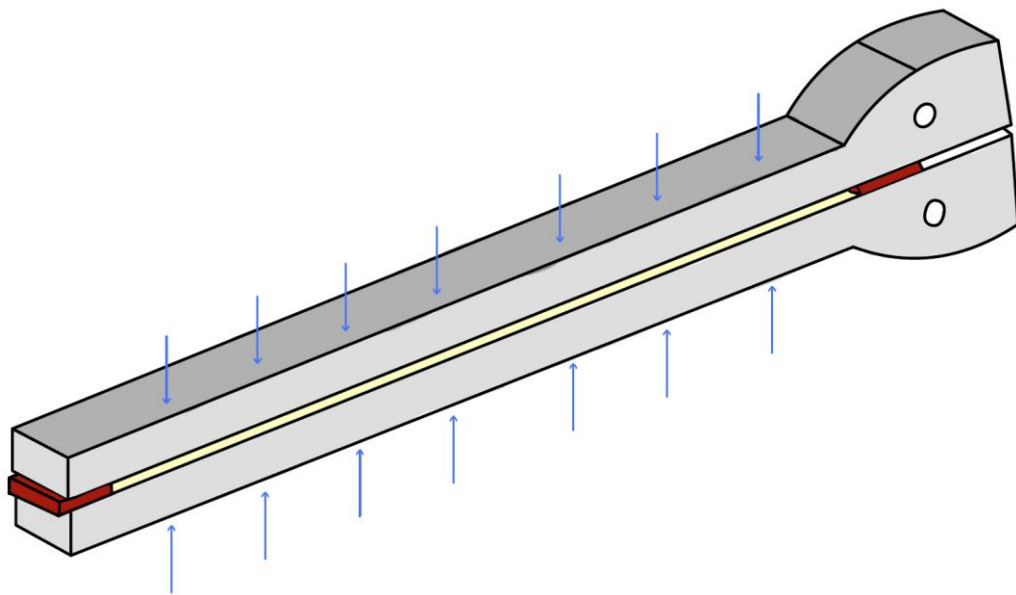


Figure 3.8 Double Cantilever Beam Adhesion Process

The initial crack has been realized by inserting a small piece of wrapped aluminum sheet in the middle of the adhesive guaranteeing, hence, in that local point, the adhesion does not happen. All the inserted elements have been covered with mold agents such to ease the release after the curing. The adhesion process of the DCBs is very similar to the one adopted for the SLJs: the roughness of the AM components has been kept as it is and the surface of the substrates has been cleaned with acetone. The curing cycle is the same followed for the SLJs, and once it is ended, the excess of adhesive in the sides has been removed through mechanical abrasion to better visualize the adhesive layer between the substrates.

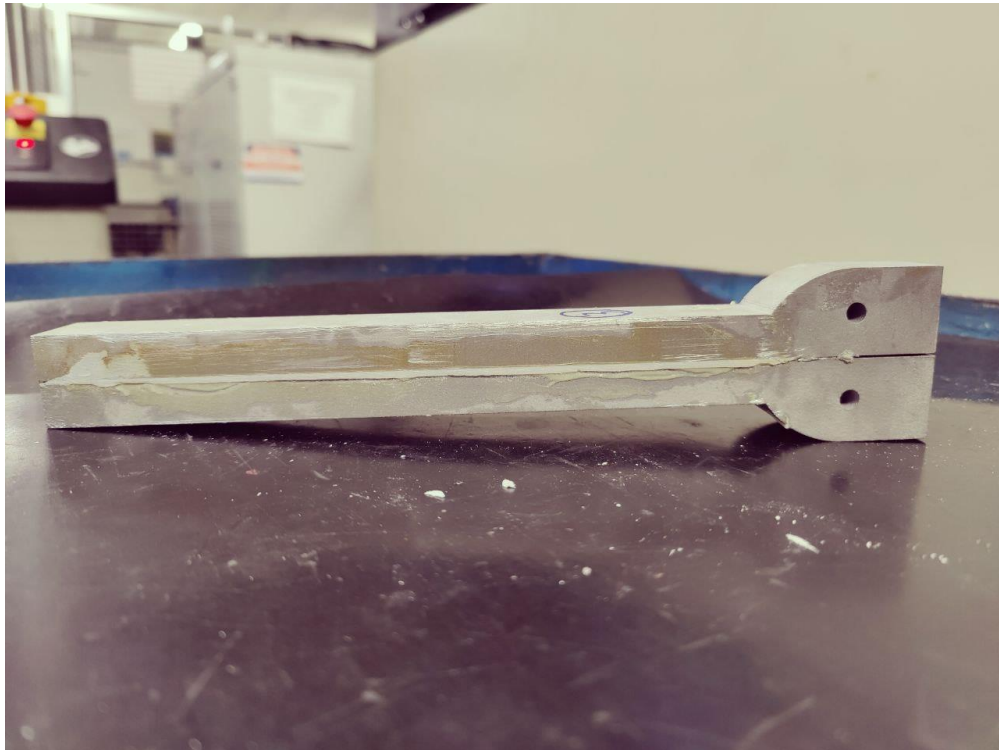


Figure 3.9 Bonded Double Cantilever Beam

### 3.3.2 Peel Testing

Double cantilever beams' specimens are fundamental in order to characterize the Mode I (tensile opening mode) fracture toughness of adhesive joints with the respective critical energy release rate  $G_I$  of the adhesive: a key parameter to insert in the traction separation law of the finite element cohesive zone modeling .

The testing is realized following the standard ASTM D3433-99 with the same machinery shown in Fig. 3.6: in addition, for each run, to avoid the blunt crack effect of the load-displacement curve , a preliminary loading is realized on each specimen to better define the initial crack and finally to perform the experiment. The evaluation of the crack propagation length is a fundamental process in DCB testing. There are several ways that might be adopted to get the “true” crack length as long as the testing is realized such:

- Visual Monitoring
- Optical Monitoring (DIC)
- Analytical Methods

Each method has its own pros and cons, that have been summarized in Table 3.4: the most reliable way to evaluate the crack propagation is exploiting analytical theories based on Timoshenko beams' and Linear Elastic Fracture Mechanics (LEFM).

Many data reduction methods have been used in the past [13-15] with proven accuracy, such as the simple beam theory (SBT), direct beam theory (DBT), experimental compliance method (ECM) and the compliance based beam method (CBBM).

The SBT method, although it considers the deflection of the beam due to bending and shear, it does not take into account the relevant contribution from the beam root rotation.

Table 3.4: Crack Length Monitoring in Double Cantilever Beam Testing

	<b>Visual Monitoring</b>	<b>Optical Monitoring</b>	<b>Analytical Methods</b>
Not Precise	X	X	
Long Setup		X	
Easy	X		X
Robust			X
Expertise Required		X	X

Generally, most data reduction schemes are based on Irwin-Kies equation [13]

$$G_c = \frac{P^2}{2b} \frac{dC}{da} \quad (19)$$

Given P as the external load, b the joint width, C as the compliance of the beam (displacement/load) and a as the crack length.

Defining E as the Young Modulus of the adherend and h as the adherend thickness, the formulation of the fracture toughness can be expressed as

$$G_{Ic}^{SBT} = \frac{4P^2}{Eb^2} \left( \frac{3a^2}{h^3} + \frac{1}{h} \right) \quad (20)$$

Unfortunately, several phenomena are not accounted for in the theory of elasticity since, in real life, beams are never fully elastic and stiff, there is always some deformation.

Additionally, stress concentrations at the crack tip within the elastic zone of the test are present and therefore the Fracture Process Zone (FPZ), where the adhesive ahead of the crack tip is damaged plastically, must be taken into account. For this, reason, a more refined model should be considered: the compliance based beam method (CBBM).

This data reduction scheme allows the direct evaluation of the equivalent crack length once the  $P-\delta$  (load/displacement) curve of the DCB is available. This latter considers also the effect of the Fracture Process Zone (FPZ) and can be calculated as follows

$$a_{eq} = \frac{A}{6\alpha} - \frac{2\beta}{A} \quad (21)$$

With

$$\alpha = \frac{8}{Bh^3E_f} \quad \beta = \frac{12}{5BhG_{13}} \quad (22)$$

Given  $C$  as the compliance and  $G$  as the Shear Modulus of the adherends

$$A = \sqrt[3]{\alpha^2 \left( 108 C + 12 \sqrt{\frac{3(4\beta^3 + 27\alpha C^2)}{\alpha}} \right)} \quad (23)$$

To account for the previous described phenomena, a flexural elastic modulus  $E_f$  is considered instead of Young's Modulus

$$E_f = \left( C_0 - \frac{12(a_0 + |\Delta|)}{5BhG_{13}} \right)^{-1} \frac{8(a_0 + |\Delta|)^3}{Bh^3} \quad (24)$$

Where  $C_0$  is the initial compliance and  $\Delta$  is the crack length correction accounting for the beam root rotation and deflection effects and is deduced from:

$$\Delta = h \sqrt{\frac{E}{11G_{13}} \left( 3 - 2 \left( \frac{\Gamma}{1 + \Gamma} \right)^2 \right)} \approx 0.67 h \quad (25)$$

With

$$\Gamma = 1.18 \frac{E}{G_{13}} \quad (26)$$

Therefore, the mode I fracture toughness according to CBBM is

$$G_{Ic}^{CBBM} = \frac{6P^2}{B^2h} \left( \frac{2a_{eq}^2}{h^2E_f} + \frac{1}{5G_{13}} \right) \quad (27)$$

The evaluation of the equivalent crack length is, therefore, one of the main advantages of exploiting a data reduction scheme like the compliance based beam method: indeed, the correct propagation of the crack tip is the most delicate step of the double cantilever beam testing.

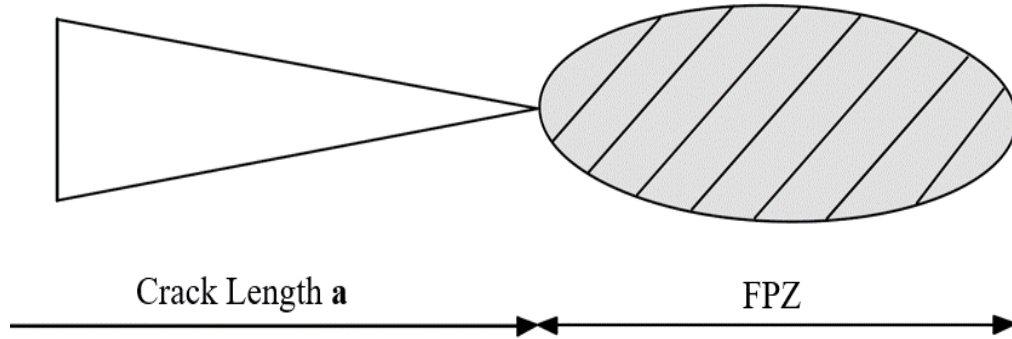


Figure 3.10 Equivalent Crack Length and Fracture Process Zone

## CHAPTER FOUR

### FINITE ELEMENT MODELS

In this section will be presented the procedure and the workflow exploited for the realization of the virtual finite element models. Moreover more details can be found on the contact definition among the adherends and the adhesive.

#### 4.1 Finite Element Modeling

The analysis of adhesively bonded joints started in the Twentieth century with the closed-form analytical models described in the second chapter. The equilibrium equation of a single lap joint led to a simple governing differential equation with a simple algebraic equation. However, if there is yielding of the adhesive and/or the adherends and substantial peeling is present, a more complex model is necessary. The more complete is an analysis, the more complicated it becomes and the more difficult it is to obtain a simple and effective solution. In such cases, it is necessary to use numerical models, like the finite element (FE) method.

The *mesh* considered for the single lap joints was built with 2mm elements, in order to properly catch the physics of the testing. Most of the modern softwares allow the possibility of including geometric non-linearities solving problems like the one proposed by the SLJ with the eccentricity of the load that causes a bending moment on the joint. The workflow adopted for this analysis starts with the definition of the geometry with SOLIDWORKS, while the pre-processing has been handled with HYPERMESH exploiting as solver and post processing ABAQUS.

## 4.2 Cohesive Zone Modeling

The Cohesive Zone Model (CZM) has become a very popular approach to analyze for example, the fracture of adhesive joints, the delamination of composites and the debonding of reinforcements. Over the last few decades, many CZMs have been successively developed. The main difference among the various CZMs proposed lies in the shape of their assumed traction-separation law (TSL). Proposed shapes include polynomial, exponential, trapezoidal, constant stress, rigid linear and bilinear forms [16,17]. With regard to the modelling of interface problems using CZMs, many researchers have concluded that the fracture toughness and cohesive strength are more important than the shape of TSL. The triangular CZM law is the most commonly used due to its simplicity, reduced number of parameters to be determined, and generally acceptable results for most real conditions: for this reason it has been chosen.

However, generically speaking, the shape of the cohesive laws can be adjusted to conform to the behavior of the material or interface they are simulating for more precise results. Obviously that, trapezoidal or more complex laws give more convergence problems because of the more abrupt change in the cohesive elements, but with more precise results. Typically, in order to determine the joint failure occurrence two approaches can be followed: the Material Strength Approach (MSA), which establishes a stress or strain criteria to assess when the adhesive fails and the Fracture Mechanics Approach (FMA), which exploits the onset of crack propagation in the singularities to predict the mechanical behavior of the joint.

The MSA is not well suited for adhesive joints, since it does not account for stress concentration points. Although the FMA considers these latter, it is difficult to assess

stress intensity factors properly. CZMs, instead, are able to combine the strength of materials and fracture mechanics approach: they have been used as an add-in to FE analyses that allows simulation of damage growth, by considering energetic principles. Cohesive elements are assumed to be under one direct component of strain (tension) and one transverse shear strain, which are computed directly from the element kinematics. The membrane strains are assumed as zero, which is appropriate for thin and compliant bonds between stiff adherends. Undamaged strength evolution is defined by a constitutive matrix relating the current stresses and strains in tension and shear across the cohesive elements. The main concern for the usage of CZM in finite element modeling is that accurate calibration of the adhesive's parameters is required: for this reason, the experimental plan presented in chapter 3 has been designed.

The values of energy release rate in tension and shear (respectively  $G_I$  and  $G_{II}$ ) along the fracture paths and relative critical values ( $G_{Ic}$ ) are required. The cohesive strengths in tension and shear ( $\sigma_n$  and  $\tau_s$ , respectively) are equally needed and they relate to damage initiation, or in other words, the end of the elastic behavior and beginning of damage. Different techniques are available for the definition of the cohesive parameters, such as the property identification technique, the direct method and the inverse method. The property identification technique consists on the separated calculation of each one of the cohesive law parameters by suitable tests, while in the inverse method the CZM parameters are estimated by iterative fitting the FE prediction with experimentally measured data (typically the load–displacement curve) up to an accurate representation. In this research, the property identification has been used, utilizing the presented SLJs and DCBs to carry out experimentally the needed parameters to tune the TSL.

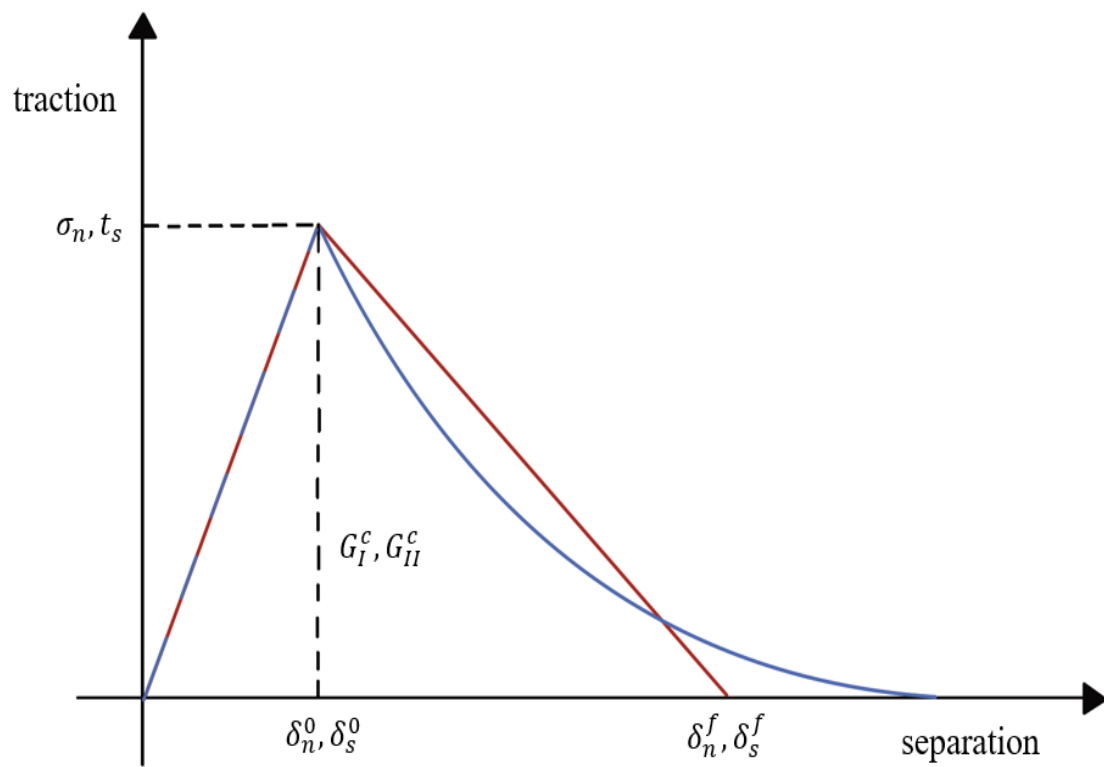


Figure 4.1 Cohesive Zone Model Traction Separation Law

### 4.3 Single Lap Joint

The definition of the finite element model for the Single Lap Joint requires different steps to follow:

- CAD Geometry Definition
- Geometry Clean Up and Mesh Creation
- Segments and Groups Creation among Adhesive and Adherends
- Material and Adhesive Properties Definition
- Load Case Definition and Simulation Run

The SLJ geometry has been realized using SOLIDWORKS and thus it has been imported in HYPERMESH. The realized model exploits a 3D mesh, which is obtained by extruding a 2D mesh uniformly in the thickness direction (i.e. z axis).

The elements used to represent the mechanical behavior of the adherends are C3D8I, full integration hexagonal elements, which are guaranteeing more precision on the calculus (even if at the expense of higher computational cost). As already mentioned, instead, for the adhesive, COH3D8 cohesive zone elements have been used, which simulate perfect adhesion among the adhesive and adherends. So far, 2 mm elements have been considered for the adherends and 1 mm size for the adhesive, the optimization of the size of the mesh, though, will be part of further studies.

Since the geometry of the SLJs is basic, the clean-up and meshing are straightforward processes, thus it is possible to define the surfaces which will simulate the contact interaction between adhesive and adherends. First, *segments* have been created and then they have been collected in *groups* (TIE), assigning the slave nodes to the most yielding part of the structure (i.e. the adhesive) and the master nodes to the adherends.

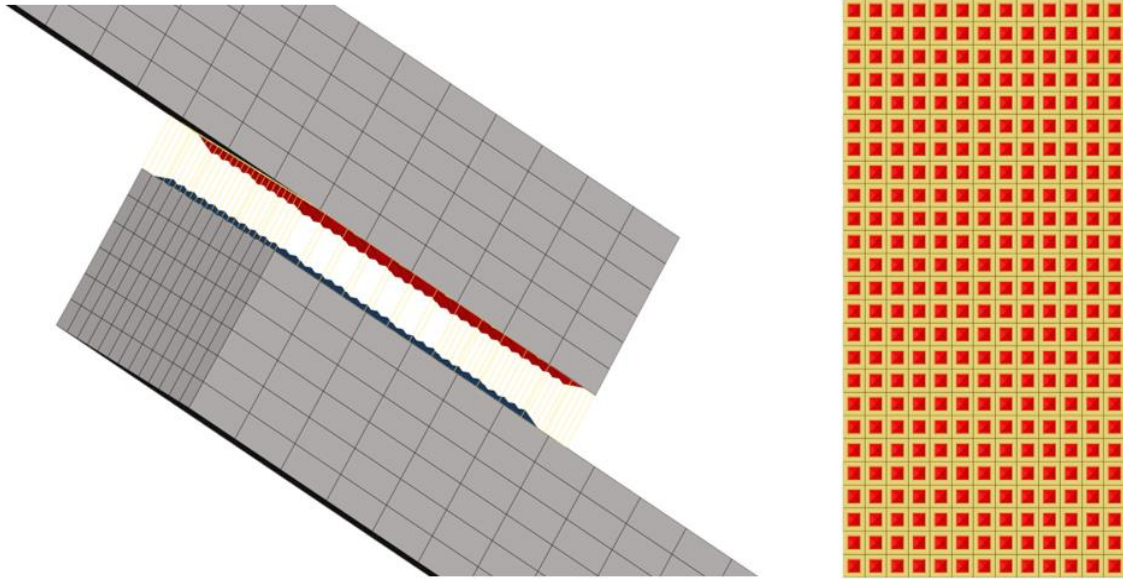


Figure 4.2 Contact Definition between Adhesive and Adherends

The connection among the adhesive and adherends could have been realized also by aligning the nodes of the elements, but exploiting the creation of *groups* there are more degrees of freedom on the meshing of the surfaces. Therefore the adherend material properties are defined, giving as input the Young modulus  $E$  and several points of the curve  $\sigma - \epsilon$  to characterize the plastic behavior of the considered 3D printed aluminum. Concerning the adhesive, instead, as already described several parameters have been input to combine the effect of the fracture mechanics and material strength approach. The load case applied to the single lap joint simulates the lap shear stress test, constraining all the nodes in the grip (6 dofs) with 1D rigid elements (RBE3) from one side and moving from the other side until the failure of the joint is verified. Once defined the material properties and the load case, the simulation can be run using as solver ABAQUS.

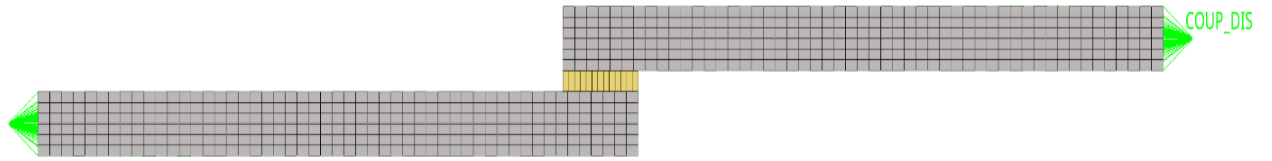


Figure 4.3 Load Case of Single Lap Joint: Lateral View

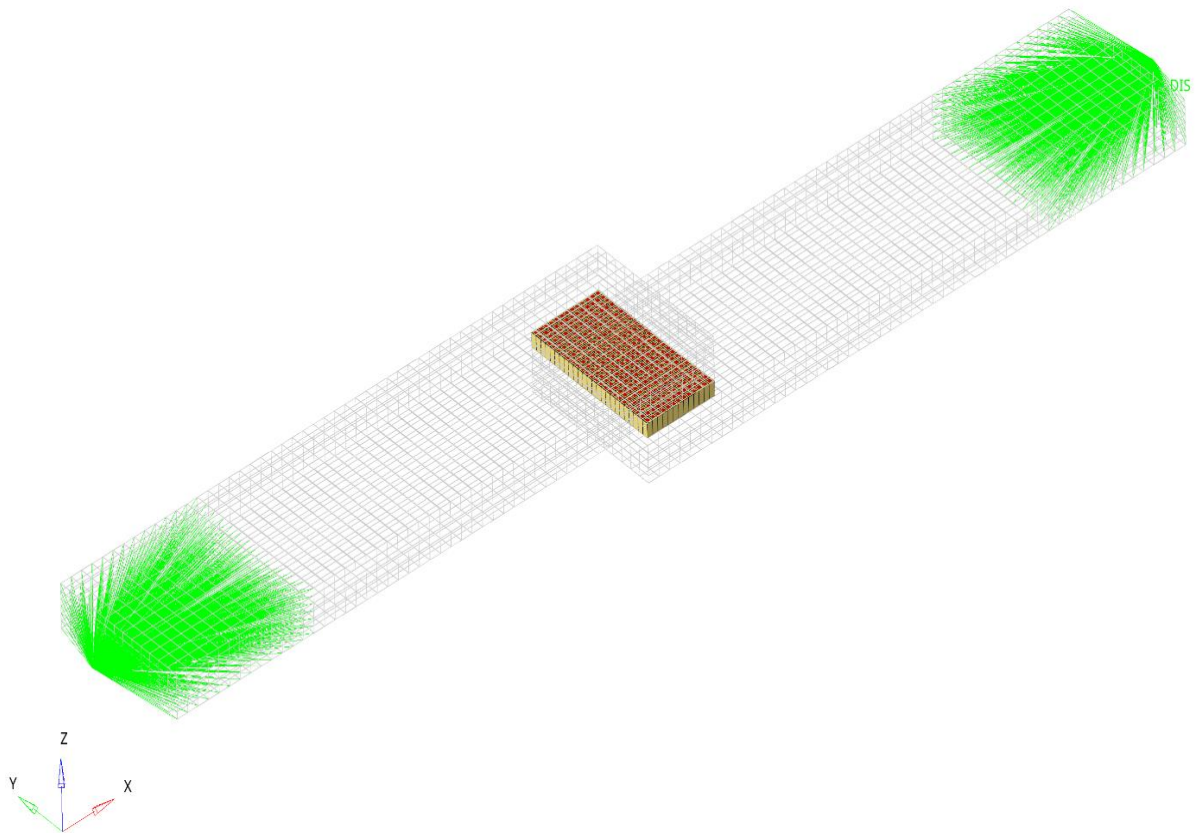


Figure 4.4 Load Case of Single Lap Joint: 3D View

#### 4.4 Automotive Bonded Joint

The building of the FE model for the SLJ is just a necessary step to properly calibrate the triangular traction separation law used to define the adhesive behavior. The core of the research is to implement effectively, in the end, the adhesion modeling implemented in the SLJ in a real joint with a much more complex geometry involving AM aluminum (AlSi 10Mg) and regular extruded aluminum profile (6082-T6). The required steps for the modeling follow the same workflow used for the SLJs, which are summarized in Figure 4.5.

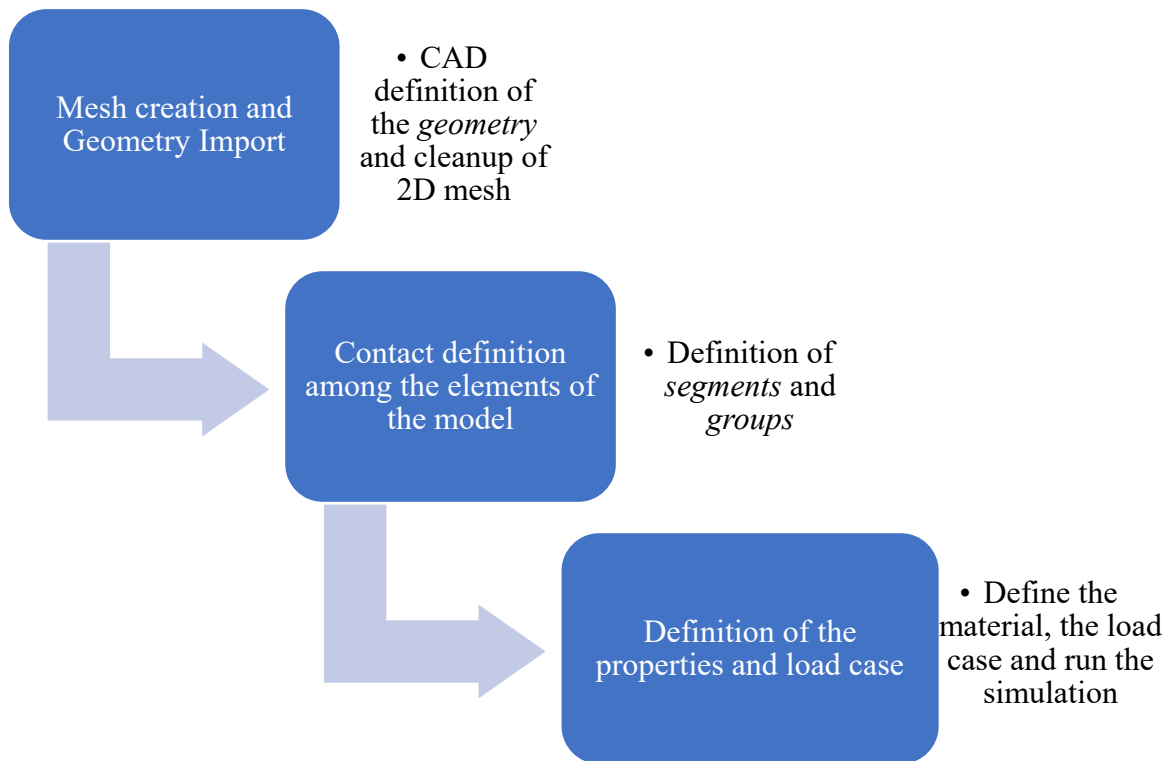


Figure 4.5 Numerical Model Workflow

In order to build the 3D final mesh of the component, it is needed that the 2D mesh (that has to be extruded later as in the SLJ) is as accurate as possible to represent the original geometry. Indeed, if not, it might happen that, internally, the elements would deform influencing the final results of the calculus. The elements used in the meshing of the real component are different from the single lap joint model: although for the adhesive and the manifold the same kind of hexagonal elements have been exploited (COH3D8 and C3D8I, respectively), for the sliding cover and the *female* joint in AM, lighter tetragonal C3D10I elements have been used. In Figure 4.6, the elements and the mesh size (1 mm) of the automotive joint are represented. In Figure 4.7, instead, the quality of the 2D mesh is reported showing no elements violating the set thresholds.

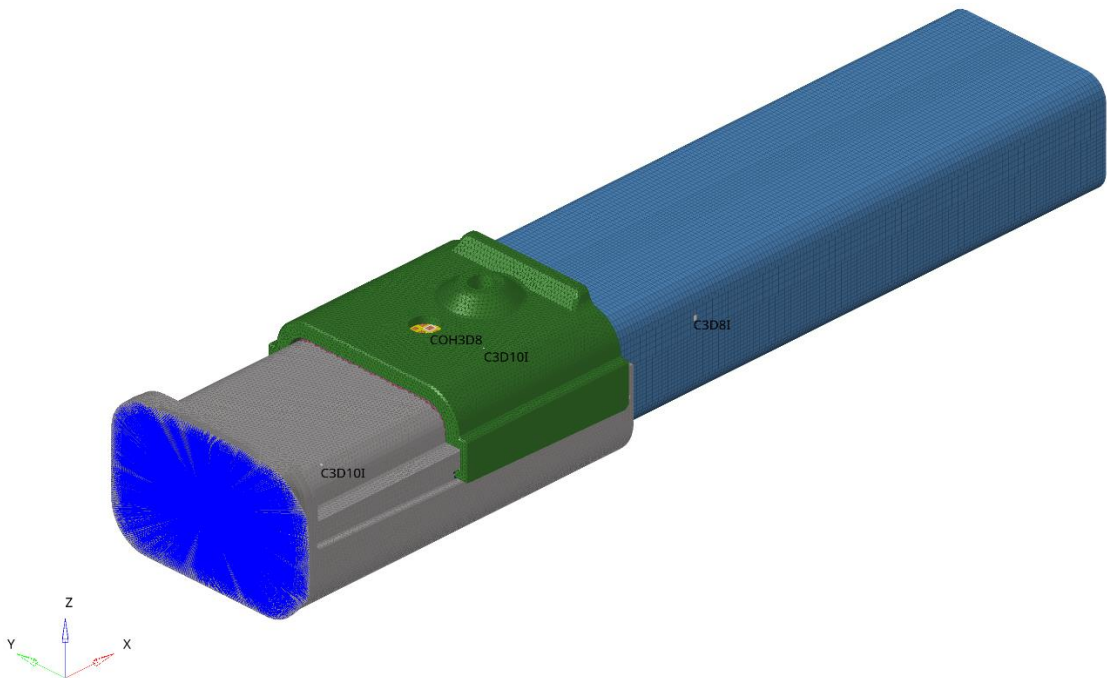


Figure 4.6 Sample Automotive Bonded Joint Mesh

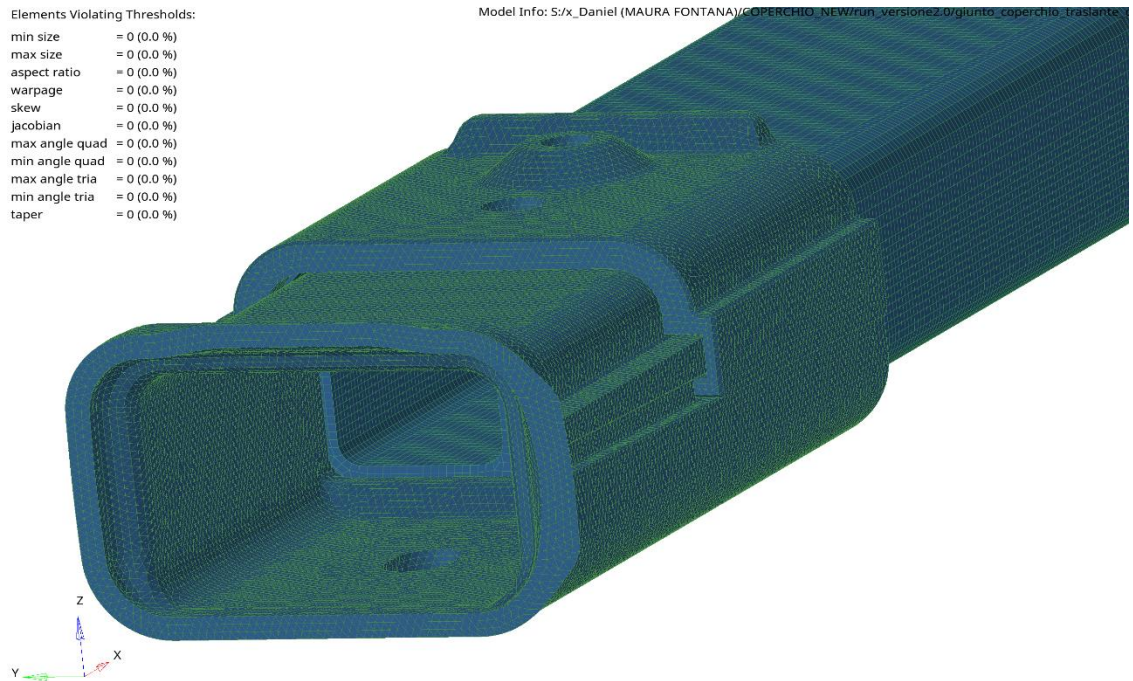


Figure 4.7 Quality of the Mesh for the Automotive Joint

A 1mm mesh was firstly considered in this analysis. From Figure 4.6, the much more complex geometry of the automotive bonded joint can be appreciated; it is composed by three main elements joined with the adhesive:

- The extruded profile (blue element) made in 6082-T6 Aluminum.
- The sliding cover (green element) made in 3D printed AlSi 10Mg Aluminum.
- The *female* node (grey element) made in 3D printed AlSi 10Mg Aluminum.

The contact definition in the FE model among the three elements is, therefore, much more complex, since there is interaction between adhesive and adherends and adherends among themselves. The interactions of the adhesive can be observed in Figure 4.8.

Moreover, the friction contacts among the extruded profile, the AM elements and the adhesive are illustrated in Figure 4.9 and 4.10.

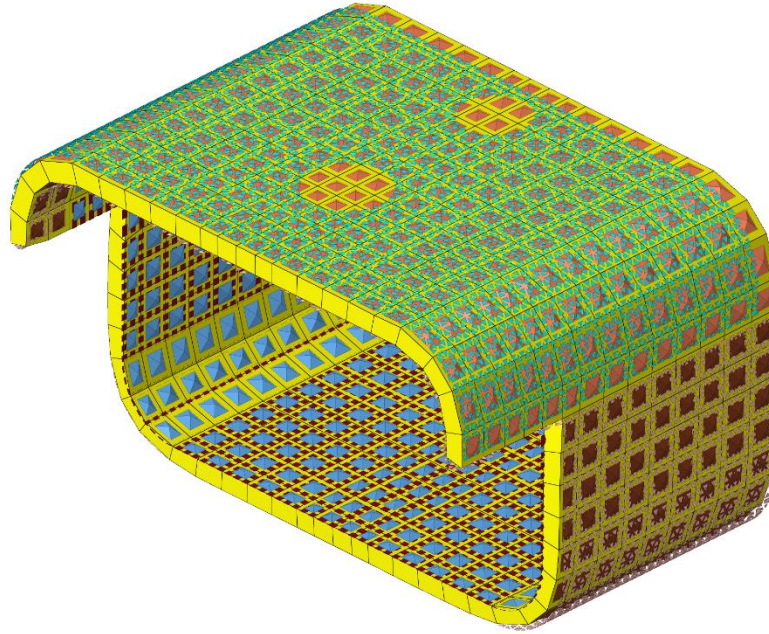


Figure 4.8 Contact Definition in the Adhesive Layer

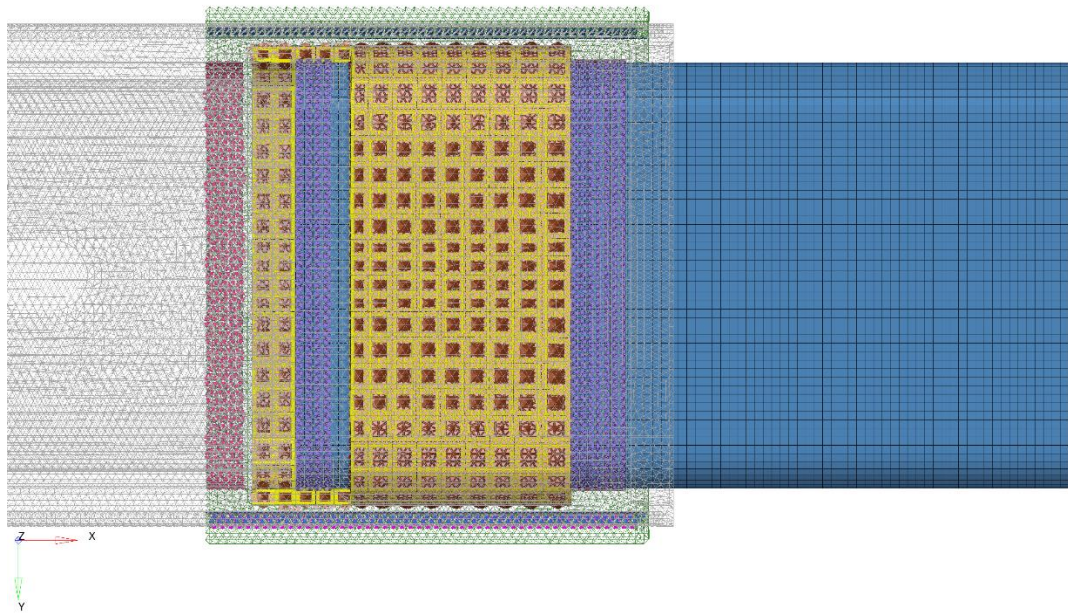


Figure 4.9 Contact Definition among Adhesive and Adherends of the Automotive Bonded Joint

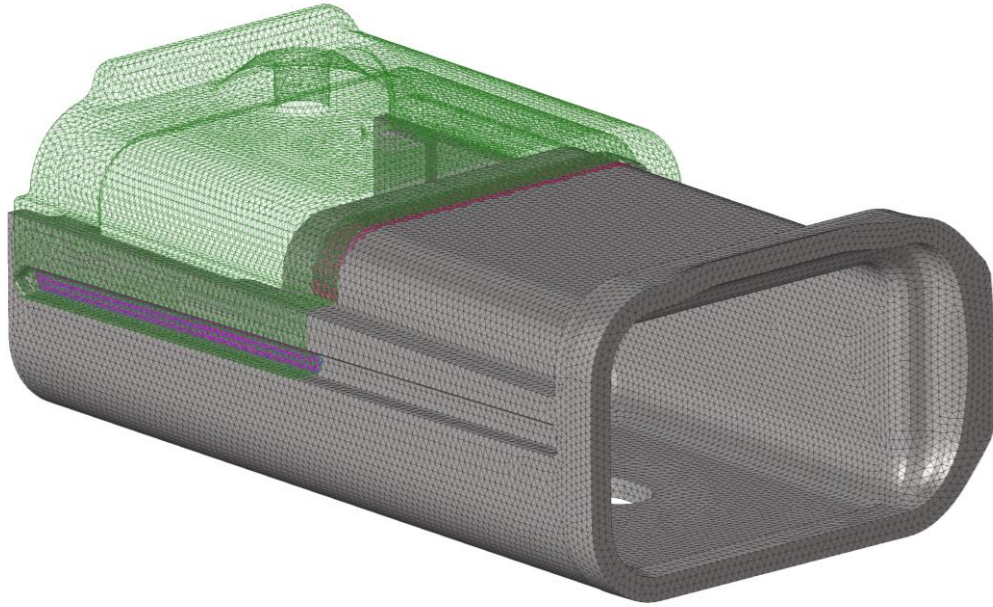


Figure 4.10 Contact Definition among the Metals of the Adherends

The defined load case is the same of the single lap joints: the nodes on one extremity are constrained in all the six degrees of freedom (dofs) and on the opposite side the only allowed displacement is the axial until the failure load is reached.

CHAPTER FIVE  
RESULTS AND DISCUSSION

Results are presented and discussed in this chapter. Experimental testing (SLJs and DCBs) allow the characterization of the adhesive parameters, creating therefore a reliable FEA model applicable for a sample automotive joint.

5.1 Experimental Testing Results

5.1.1 Single Lap Joint

Single Lap Joint shear tests are crucial in order to evaluate the shear strength of the adhesive such to obtain the required parameter for the cohesive zone model. When analyzing the results of these tests, it is important to observe the failure mode of the adhesive. In Fig. 5.1, the two main kind of failure modes are reported.

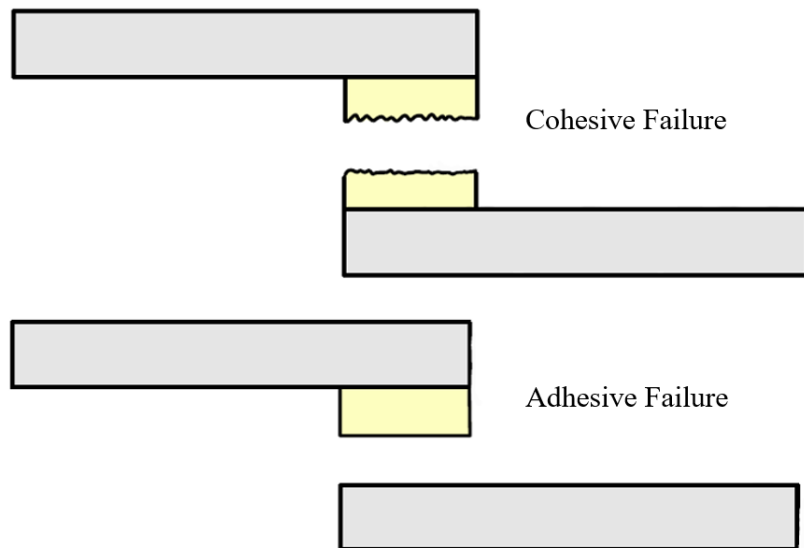


Figure 5.1: Illustration of some Failure Modes of Bonded Single Lap Joints

Although it may seem a marginal difference, in reality, it is affecting considerably the discussion of the obtained results. Indeed, so far, there is not a model of the stresses at the interface between adherend and adhesive: hence, to obtain a reliable finite element model, the parametrization of the adhesive should be based on cohesive failures.

Adhesive or mixed mode (partially cohesive and partially adhesive) failures might happen when the surface preparation is not appropriate to bond the given substrates.

In this study, the effect on the failure loads and the mechanical behavior of the SLJs has been studied by varying three adhesive thicknesses, two overlap lengths and considering also two different interfaces: the additive-additive (AM-AM) configuration and a mixed configuration (AM-EXTR) with a regular extruded aluminum.

#### 5.1.1.1 Effect of Adhesive Thickness

The adhesive thickness has shown to be a significant variable affecting the mechanical behavior of single lap joint: increasing the thickness, the failure load of the joint decreases remarkably. For each configuration, four tests have been repeated in order to obtain more robust results from a statistical point of view: the reported standard deviations of the samples are very low and this is an indication of the good reliability of the results. In Figures 5.2, 5.3 and 5.4 are reported respectively the SLJ tested with adhesive thickness equal to 0.5mm, 1mm and 2mm. The curves have been post-processed with MATLAB considering a filter to lower the effect of noise of the measurements.

When considering the lowest adhesive thickness (0.5 mm) the failure load increases of about 6% with respect to the baseline (1.0 mm). In case of 2 mm of adhesive thickness, instead, the performance is decreasing of more than 25% with respect to the baseline and about 34% in comparison with 0.5 mm configuration.

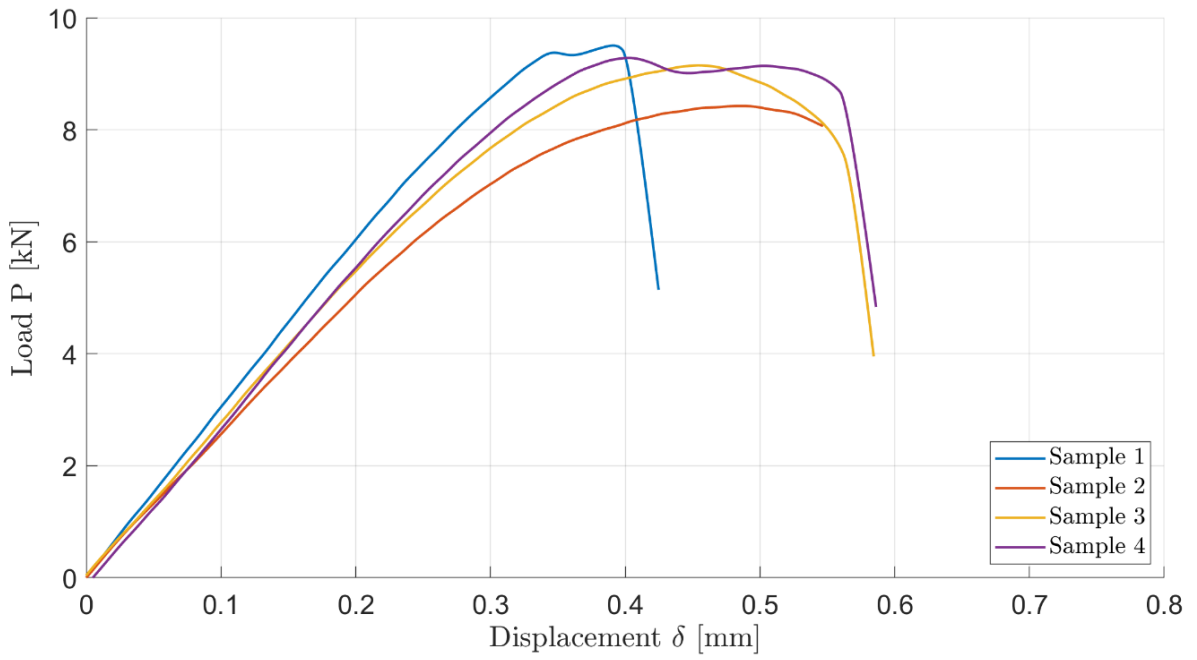


Figure 5.2 Load-Displacement Data for Adhesive Thickness = 0.5 mm

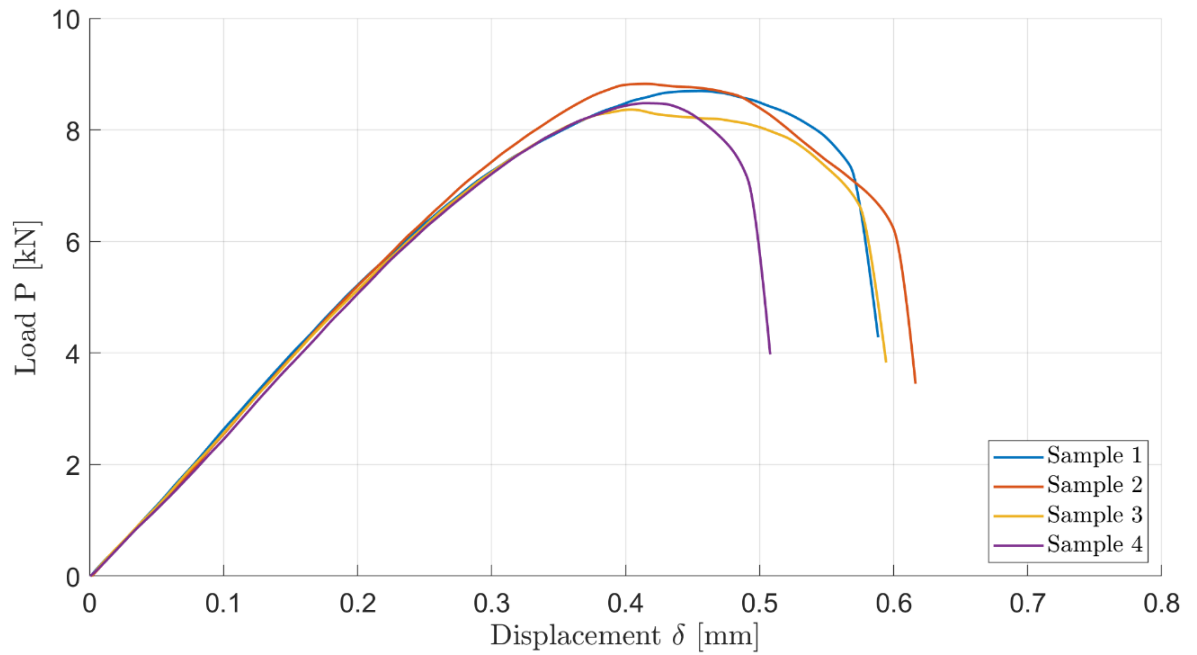


Figure 5.3 Load-Displacement Data for Adhesive Thickness = 1 mm

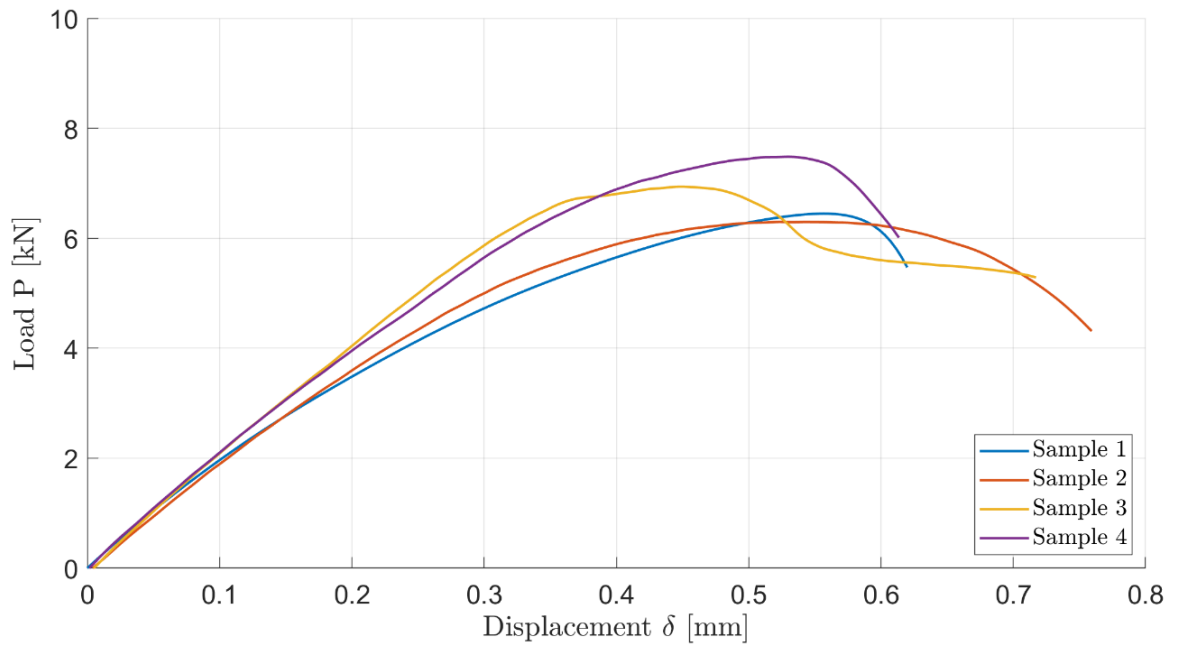


Figure 5.4 Load-Displacement Data for Adhesive Thickness = 2 mm

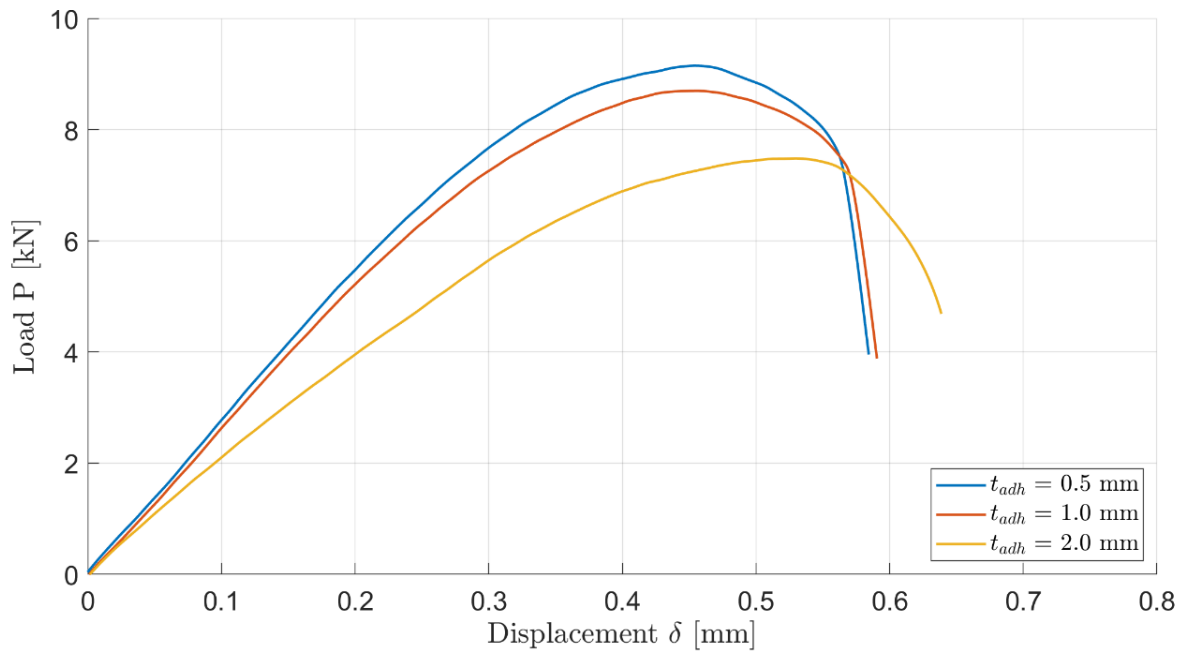


Figure 5.5 Average Load-Displacement Data for Different Adhesive Thicknesses

For each repetition of the tested configurations, the most representative has been chosen in order to compare visually the differences in Figure 5.5. By considering the SLJ dimensions described in Fig. 3.3 with three different adhesive thicknesses, it is possible to summarize the obtained results for the failure loads in Table 5.1. The decrease of the failure loads, and therefore in shear strength of the adhesive, is not the only effect on the mechanical behavior of the SLJ: with higher adhesive thickness also the joint stiffness decreases. In Table 5.2, the effect on the stiffness for each configuration can be observed. Moreover, in order to have a visual impact of the obtained results, bar charts with the respective standard deviations of the testing for the failure loads are shown in Figure 5.6. It must be noted that it is a two-axis plot where on the left side the failure load of the joint is reported and on the right side, it can be observed the trend of the shear strength of the adhesive, normalizing by the bonding area.

Table 5.1 Effect of Adhesive Thickness on Joint Failure Loads

<b>Failure Loads [kN]</b>							
Overlap Length [mm]	Adhesive Thickness [mm]	#1	#2	#3	#4	Average	Standard Deviation
<b>12.7</b>	<b>0.5</b>	9.50	8.42	9.15	9.28	9.09	0.467
<b>12.7</b>	<b>1.0</b>	8.70	8.82	8.36	8.48	8.59	0.208
<b>12.7</b>	<b>2.0</b>	6.49	6.30	6.94	7.48	6.79	0.535

Table 5.2 Effect of Adhesive Thickness on Joint Stiffness

Overlap Length [mm]	Adhesive Thickness [mm]	Average Joint Stiffness (Sample Size = 4) [kN/mm]	Standard Deviation [kN/mm]
12.7	0.5	29.5	1.80
12.7	1.0	26.7	1.88
12.7	2.0	23.2	1.90

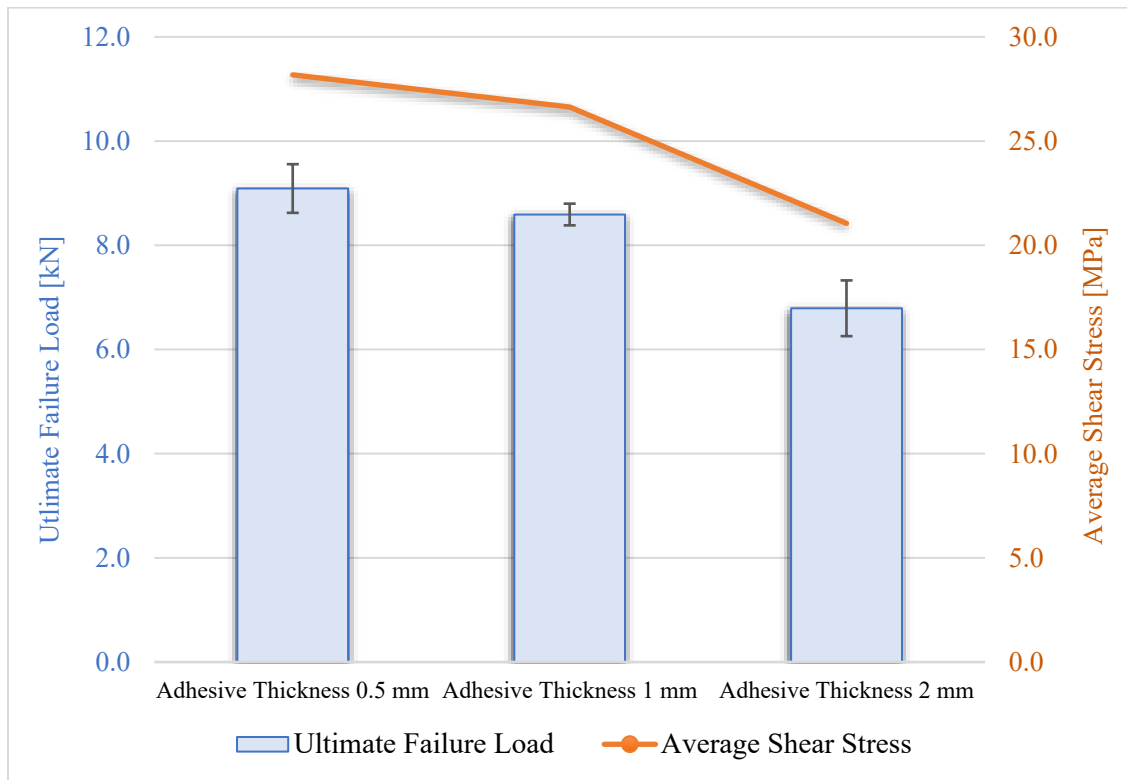


Figure 5.6 Effect of Adhesive Thickness on Single Lap Joints Bonded with Additive Manufacturing Substrates

The decrease in the mechanical performances of the SLJ concerning adhesive thickness is in contrast with the analytical models described: this means that they do not predict properly the performance of joints with different adhesive thicknesses. The reason for which the adhesive thickness lowers the ultimate failure load and the stiffness of the SLJ can be found in mainly two aspects:

- State of stress in the adhesive
- Failure mode shift

When considering higher adhesive thicknesses, the distance from the two adherends increases causing higher eccentricity of the loading and therefore higher peel stress.

The decrease of the stiffness can be discussed also from an analytical point of view; since the shear stress is proportional to the relative displacement between the two substrates and inversely proportional to adhesive thickness, defining  $K$  as the joint stiffness and  $u_1$ ,  $u_2$  as the displacements of the upper and lower substrates, respectively

$$K \propto \frac{F}{u_1 - u_2} \propto \frac{1}{t_{adh}} \quad (28)$$

The experimental measurements of the stiffness decrease, therefore, match with the analytical definitions of shear stress and stiffness. Moreover, the performance of the joint has decreased is due to the shift in failure mode: in the 0.5 mm adhesive thickness configuration, the failure has been perfectly cohesive, whereas, increasing the thickness, the failure tends to be more unbalanced. Indeed, in the 1 mm configuration, a crack in the middle of the adhesive can be noticed going from one substrate to the other, whereas in the 2mm joint, the adhesive remains attached completely just on one substrate leaving just a very thin layer on the other side (mixed mode failure).



Figure 5.7 Fracture Surface: Adhesive Thickness = 0.5 mm

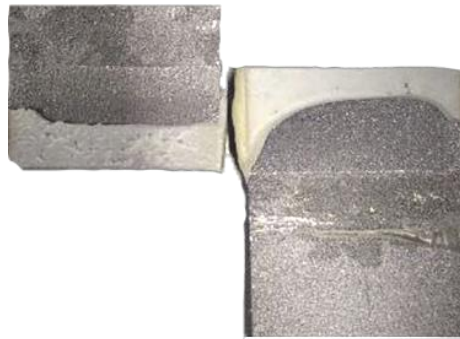


Figure 5.8 Fracture Surface: Adhesive Thickness = 1 mm

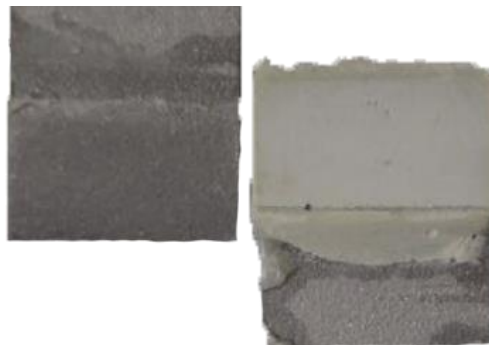


Figure 5.9 Fracture Surface: Adhesive Thickness = 2 mm

### 5.1.1.2 Effect of Overlap Length

The overlap length has shown to be a remarkable variable affecting the mechanical behavior of single lap joint: increasing the overlap (and thus the bonding area), the failure load of the joint increases noticeably. Also for this variable, four repetitions with the same adhesive thickness (i.e. 0.5 mm) have been performed to have statistically robust results. Two different overlaps have been considered: 12.7 mm and 19.05 mm (i.e. 0.5'' and 0.75'') and the P- $\delta$  curves for the increased overlap are shown in Figure 5.10. By choosing the most representative curve for each repetition, it is possible to appreciate the differences between the two configurations in Figure 5.11.

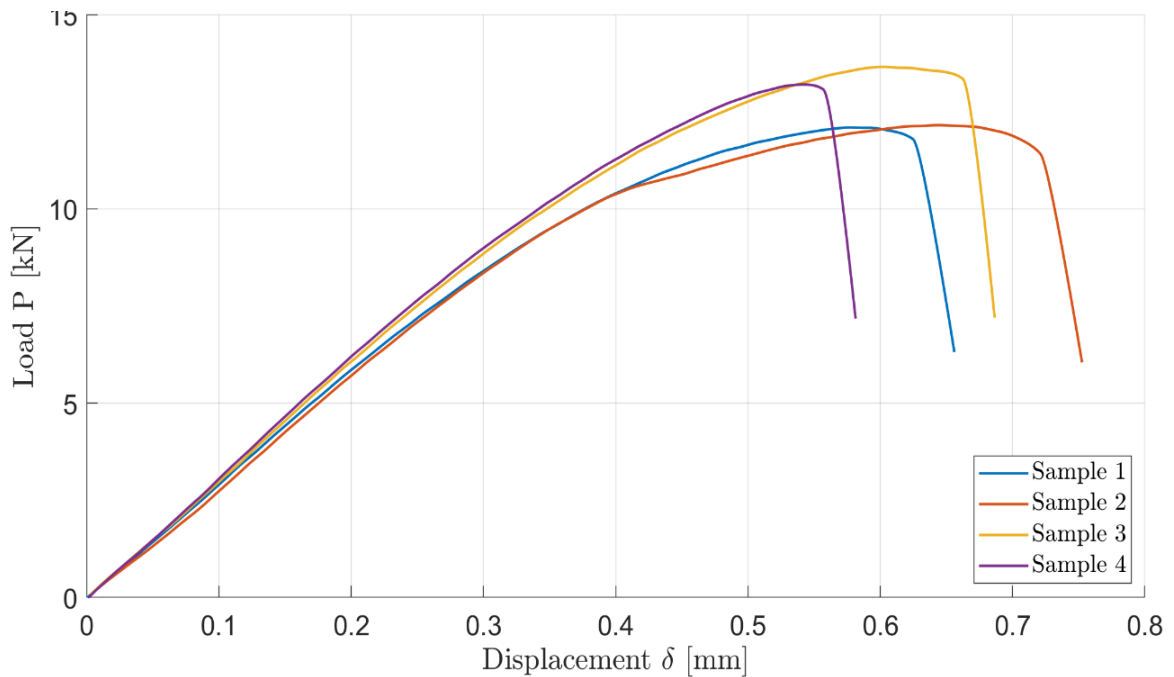


Figure 5.10 Load-Displacement Data for Overlap Length = 19.05 mm and Adhesive Thickness = 0.5 mm

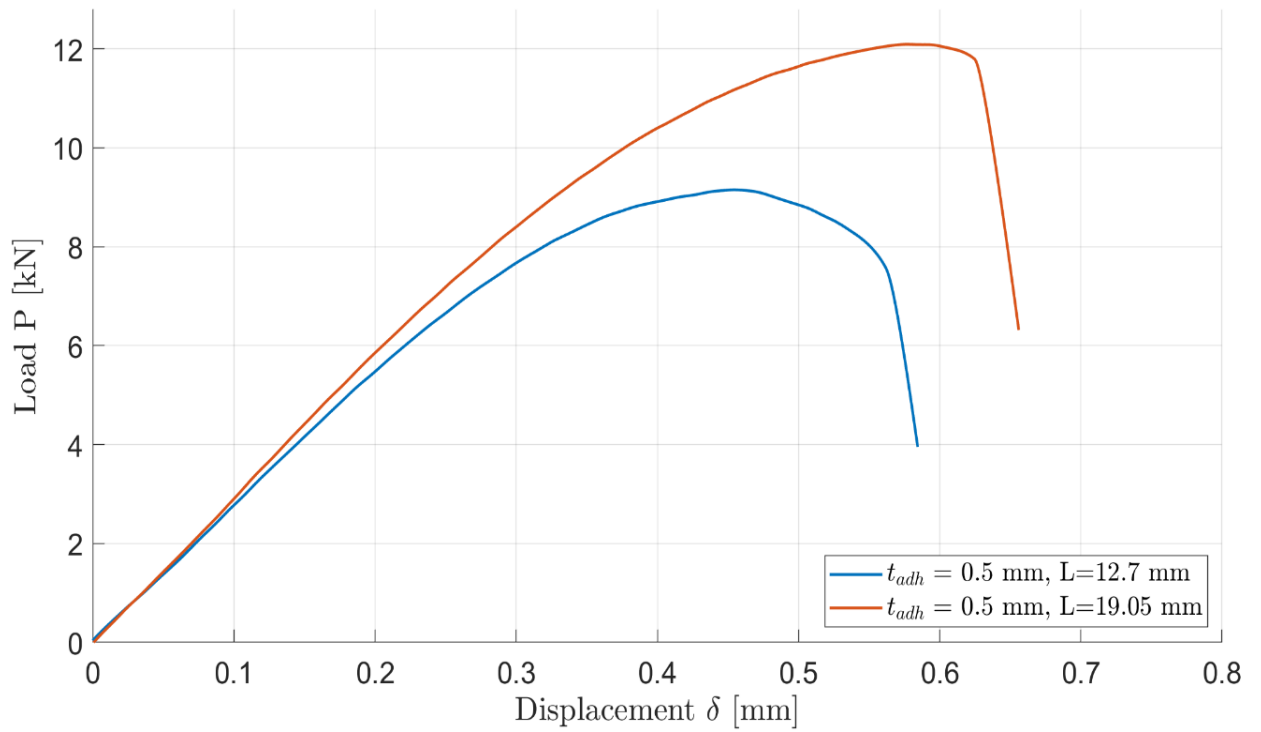


Figure 5.11 Average Load-Displacement Data for Different Overlap Lengths

Table 5.3 Effect of Overlap Length on Joint Failure Loads

		Failure Loads [kN]						
Overlap Length [mm]	Adhesive Thickness [mm]	#1	#2	#3	#4	Average	Standard Deviation	
12.7	0.5	9.50	8.42	9.15	9.28	9.09	0.467	
19.05	0.5	12.1	12.2	13.6	13.2	12.8	0.776	

Increasing the overlap length, also the stiffness of the joint tends to slightly increase (i.e. about 5%), whereas the ultimate failure load increases dramatically up to 40%. Indeed, when considering the largest overlap configuration, the load displacement curve tends to flatten close to the higher loads since there is a slight deformation of the substrates. In Figure 5.12, the results of the failure loads have been summarized with bar charts with the respective standard deviations. Analyzing the results obtained from the experimental testing, an interesting observation can be assessed: although the failure load increases dramatically, the average shear strength of the adhesive decreases when larger overlaps are considered.

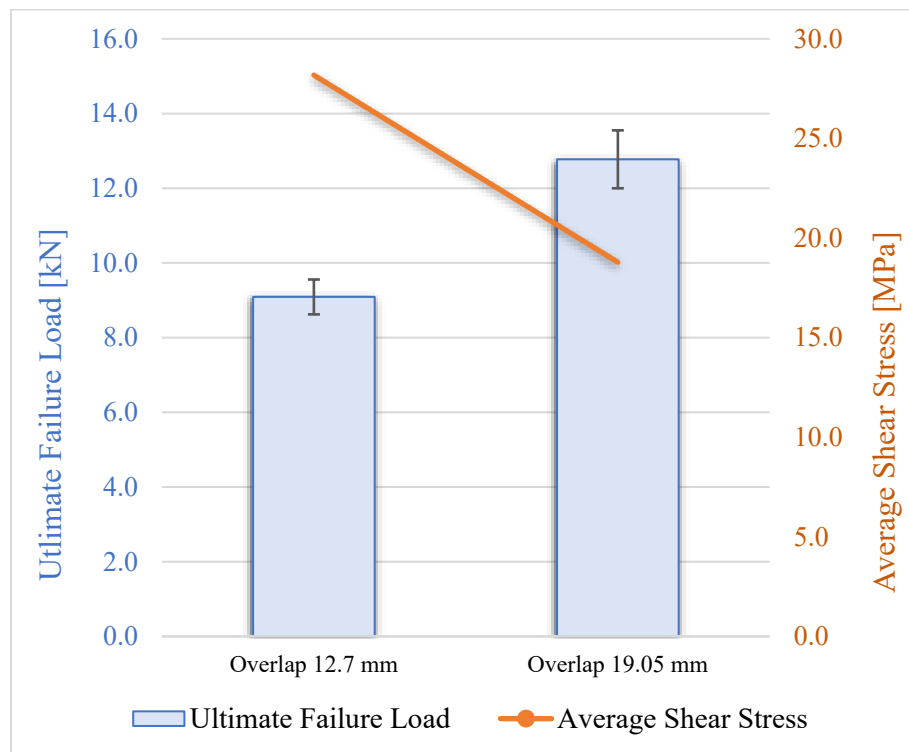


Figure 5.12 Effect of Overlap Length on Single Lap Joints Bonded with Additive Manufacturing Substrates

This can be explained in two different ways:

- The substrates start to slightly yield when loads beyond 10 kN are considered.
- The wave form of the stresses along the overlap of the adhesive: as shown in chapter two, analytical models show clearly that the shear stress have a U-shape, and the average shear stress is just an approximation. When the larger overlap is considered, the stresses in the ends of the overlap are much higher with respect to the average and therefore the final average will approximate worse the real performance of the adhesive.

Concerning the failure mode, although the adhesive thickness is the same (i.e. 0.5mm), the failure in the adhesive is shifted in the edges of the overlap (Fig. 5.13), where the stresses are higher with respect to Figure 5.7.

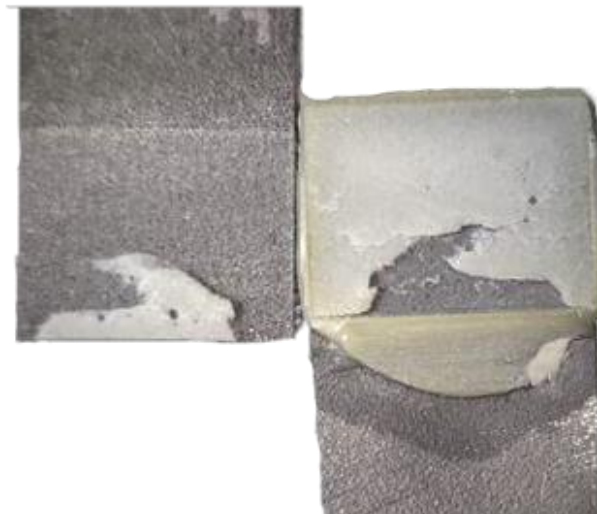


Figure 5.13 Fracture Surface of the Single Lap Joint with  $L = 19.05$  mm

### 5.1.1.3 Effect of Substrate Material

The substrate's material and surface roughness are fundamental for the bonding process of the joints. All the tests previously shown were conducted with the same substrate material for both adherends: 3D printed aluminum (i.e. AlSi 10 Mg). Comparing the obtained results with preliminary tests made by Stellantis with different substrates, it is possible to assess the influence of the surface on the adhesion and therefore, on the mechanical behavior of the SLJ. The considered geometry for these tests is quite different: the overlap length is 20 mm, the adhesive thickness 2mm and the joint is 60 mm wide. For this purpose, to compare the performances, it is necessary to divide the failure loads by the bonding area, considering the average shear strengths. In Figure 5.14 and 5.15, the AM-AM and AM-EXTR shear strengths are respectively reported.

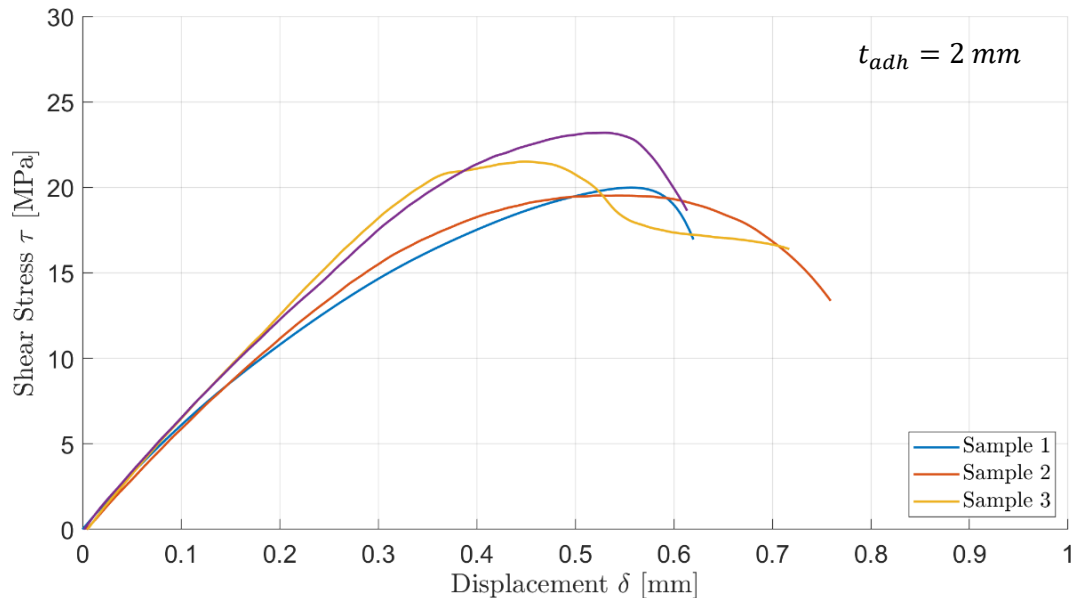


Figure 5.14 Joint Average Shear Stress with Additive Manufacturing Substrates

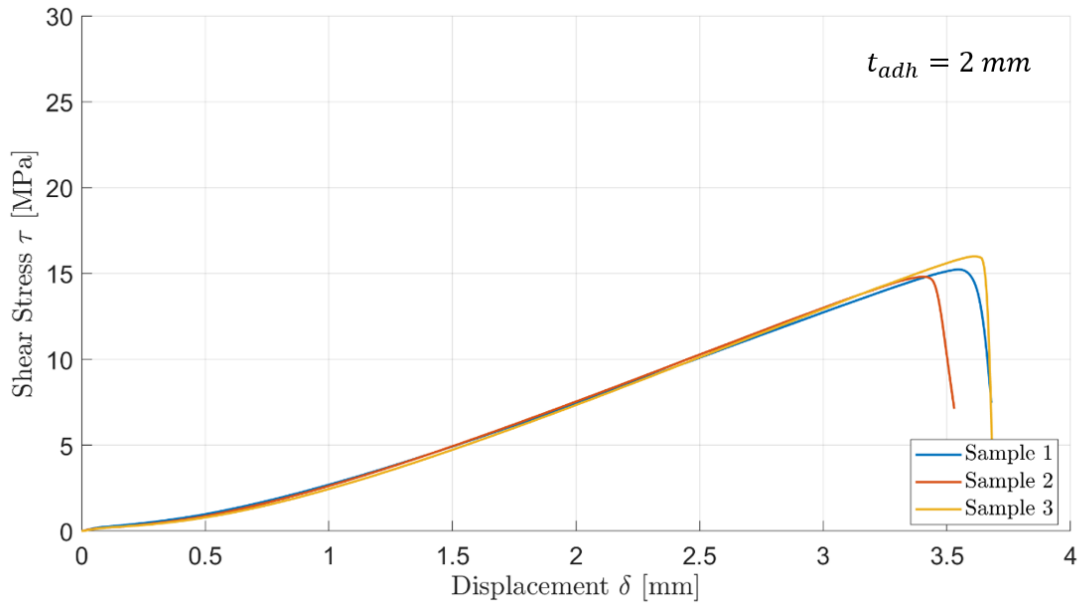


Figure 5.15 Joint Average Shear Stress with Additive Manufacturing and Extruded Substrates

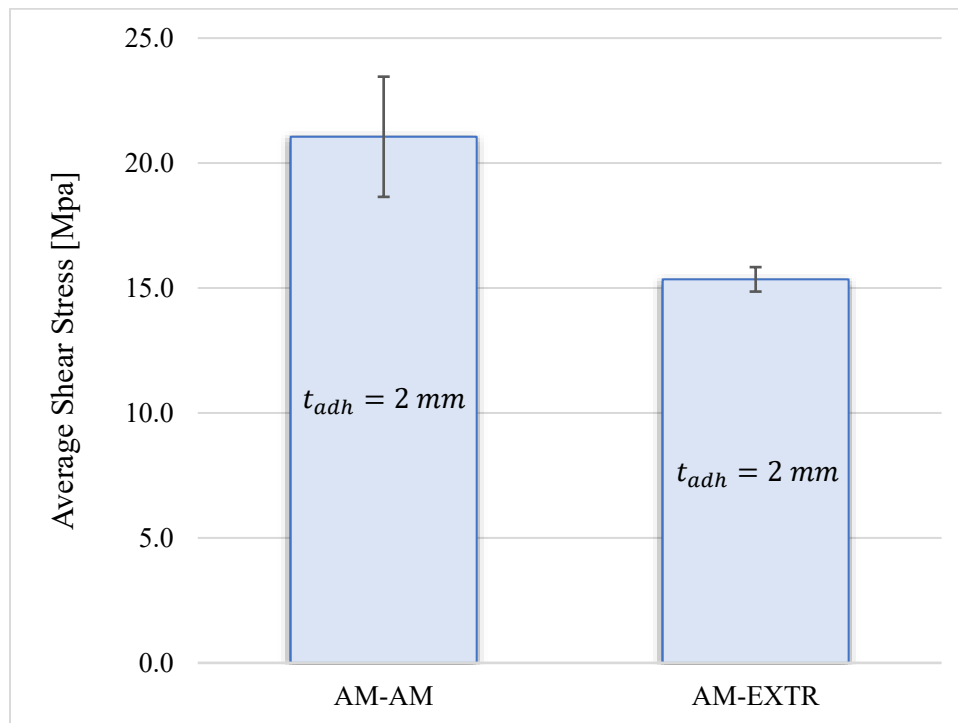


Figure 5.16 Comparison of Joint Strength: Additive Manufacturing vs. Extruded Substrates

Figure 5.16 shows that joint shear strength is higher when both substrates are made with additive manufacturing since the average shear stress increases by more than 40%, due to the stronger interfacial adhesion with AM substrates. When 2mm adhesive thickness configuration is considered, the failure mode is cohesive but shifted towards the interface leaving just a thin layer of adhesive on the other side. In the mixed configuration, the interaction between the adhesive and the substrate made with regular extruded aluminum (6082-T6) is much weaker, decreasing remarkably the mechanical performances of the joint. All the results are summarized in Table 5.4.

Table 5.4 Summary of the Single Lap Joint Shear Tests with Additive Manufacturing Substrates

Substrates	Adhesive Thickness [mm]	Overlap Length [mm]	Ultimate Failure Load [N]	Average Shear Stress [MPa]	Experimental Stiffness [kN/mm]	Failure Mode
<b>AM-AM</b>	0.5	12.7	9,090 ± 467	28.2	29.5 ± 1.80	COHESIVE
<b>AM-AM</b>	1	12.7	8,591 ± 208	26.6	26.7 ± 1.88	COHESIVE
<b>AM-AM</b>	2	12.7	6,791 ± 535	21.1	23.2 ± 1.90	MIXED MODE
<b>AM-AM</b>	0.5	19.05	12,774 ± 776	18.8	31.9 ± 2.14	COHESIVE

### 5.1.2 Fracture Toughness Tests

Double Cantilever Beam testing is used for evaluating the mode I fracture toughness of the adhesive joints for the cohesive zone modeling using FEA. Each test is repeated five times. In Fig. 5.17, the load displacement curves have been reported showing very good repeatability of the experiment since the adhesive behavior does not change much.

The  $P$ - $\delta$  curves are crucial for the estimation of the equivalent crack length during the experiment: indeed, the considered crack length is not the one visualized during the testing but it is evaluated through the CBBM which takes into account of the plasticity of the fracture process zone. In Fig. 5.18 and 5.19 respectively, the compliance from the ratio  $\delta/P$  and the calculated equivalent crack length are reported.

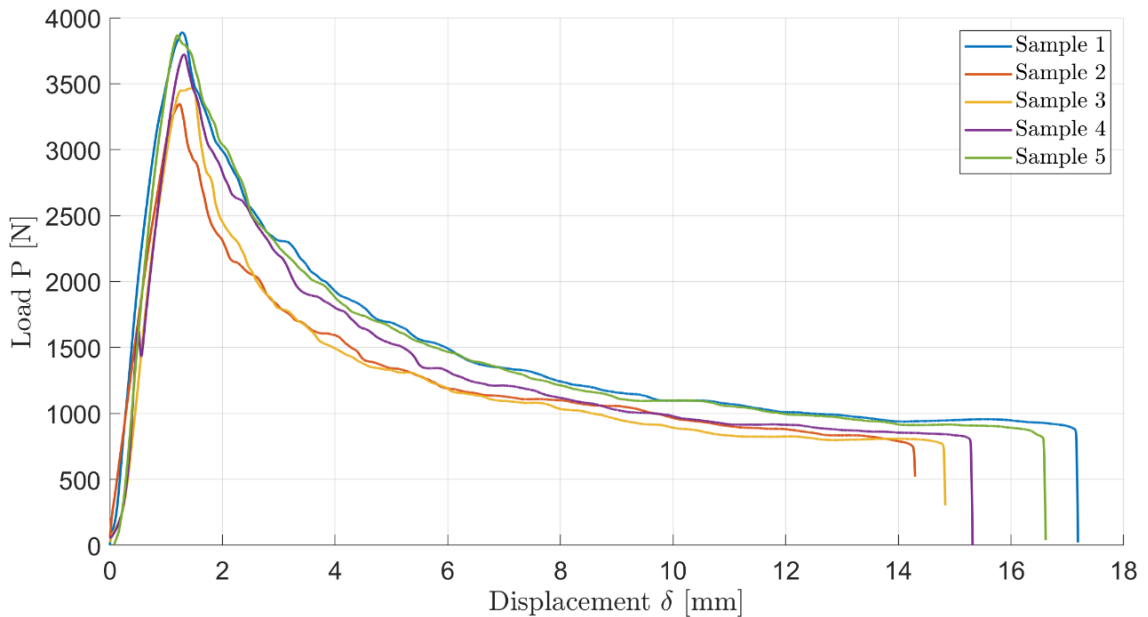


Figure 5.17 Double Cantilever Beam Load-Displacement Curves

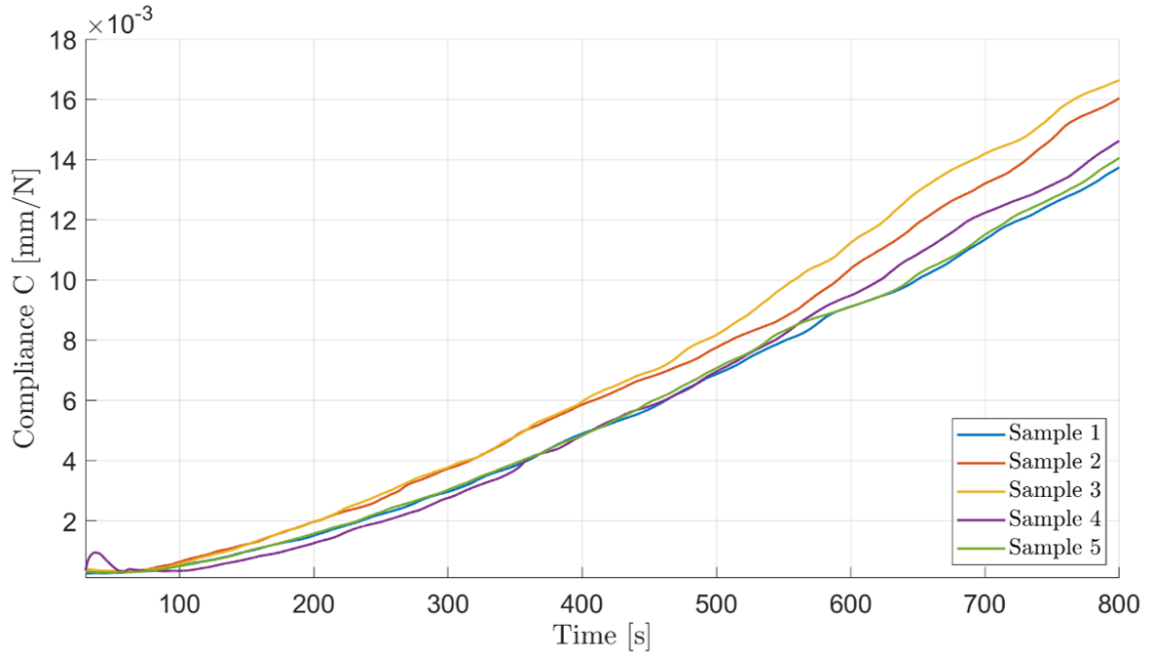


Figure 5.18 Double Cantilever Beam Compliance

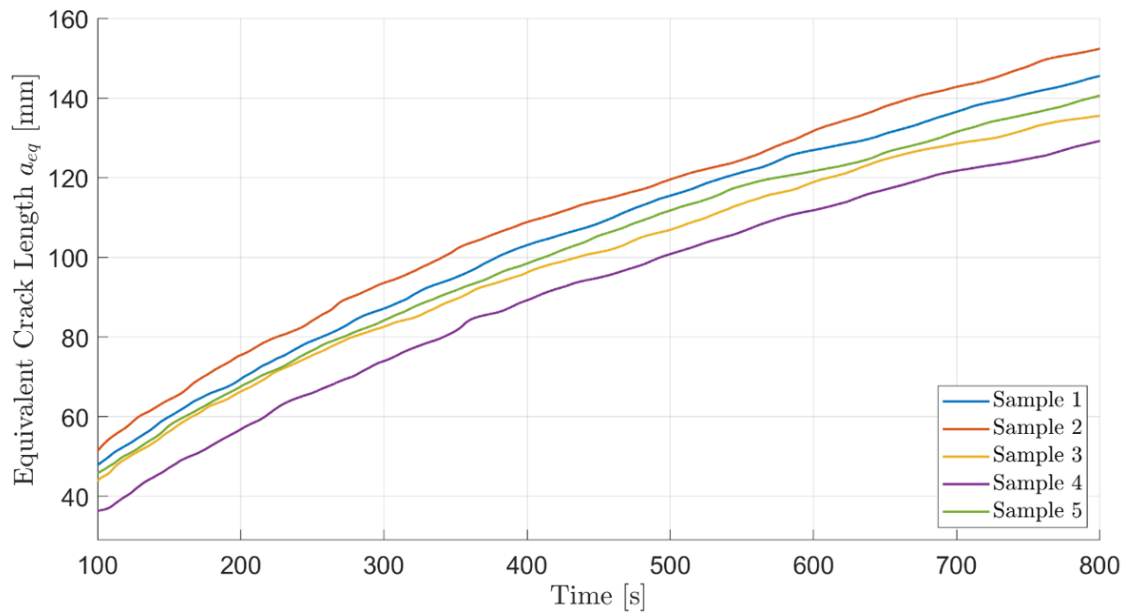


Figure 5.19 Double Cantilever Beam Equivalent Crack Length

From Fig. 5.18, it is possible to evaluate the parameter  $C_0$  which is crucial for the estimation of the flexural modulus of the beams: it can be read in the constant part of the curve for each repetition. In this way it is possible to calculate the equivalent crack length in Fig. 5.19, which is slightly larger than the one that could be observed by external monitoring of the experiment (Fig. 5.20).



Figure 5.20 Crack Length Measurement

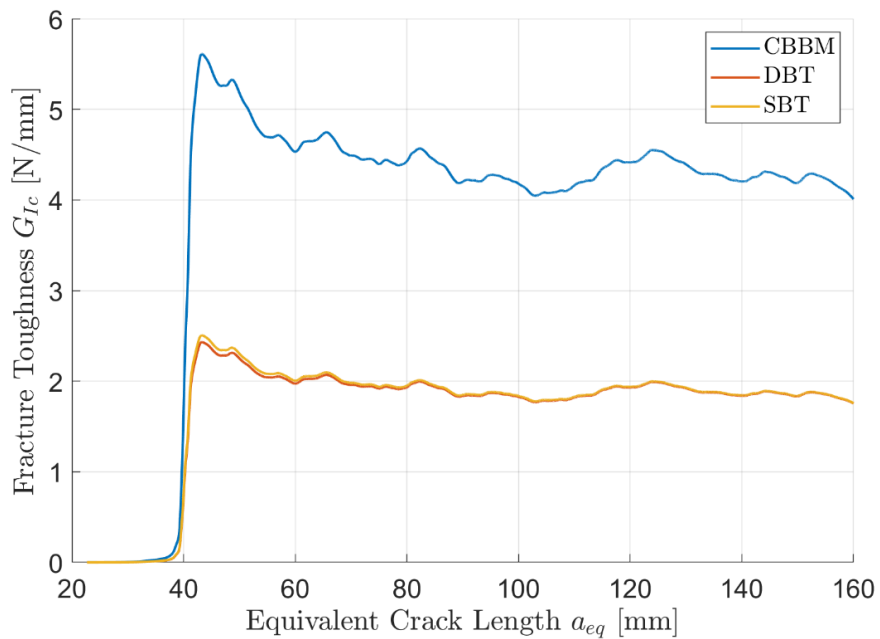


Figure 5.21 Comparison of Single Beam Theory, Double Beam Theory and Compliance Based Beam Method

From Figure 5.21, the fracture toughness evaluated with the compliance based beam method is compared to the ones obtained with the simple beam theory and double beam theory by considering the same equivalent crack length calculated through CBBM. It is worth noting that the substantial difference among the considered data reduction schemes is due to the huge difference of the flexural modulus with respect to Young's one and the fact that the crack tip is not measured visually for SBT and DBT. The CBBM, therefore, allows better evaluation of the crack tip position, thus more precision with respect to SBT or DBT, by just measuring the P- $\delta$  curve. From Table 5.4, the summary of the results obtained by the double cantilever beams are reported showing very good repeatability on the mode I fracture toughness. This numerical parameter is fundamental to properly tune and characterize the finite element cohesive model of the adhesive that will be discussed in the next paragraph.

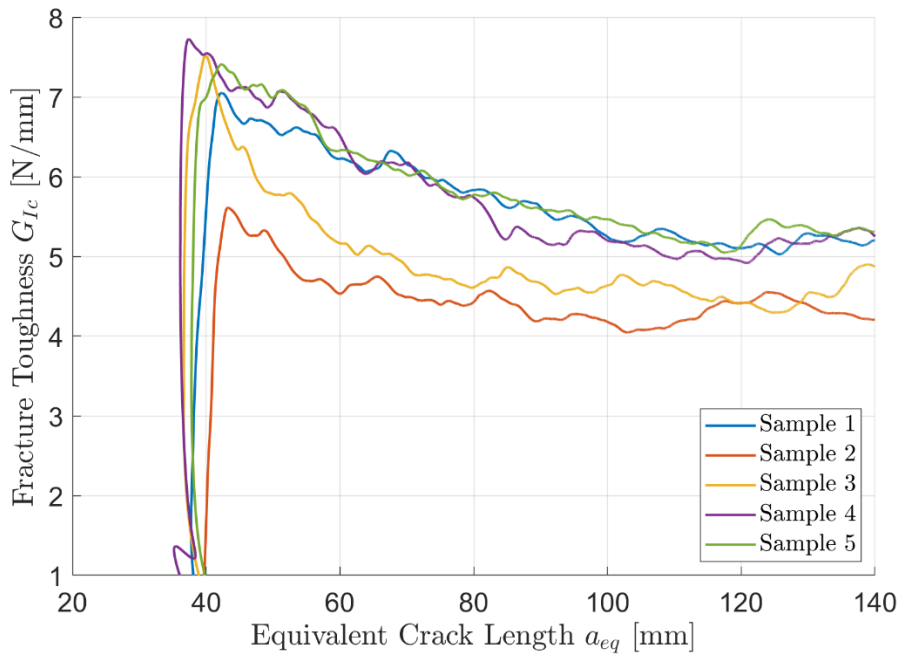


Figure 5.22 Mode I Fracture Toughness from Double Cantilever Beam

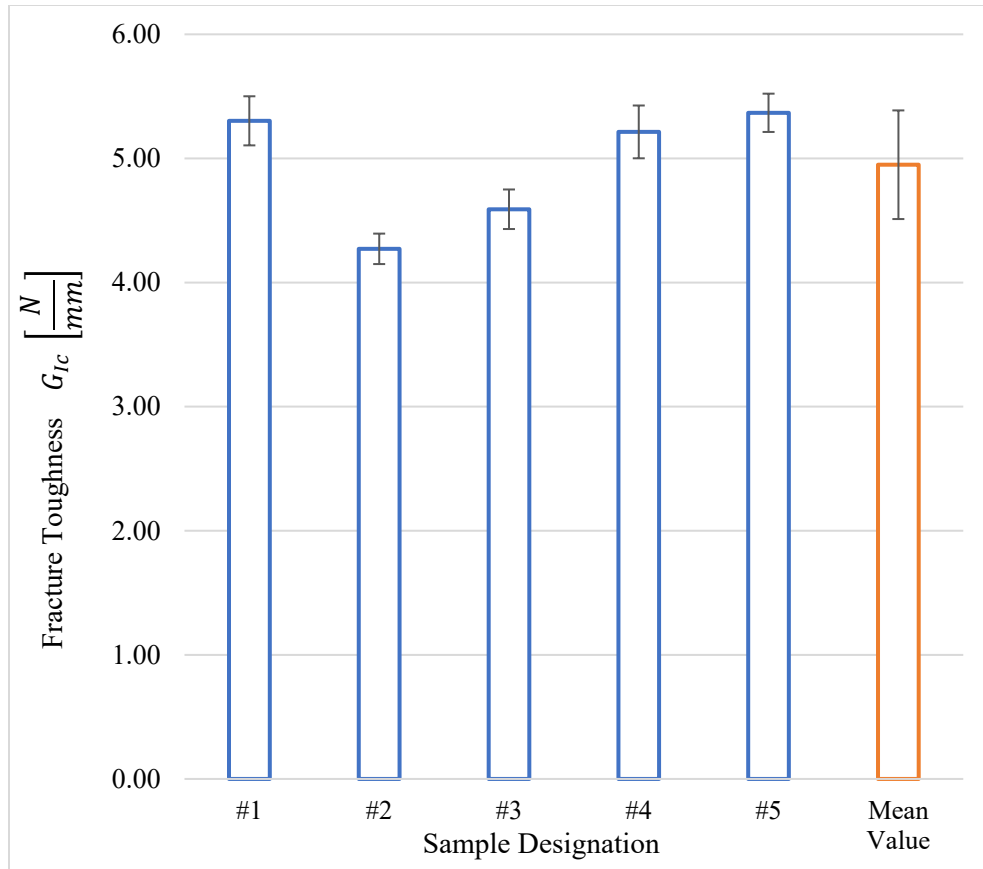


Figure 5.23 Mode I Fracture Toughness Test Data

Table 5.5 Mode I Fracture Toughness

Overlap Length [mm]	Adhesive Thickness [mm]	#1 [N/mm]	#2 [N/mm]	#3 [N/mm]	#4 [N/mm]	#5 [N/mm]	Average Value [N/mm]
250	1.0	5.30	4.27	4.59	5.21	5.37	4.95 ± 0.44

## 5.2 Finite Element Results

### 5.2.1 Single Lap Joint

In this section, the FEA results can finally be obtained after having characterized the main adhesive parameters for each configuration: indeed the main drawback of the CZM is the need of calibrating for each adhesive thickness the right numerical values. Therefore, in Figures 5.24, 5.25, and 5.26 the mechanical behavior predicted with the FEA of the SLJs with different adhesive thicknesses can be appreciated. The very first observations to do are concerning the adherends:

- Stress distributions are symmetric.
- The stress in the adherends (Von Mises) increases up to 190 MPa until the adhesive gets damaged and starts to lose its load transfer capability.
- The deflections and the rotations of the adherends due to the eccentric load are limited and the yielding limit is not reached.

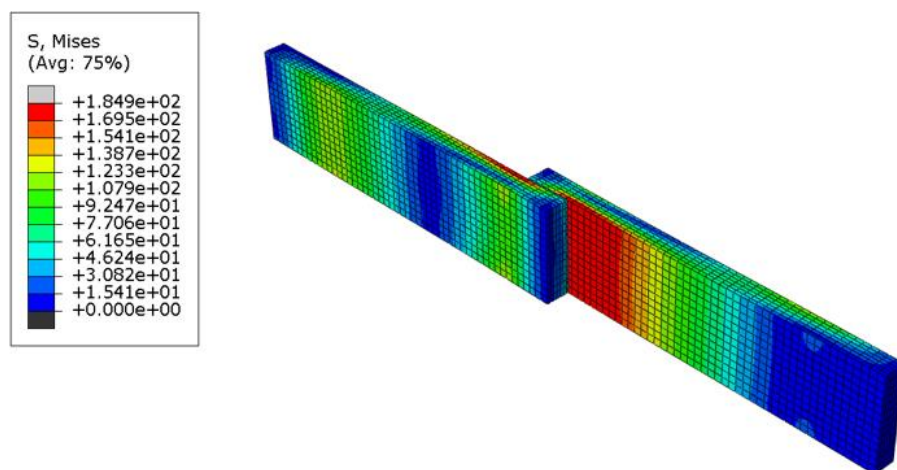


Figure 5.24 Finite Element Analysis: Single Lap Joint Shear Testing with Adhesive Thickness 0.5 mm and Overlap Length 12.7 mm

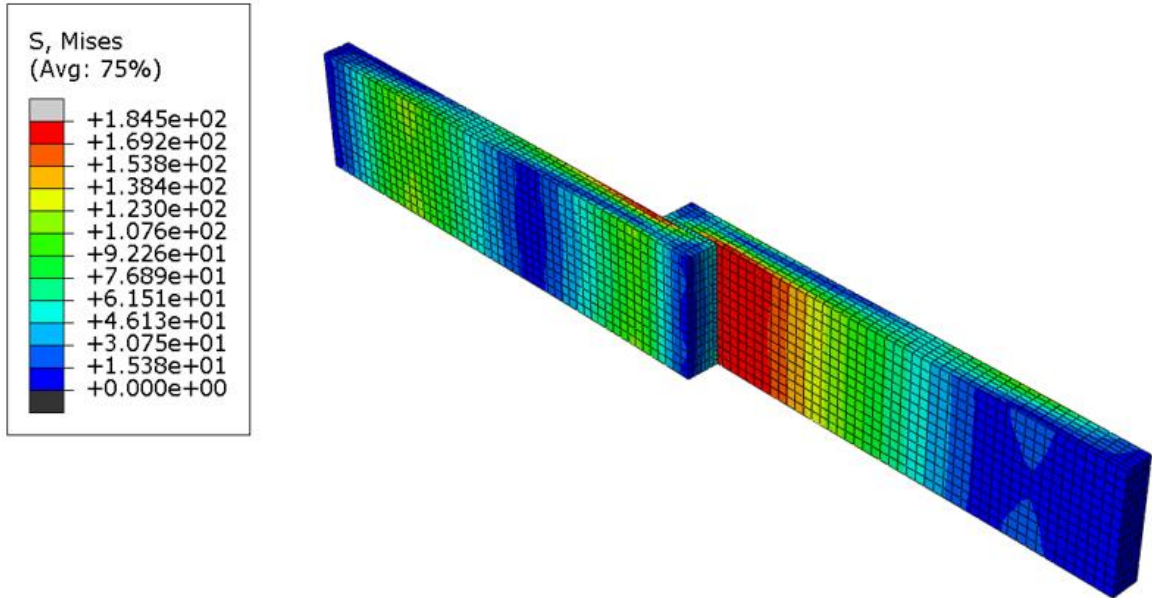


Figure 5.25 Finite Element Analysis: Single Lap Joint Shear Testing with Adhesive Thickness 1 mm and Overlap Length 12.7 mm

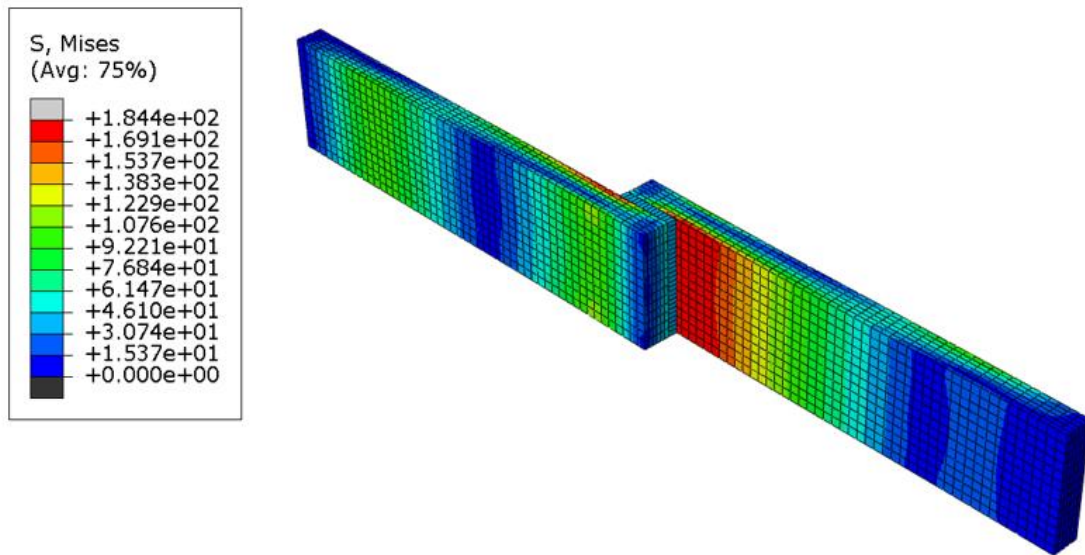


Figure 5.26 Finite Element Analysis: Single Lap Joint Shear Testing with Adhesive Thickness 2 mm and Overlap Length 12.7 mm

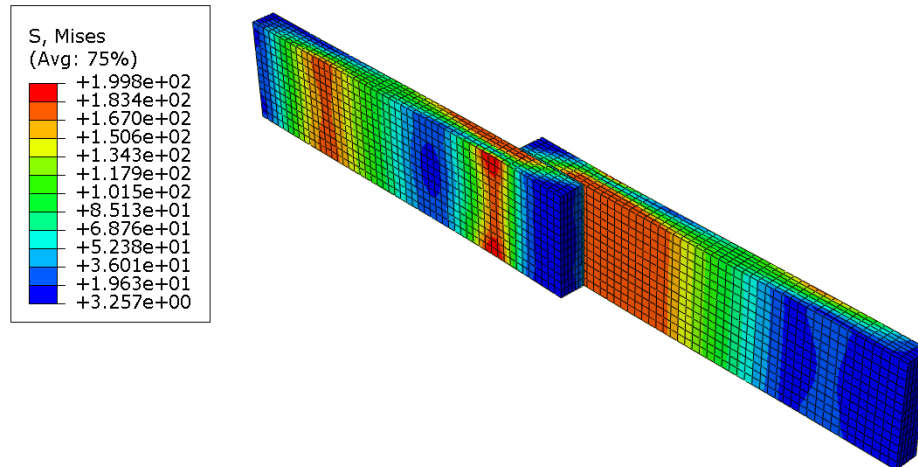


Figure 5.27 Finite Element Analysis: Single Lap Joint Shear Testing with Adhesive Thickness 0.5 mm and Overlap Length 19.05 mm

In Figure 5.27, the overlap length has been increased, and therefore a larger region of the adherend is more loaded (up to 200 MPa). It is very interesting to also observe the behavior of the adhesive in the finite element model; many parameters can be used to check the evolution of the adhesive characteristics during the test, such as the Quadratic Nominal Stress Damage Initiation Criterion (QUADSCRT) which allows to understand when the adhesive starts to get damaged, or the Stiffness Degradation (SDEG) which instead allows to understand how far the damage has gone. In Figure 5.28, QUADSCRT in the adhesive is reported showing how the adhesive passes almost uniformly over its elastic limit (when the DAMAGE=1). Indeed, there are, as expected in a proper modeling of the adhesive behavior, more loaded zones on the overlap ends of the adhesive. Nevertheless, since the considered overlaps are really small, the adhesive layer will more or less degrade uniformly as shown in Figure 5.29. This is due mainly to the short overlap, showing that the simplified stress model can represent this phenomenon.



Therefore, the load displacement curves obtained through FE analysis can be compared with the experimental ones. Concerning the influence of adhesive thickness, looking at Figure 5.30, it is possible to appreciate how the numerical curves fit the experimental ones. The stiffness of the experimental curves slightly changes when the displacement increases, showing how in reality the non-perfect adhesion of the bonding with the substrates cannot be fully modelled with the cohesive zone elements. Therefore the numerical stiffness is very close just to the initial values of the experimental curves. As it can be noticed, the FEA is a much more reliable tool with respect to the analytical models, since it is able to predict with much more accuracy the final failure load of the joint when different thicknesses of the adhesive are considered.

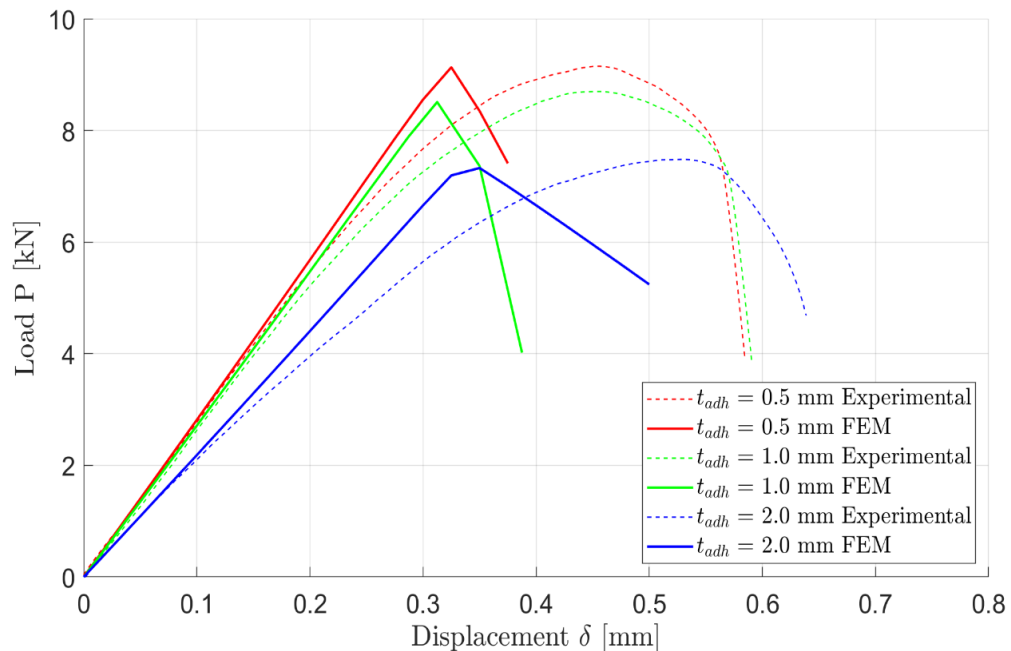


Figure 5.30 Effect of Adhesive Thickness on Load-Displacement Curves: Comparison Finite Element Analysis vs. Experimental Tests

The results can be numerically summarized in Table 5.6, the slight differences among the numerical models and the actual tests can be noticed. The prediction of the final failure load is very reliable based on the data provided by the different shear tests made, whereas the stiffness of the FEM tends to be slightly higher than the real testing (of about 10%). This can be explained with the lateral contraction blocking phenomenon, which in the FEM is present: in other words, all the elements of the adhesive are perfectly stretched by the adherend displacement, whereas in reality, each element of the adhesive is stretched in a different way slightly influencing the final stiffness of the joint.

Table 5.6 Effect of Adhesive Thickness on Joint Behavior: Comparison FEA vs. Experimental Tests

Substrates	Adhesive Thickness [mm]	Overlap Length [mm]	EXP Ultimate Failure Load [N]	FEM Ultimate Failure Loads [N]	EXP Stiffness [kN/mm]	FEM Stiffness [kN/mm]
<b>AM-AM</b>	0.5	12.7	9,090 ± 467	9,130	29.5 ± 1.80	28.0
<b>AM-AM</b>	1	12.7	8,591 ± 208	8,510	26.7 ± 1.88	26.96
<b>AM-AM</b>	2	12.7	6,791 ± 535	7,330	23.2 ± 1.90	21.74

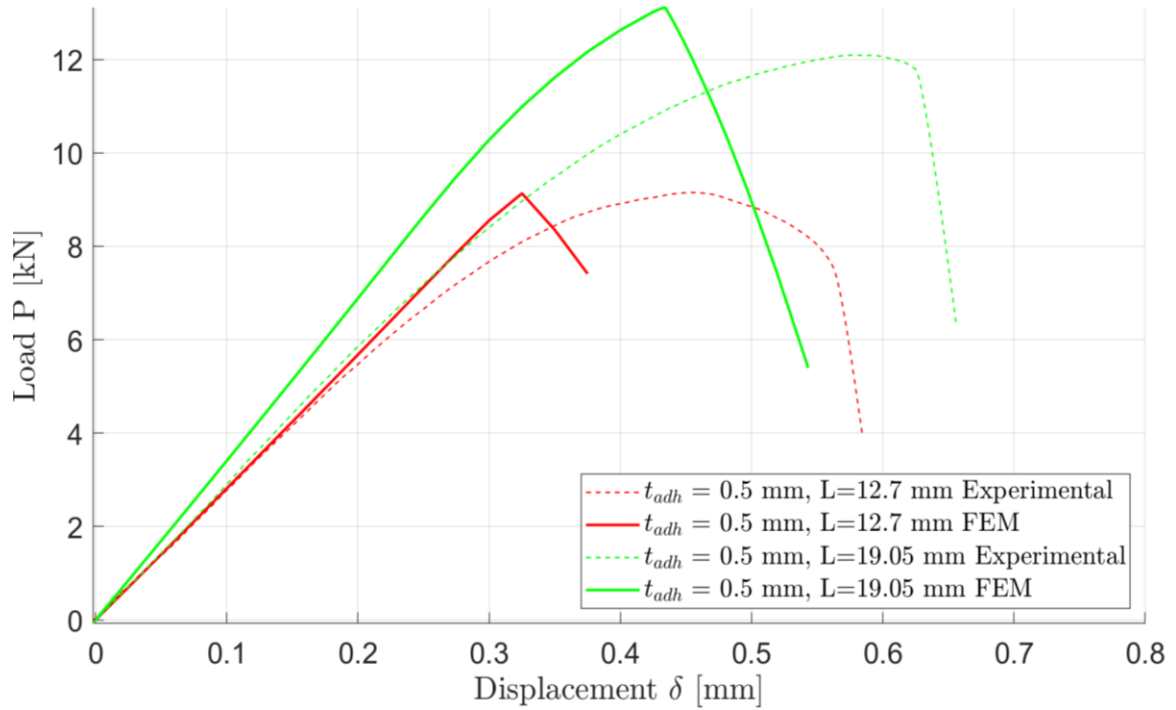


Figure 5.31 Effect of Overlap Length on Joint Load-Displacement Data: Comparison Finite Element Analysis vs. Experimental Tests

Table 5.7 Effect of Overlap Length on Joint Behavior: Comparison FEA vs. Experimental Tests

Substrates	Adhesive Thickness [mm]	Overlap Length [mm]	EXP Ultimate Failure Load [N]	FEM Ultimate Failure Loads [N]	EXP Stiffness [kN/mm]	FEM Stiffness [kN/mm]
AM-AM	0.5	12.7	9,090 ± 467	9,130	29.5 ± 1.80	28.0
AM-AM	0.5	19.05	12,774 ± 776	12,659	31.9 ± 2.14	33.89

The overlap length effect on the mechanical behavior of SLJs is assessed: it matches exactly with what has been predicted with the analytical models. Indeed, analytically the stress in the adhesive along the overlap decreases as the overlap length increases: it means that the joint will be able to resist to higher loads and this is verified by the FEA model passing from 9.13 kN as ultimate failure load up to 12.7 kN with an increase of about 30%. The FEA is also to predict the increased stiffness of the joint when larger overlaps are considered.

### 5.2.2 Sample Automotive Application

After the experimental characterization of the adhesive and the numerical validation of the models, it is possible to apply the traction separation law (TSL) used for each adhesive thickness to a real automotive joint application. A sample automotive joint made with extruded aluminum and 3D printed AlSi 10 Mg that were bonded together with the previously described NCA adhesive (Figures 5.32 and 5.33) is considered. FEA results show some plasticity zones in the aluminum sliding *female* joint, indicating that the adhesive is not the *weak link* in the design: this highlights the advantage of using a reliable predictive FEA tool for structural design, which saves both time and cost of experimental testing of the components. Examination of damage initiation zones in the adhesive layer (Fig. 5.34) allows further processes iterations in order to allow better adhesion and to reduce or even eliminate the adhesive in other locations with low stress. It can be observed that the adhesive stiffness is not completely degraded in the joint, indicating that the adherends are less resistant with respect to the adhesive and that the capability of the adhesive is not fully utilized. Moreover the upper part of the structural adhesive layer is not loaded at all, whereas in the bottom side, the damage has started and

therefore, the performances will be affected. In the end, the load displacement curve associated to the sample automotive bonded joint is reported in Fig. 5.35, highlighting the point where the damage in the adhesive starts (i.e. QUADSCRT=1.0).

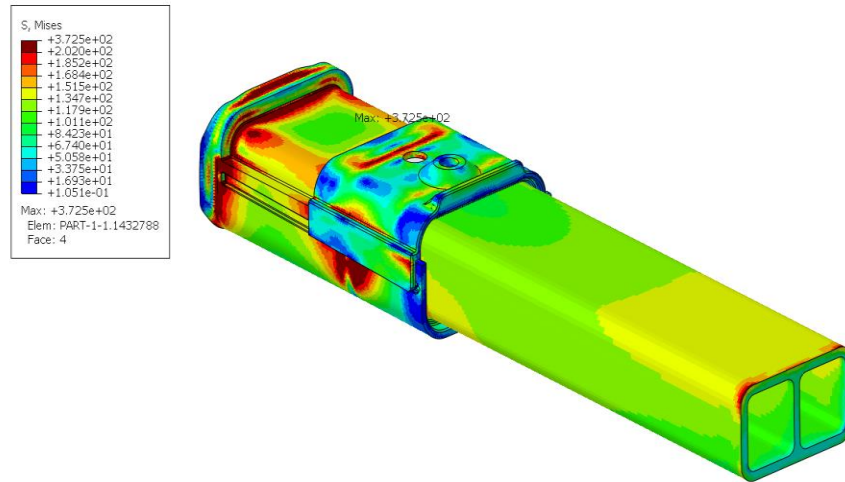


Figure 5.32 Equivalent Stress in the Sample Automotive Bonded Joint: Overall View

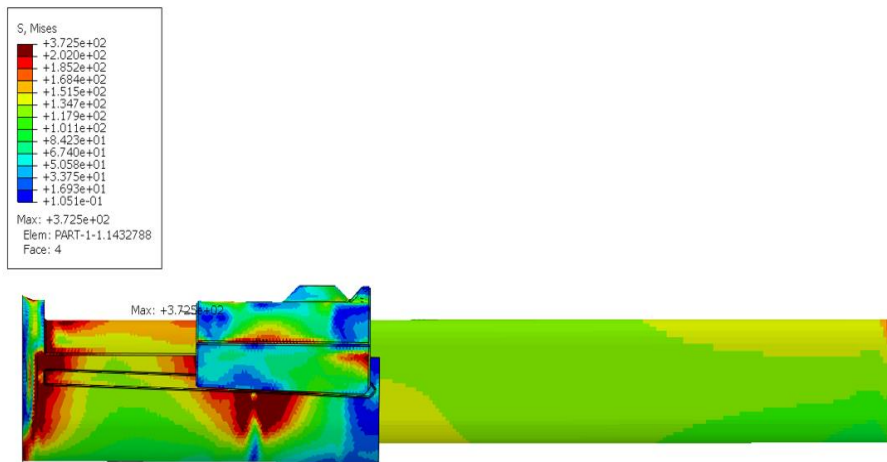


Figure 5.33 Equivalent Stress in the Sample Automotive Bonded Joint: Lateral View

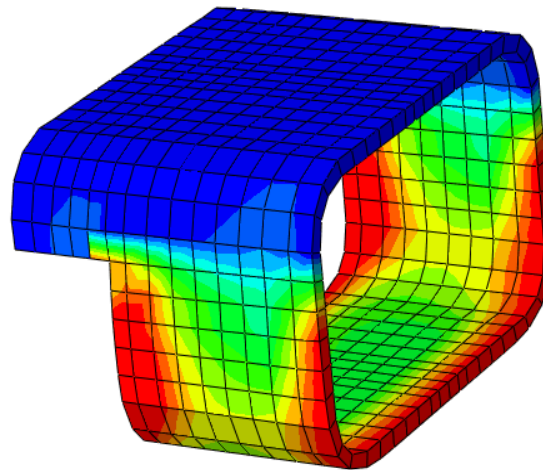
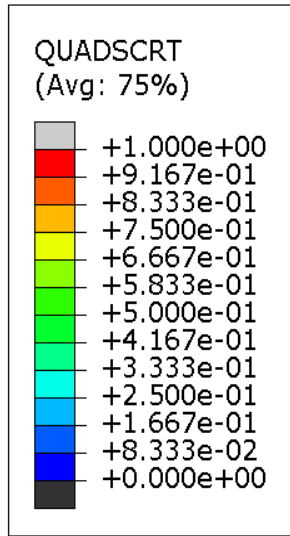


Figure 5.34 Quadratic Nominal Stress in the Sample Automotive Bonded Joint Adhesive

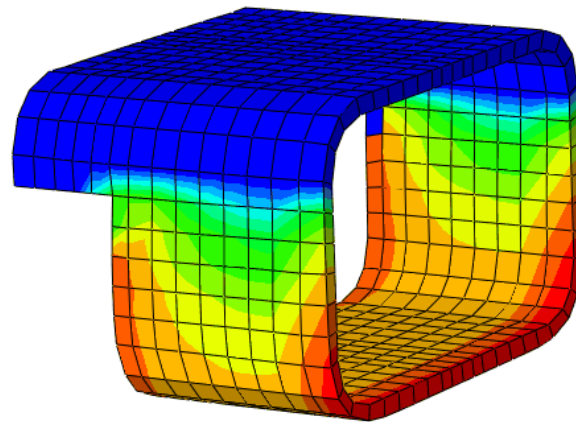
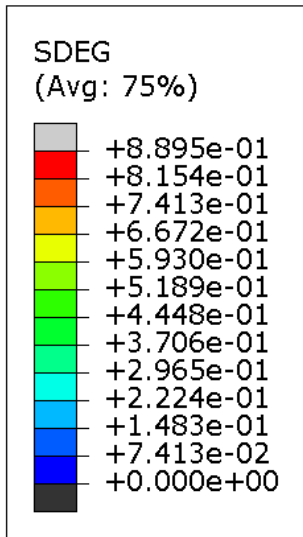


Figure 5.35 Stiffness Degradation in the Sample Automotive Bonded Joint Adhesive

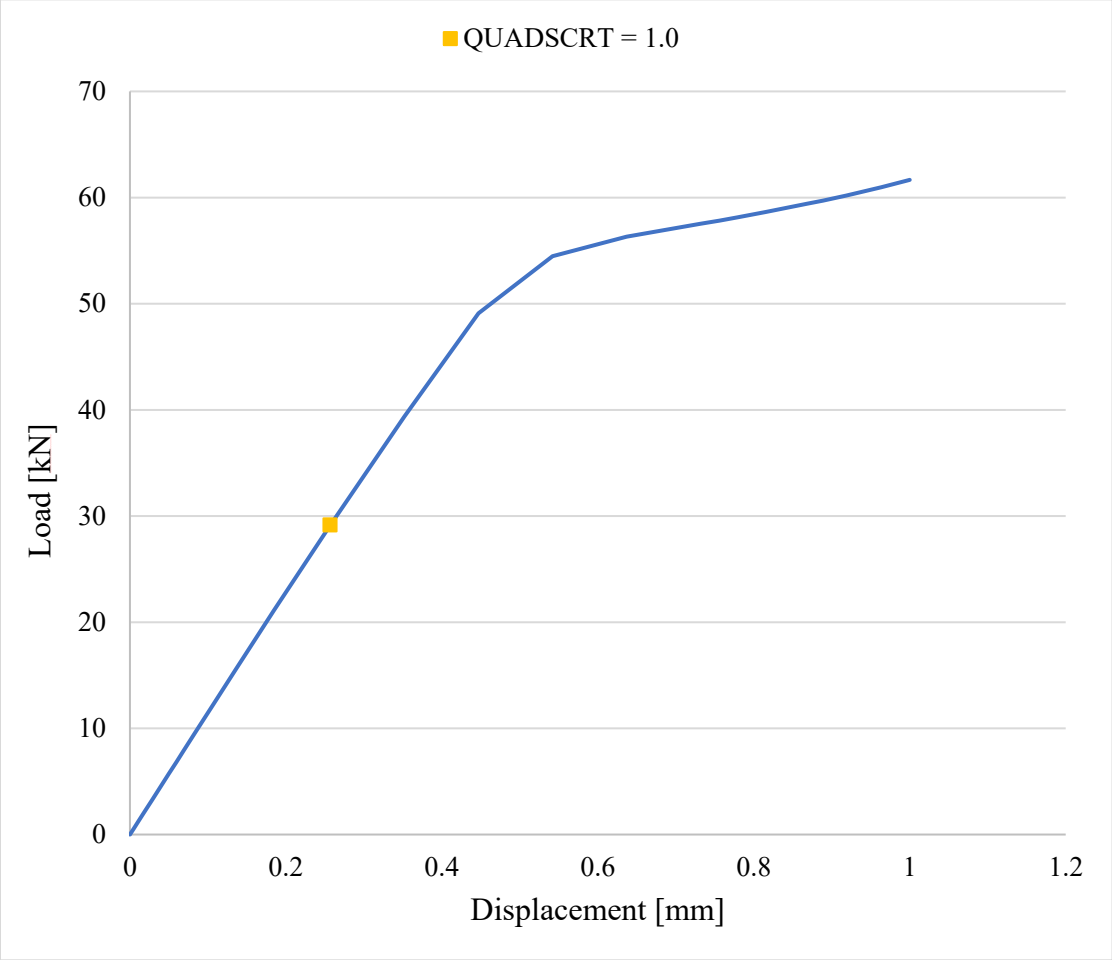


Figure 5.36 Sample Automotive Bonded Joint Load Transfer Capacity

## CHAPTER SIX

### CONCLUSIONS

#### 6.1 Conclusions

In this study, the effect of key design variables on adhesively bonded joints made with additive manufacturing substrates are assessed and compared with extruded substrates using analytical and experimental methods. Experimental results showed a substantial difference in the performances of the single lap joint made with additive manufacturing substrates as compared to regularly extruded substrates; higher AM surface roughness allowed better adhesion with the adhesive that resulted in higher shear strength of the joint.

Increasing the adhesive thickness lowers the shear strength of the joint, which is in contrast with the predictions by Volkersen and Goland-Reissner models that do not include the adhesive thickness strength variations.

#### 6.2 Continuation Studies

Future work could involve considering other load cases (e.g. Fatigue and Impact) to assess the overall mechanical characteristics of adhesive joints also on dynamic loads.

Other variables may be investigated such as the strain rate, the heat and moisture effect.

## REFERENCES

- [1] Lucas F.M. da Silva, Paulo J.C. das Neves, R.D. Adams, J.K. Spelt, 2009, *International Journal of Adhesion & Adhesives*, “Analytical Models of Adhesively Bonded Joints – Part I: Literature Survey”, V.29, pp. 319-330.
- [2] Lucas F.M. da Silva, Paulo J.C. das Neves, R.D. Adams, A. Wang, J.K. Spelt, 2009, *International Journal of Adhesion & Adhesives*, “Analytical Models of Adhesively Bonded Joints – Part II: Comparative Study”, V.29, pp. 331-341.
- [3] R.D. Adams, N.A. Peppiat, 1974, *The Journal of Strain Analysis for Engineering Design*, “Stress Analysis of Adhesive-Bonded Lap Joints”, V.9, pp.185-196.
- [4] M. Banea, M. Rosioara, R.Carbas, L. da Silva, 2018, “Multi Material Adhesive Joints for Automotive Industry”, *Composite Part B, Volume 150*, pp.71-77
- [5] R. Garcia, P. Prabhakar, 2017 “Bond interface design for single lap joints using polymeric additive manufacturing”, *Composite Structures, Volume 176*, pp. 547-555.
- [6] J. M. Arenas, Cristina Alia, F. Blaya, A. Sanz, 2012, *International Journal of Adhesion & Adhesives*, “Multi-criteria selection of structural adhesives to bond ABS parts obtained by rapid prototyping”, V.33, pp. 67-74.
- [7] M. Frascio, L. Bergonzi, M. Jilich, F. Moroni, M. Avalle, A. Pirondi, M. Monti, M. Vettori, 2019, *Acta Polytechnica CTU Proceedings*, “Additive Manufacturing Process Parameter Influence on Mechanical Strength of Adhesive Joints, Preliminary Activities”, V.25, pp.41-47.
- [8] M. Frascio, C. Mandolino L. Bergonzi, M. Jilich, F. Moroni, M. Avalle, A. Pirondi, M. Monti, M. Vettori, 2021, *International Journal of Adhesion & Adhesives*, “Appraisal of surface preparation in adhesive bonding of additive manufactured substrates”, V.106, pp.1-9.
- [9] Raul D.S.G. Campilho, 2017, “Strength Prediction of Adhesively-Bonded Joints”, Taylor & Francis Group.
- [10] Lucas F.M. da Silva, A. Ochsner, R. D. Adams, 2008, “Modeling of Adhesively Bonded Joints”, Springer.

## REFERENCES

- [11] Lucas F.M. da Silva, A. Ochsner, R. D. Adams, 2018, “Handbook of Adhesion Technology”, Springer.
- [12] X. Zhao, R.D. Adams, Lucas F.M. da Silva, 2010, International Journal of Adhesion & Adhesives, “A New Method for the Determination of Bending Moments in Single Lap Joints”, V.30, pp. 63-71.
- [13] M.F.S.F. de Moura, R.D.S.G. Campilho, J.P.M. Goncalves, 2008, “Crack Equivalent Concept applied to the fracture characterization of bonded joints under pure mode I loading”, Composites Science and Technology, Volume 68, pp. 2224-2230.
- [14] M.F.S.F. de Moura, J.J.L. Morais, N. Dourado, 2008, “A New Data Reduction Scheme for Mode I Wood Fracture Characterization using the DCB test”, Engineering Fracture Mechanics, Volume 75, pp. 3852-3865.
- [15] F. Sun, B.R.K. Blackman, 2020, “A DIC Method to Determine the Mode I Energy Release Rate  $G$ , the  $J$ -integral and the Traction-Separation Law simultaneously for Adhesive Joints”, Engineering Fracture Mechanics, Volume 234, pp. 1-13.
- [16] R.L. Fernandes & R.D.S.G. Campilho (2019) Accuracy of cohesive laws with different shape for the shear behavior prediction of bonded joints, The Journal of Adhesion, 95:4, 325-347
- [17] J.J.G. Oliveira, R.D.S.G. Campilho, F.J.G. Silva, E.A.S. Marques, J.J.M. Machado & L.F.M. da Silva (2020) Adhesive thickness effects on the mixed-mode fracture toughness of bonded joints, The Journal of Adhesion, 96:1-4, 300-320
- [18] Yu Sekiguchi, Masato Katano & Chiaki Sato (2017) Experimental study of the Mode I adhesive fracture energy in DCB specimens bonded with a polyurethane adhesive, The Journal of Adhesion, 93:3, 235-255
- [19] R.D.S.G. Campilho, M.D. Banea, J.A.B.P. Neto, L.F.M. da Silva (2013), “Modelling adhesive joints with cohesive zone models: effect of the cohesive law shape of the adhesive layer”, International Journal of Adhesion & Adhesives, Volume 44, pp. 48-56.
- [20] E.F. Karachalios, R.D. Adams, Lucas F.M. Da Silva (2013), “Single lap joints loaded in tension with high strength steel adherends”, International Journal of Adhesion & Adhesives, Volume 43, pp. 81-95.

## REFERENCES

- [21] Volkersen O., 1938, Luftfahrtforschung, “ Die niekraftverteilung in zugbeanspruchten mit konstanten laschenquersritten”, V.15, pp. 41-47.
- [22] M. Goland, E. Reissner, 1944, Journal of Applied Mechanics, “The stresses in cemented joints”, V.66, pp.17-27.
- [23] R.D. Adams, J. Comyn, W.C. Wake, 1997, Chapman & Hall, “Structural Adhesive Joints in Engineering”.
- [24] Hart-Smith L.J., 1973, NASA Contractor Report 112235- 112236, “Adhesive-bonded double-lap joints”.